T.C.
MARMARA UNIVERSITY
INSTITUTE FOR GRADUATE STUDIES IN
PURE AND APPLIED SCIENCES

INVESTIGATION OF PEPTIDE INHIBITOR BINDING TO β-LACTAMASE

Nilay BÜDEYRİ

THESIS

FOR THE DEGREE OF MASTER OF SCIENCE

IN

BIOENGINEERING

SUPERVISOR
Assist. Prof. Berna SARIYAR AKBULUT
Co-ADVISOR
Assist. Prof. Elif ÖZKIRIMLI ÖLMEZ

İSTANBUL 2009

T.C.
MARMARA UNIVERSITY
INSTITUTE FOR GRADUATE STUDIES IN
PURE AND APPLIED SCIENCES

INVESTIGATION OF PEPTIDE INHIBITOR BINDING TO β-LACTAMASE

Nilay BÜDEYRİ
(141103820070510)

THESIS

FOR THE DEGREE OF MASTER OF SCIENCE
IN
BIOENGINEERING

SUPERVISOR
Asist. Prof. Berna SARIYAR AKBULUT
Co-ADVISOR
Assist. Prof. Elif ÖZKIRIMLI ÖLMEZ

İSTANBUL 2009

ACKNOWLEDGMENTS

I would like to express my deep and sincere gratitude to my thesis supervisor Assist. Prof. Berna SARIYAR AKBULUT for her understanding, encouragement, moral support and valuable guidance which have provided a good basis for the present thesis.

I would also like to express my appreciation to my co-advisor Assist. Prof. Elif ÖZKIRMLI ÖLMEZ for her assistance, valuable guidance and advices throughout this research.

I am deeply indebted to thank Prof. Dr. Amable HORTAÇSU and Prof. Dr. Dilek KAZAN for their valuable suggestions and encouragement during my thesis work.

I am very grateful to Assist. Prof. Burak ALAKENT for providing all of the MATLAB scripts used in my thesis work.

My special thanks are to Mehmet Ali GÖKGÖZ for his love, valuable friendship, patience and support during the days of hard study.

I would like to thank my friends; Selim CEYLAN, Çağakan ÖZBALCI, Pınar KANLIKILIÇER, A. Ezgi AKKAYA, Burcu ÖZKARAL, Celal CEYLAN, Ahmet ÖZCAN for sharing all good and bad times with me.

My special gratitude is to my family for their patience, encouragement and deep love. This thesis is dedicated to them.

It is a pleasure for me to thank TÜBİTAK-BİDEB for providing the National MSc Scholarship throughout my thesis work.

Financial support provided by Marmara University BAPKO project FEN-C-YLP-181208-0290, Boğaziçi University BAP project 08A502 and TÜBİTAK 108M644 is gratefully acknowledged.

July, 2009 **Nilay BÜDEYRİ**

CONTENTS

PAGE

ÖZET

β-LAKTAMAZA PEPTİT İNHİBİTÖRLERİN BAĞLANMASININ İNCELENMESİ

β-laktamazın neden olduğu antibiyotik direnci önemli bir sağlık sorunudur. Bu sorun ile mücadelede β-laktamaz enzimi önemli bir hedef haline gelmiştir. β-Laktamaz inhibitör proteini (BLIP), TEM-1 ve SHV-1 gibi A sınıfı β-laktamazları yüksek ilgiyle inhibe eder. Bu çalışmanın ilk bölümünde, β-laktamaz inhibitör proteininin yapısı temel alınarak oluşturulan peptit inhibitörlerinin (BLIP'in 45-52 kalıntıları) inhibisyon etkisi hesapsal yöntemlerle araştırılmıştır. Moleküler Dinamik Simülasyonları ile β-Laktamaz inhibitör proteini ve seçilen peptid üzerinde çeşitli kalıntılar alanine dönüştürülerek bu kalıntıların SHV-1 β-laktamaza bağlanması değerlendirilmiştir. Peptidin üzerindeki D49A ve Y50A mutasyonları SHV-1 β-laktamazın yapı ve dinamiğini BLIP'ten farklı şekilde etkilerken Y51A mutasyonu SHV-1 β-laktamazın yapı ve dinamiğini BLIP'e benzer şekilde etki etmiştir. Çalışmanın ikinci kısmında ise *in-vitro* ve *in-vivo* β-laktamaz inhibisyonu, farklı uzunluktaki iki peptit (β-laktamaz inhibitör Proteinin A46-Y51 ve C30-D49 kalıntıları) ile incelenmiştir. *In-vitro* ortamda 400 μM konsantrasyonda her iki peptidin de β-laktamazı inhibe ettiği görülmüştür. *In-vivo* ortamda ise, aynı peptitler 28 μM konsantrasyonda yeteri kadar inhibisyon etkisi gösterememiştir.

Temmuz, 2009 **Nilay BÜDEYRİ**

ABSTRACT

INVESTIGATION OF PEPTIDE INHIBITOR BINDING TO β- LACTAMASE

β-Lactamase is an important drug target in combating the increasing problem of β-lactamase antibiotic resistance. β-Lactamase inhibitor protein is an effective inhibitor of class A β-lactamases such as TEM-1 and SHV-1. In the current research, β-Lactamase inhibitor protein structure was used as the starting point to develop new β-lactamase inhibitors. In the first part of this study, the inhibition effect β-lactamase inhibitor protein based peptides (residues 45-52), was investigated by computational methods. Molecular dynamics simulations were performed on various alanine mutants of the β-lactamase inhibitor protein and the peptides to investigate the contribution of these residues to SHV-1 β-lactamase structure and dynamics. Y51A mutation on the peptide affected SHV-1 structure and dynamics similar to BLIP while D49A and Y50A mutations altered the SHV-1 structure and dynamics differently from BLIP. In the second part of the study, β-Lactamase inhibitor protein based peptides of different lengths (A46-Y51 and C30-D49) were used to investigate *in-vitro* and *in-vivo* β-lactamase inhibition. *In-vitro* β-lactamase inhibition was observed by both peptides at a concentration of 400 μM. Under *in-vivo* conditions, inhibition effect of the same peptides at a concentration of 28 μM was not sufficiently high.

July, 2009 **Nilay BÜDEYRİ**

SYMBOLS

$\boldsymbol{a_i}$	: Acceleration of particle *i*
$\boldsymbol{F_i}$	: Force acting on particle *i*
$\boldsymbol{M_i}$	: Virtual bond vector of particle *i*
$\boldsymbol{m_i}$	: Mass of particle *i*
ns	: nanosecond
$\boldsymbol{R_i}$	: Position of particle *i*
$\boldsymbol{V}$	: Potential energy
Å	: Angstrom
A	: Ala, Alanine
D	: Asp, Aspartic acid
E	: Glu, Glutamine acid
F	: Phe, Phenylalanine
G	: Gly, Glycine
H	: His, Histidine
K	: Lys, Lysine
L	: Leu, Leucine
M	: Met, Methionine
N	: Asn, Asparagine
P	: Pro, Proline
R	: Arg, Arginine
S	: Ser, Serine
T	: Thr, Threonine
U	: Enzyme Units
V	: Val, Valine
W	: Trp, Tryptophan
Y	: Tyr, Tyrosine
$\boldsymbol{\varphi}$	: dihedral angle

ABBREVIATIONS

3-D	: Three-Dimensional
Da	: Dalton
fs	: femtosecond
kDa	: kilodalton
ml	: mililiter
mM	: milimolar
ng	: nanogram
nM	: nanomolar
ns	: nanosecond
µM	: micromolar
BLIP	: β-Lactamase Inhibitor Protein
Cα	: Carbon Alpha
CA	: Carbon Alpha Atom on The Protein Backbone
CE	: Terminal Carbon Atom of Methionine Sidechain
CFU	: Colony Forming Unit
CHCA	: α-cyano-4-hydroxycinnamic acid
CZ	: Terminal Carbon Atom of Tyrosine Sidechain
EDTA	: ethylenediaminetetraacetic acid
MALDI	: Matrix Assisted Laser Desorption/Ionization
MD	: Molecular Dynamics
MSF	: Mean Square Fluctuations
MW	: Molecular Weight
NZ	: Terminal Nitrogen Atom of Lysine Sidechain.
ND2	: Terminal Nitrogen Atom of Asparagine Sidechain
OD	: Terminal Oxygen Atom of Glutamine Acid Sidechain
OG	: Terminal Oxygen Atom of Serine Sidechain

PCA : Principal Components Analysis

pdb : Protein Database Bank

RMSD : Root Mean Square Deviation

rpm : rotation per minute

SDS-PAGE : Sodium Dodecyl Sulfate- Polyacrylamide Gel Electrophoresis

TEMED : N,N,N,N-tetramethylethylendiamine

vdW : van der Waals

LIST OF FIGURES

PAGE

LIST OF TABLES

CHAPTER I

INTRODUCTION and AIM

Many strains of bacteria resistant to β-lactam antibiotics have emerged in clinical care settings due to the heavily usage of β-lactam antibiotics since the 1940's (Palumbi et al., 2001). β-lactam antibiotics form about 50% of the global market of antibiotics which was estimated to be US$ 25 billion in 2002 (Coates et al., 2002). On the other hand, the cost of the resistance to the β-lactam antibiotics was estimated to be between US$ 10-17 billion annually (Palumbi et al., 2001). Resistance to β-lactam antibiotics is an especially severe threat since, as well as killing a broad spectrum of bacteria, β-lactams have very low toxicity to humans (Livermore et al., 1996). The primary mechanism of β-lactam resistance is the enzymatic cleavage of the β-lactam ring by β-lactamases that is produced by bacteria (Fisher et al., 2005). This makes β-lactamase an important drug target to combat antibiotic resistance.

β-lactamases are classified into four groups (class A-D) based on their primary sequences. β-lactamases and especially class A family of these enzymes are the most common form of resistance against the very important group of β-lactam antibiotics. To overcome the antibiotic resistance mechanism mediated by β-lactamase, small molecule β-lactamase inhibitors such as clavulanic acid and sulbactam are used in combination therapies (Page and Laws, 1998). However, mutations in β-lactamases render them no longer sensitive to β-lactamase inhibitors and therefore β-lactamase inhibitor design is an interesting field of research.

β-lactamase inhibitory protein (BLIP), a 165 amino acid protein, produced by *Streptomyces clavuligerus*, binds and inhibits class A β-lactamases such as TEM-1 and SHV-1 with high potency (Rudgers et al., 2001). Therefore, mimicking the binding and inhibition activity of BLIP in a small peptide would be very beneficial for the development of novel β-lactamase inhibitors and antibiotics.

Computational simulations act as a bridge between microscopic length and time scales and the macroscopic world of the laboratory. Molecular Dynamics (MD) calculations have been shown to be a powerful tool to understand conformational changes involved in ligand binding, catalysis or other functions of biological macromolecules at an atomic level. They are routinely used to investigate structure, dynamics and thermodynamics of biological molecules and their complexes (Reichmann et al., 2005). Although MD Simulations give valuable information on the binding properties of biological molecules, the findings must be experimentally verified.

The aim of this research was to propose BLIP based peptide inhibitors for β-lactamase and then verify the inhibition potential of peptides using experimental techniques. The first part of the work involved the analysis of crystal structures of apo and BLIP bound SHV-1 β-lactamases (a class A β-lactamase). These structures were also analyzed by MD simulations on apo and BLIP and peptide bound SHV-1 complexes. The importance of residue $D49_{BLIP}$ to SHV-1 binding was investigated by mutating this residue to alanine and investigating its effect on SHV-1 conformation and dynamics. The peptide of interest was based on residues 45 to 52 of BLIP. Residues D49, Y50, Y51 of the peptide were mutated to alanine and changes in conformation, dynamics and interactions of the peptides carrying these point mutations with SHV-1 were examined.

The second part of the work involved experimental analysis to study *in-vivo* and *in-vitro* binding of two BLIP derived peptides to RTEM-1 β-lactamase, an other class A β-lactamase. The similarities in sequence and catalytic mechanisms between these two class A enzymes allow specific information to be generalized. The peptides derived from BLIP, residues 46 to 51 and 30 to 49, were synthesized and their inhibition effect was investigated on the pUC18 derived RTEM-1 β-lactamase in the osmotic shock fluid and intact cells. The results of this study with integration of computational and experimental methods for inhibitor design should help to speed up the efforts to fight with increasing bacterial resistance.

CHAPTER II

GENERAL BACKGROUND

II.1. MECHANISM AND ACTION OF β-LACTAM ANTIBIOTICS AND β-LACTAMASE MEDIATED RESISTANCE TO β-LACTAM ANTIBIOTICS

β-Lactam antibiotics are the most widely used of all different groups of antimicrobials. Today, about 100 different β-lactam antibiotics are used clinically in the antibacterial treatment of humans. Penicillins including ampicillins, cephalosporins, imipenem and clavulanate are all considered β-lactam antibiotics (Kasier, 2004). These antibiotics share a three carbon, one nitrogen structure also known as the β-lactam ring (Figure II.1). An intact β-lactam ring is required for these antibiotics to exert its bacterial activity.

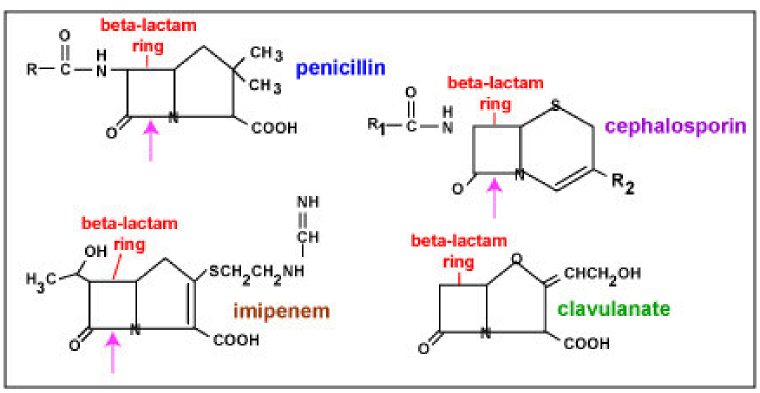

Figure II.1. β-lactam rings of penicillins, cephalosporin, imipenem and clavulanate (Kasier, 2004).

The β-lactam antibiotics act by interfering with the enzymes involved in the growth of bacterial cell wall of both gram negative and gram positive bacteria. The cell wall not only determines the shape of an organism, but also protects it as well. The cell wall is composed of, amongst other things, a peptidoglycan layer that is formed from linear chains of two alternating amino sugars, N-acetyl-glucosamine (NAG) and N-acetyl-muramic acid (NAM). The NAM/NAG-peptide subunits are then cross-linked together by a short amino acid chain containing D-alanine, D-glutamine and mesodiaminopimelic acid (or lipid II). The amino acid composition varies between species. The final transpeptidation step is facilitated by membrane bound DDtranspeptidases, also known as penicillin binding proteins (PBPs) [Figure II.2A]. The β-lactam antibiotics are analogues of D-alanyl-D-alanine, and thus act as pseudosubstrates of the PBPs. Once bound in the active site, the β-lactam ring is hydrolysed, acylating the active site serine to form a stable covalent acyl-enzyme complex [Figure II.2B]. For a long time it was thought that the inactivation of the PBP prevented the crosslinking of the NAG/NAM subunits in the peptidoglycan layer, in turn weakening the cell wall, eventually leading to bacteriolysis (Tipper and Strominger, 1965). However the lysis of the bacterial cell wall has been shown to be enzymatically mediated (Rogers and Forsberg, 1971; Tomasz et al., 1970).

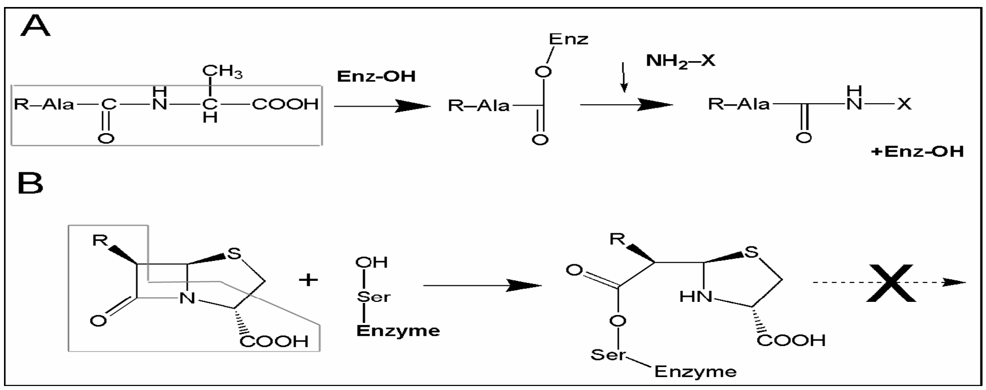

Figure II.2. A. The reaction catalysed by PBPs, and **B.** their inhibition by β-lactam antibiotics (Bayles, 2000).

The most prevalent mechanism of β-lactam resistance employed by bacteria involves the enzymatic destruction of the β-lactam ring by a group of enzymes known as β-lactamases. The β-lactamases are structurally related to PBPs (Massova and Mobashery, 1998), and are capable of hydrolysing the β-lactam ring [Figure II.3]; thus they are potentially active upon a number of different β-lactam antibiotics. Secreted into the periplasm, these enzymes can destroy the β-lactam antibiotics before they can even reach their target.

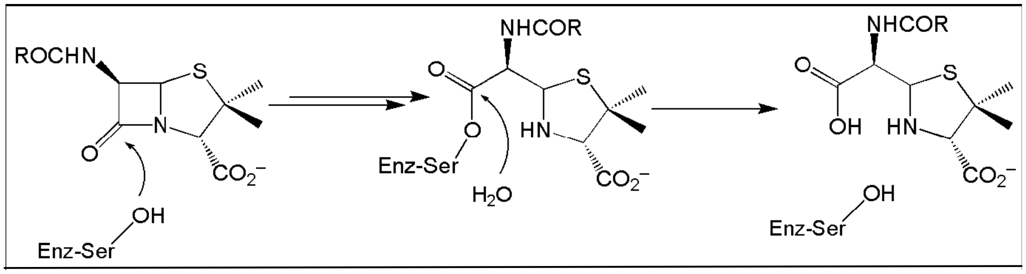

Figure II.3 The hydrolysis of acyl-enzyme complex catalysed by a serine β-lactamase (Massova and Mobashery, 1998).

II.2. CLASSIFICATION OF β-LACTAMASES

The spread of β-lactamase genes was aided by their integration with mobile genetic elements such as plasmids or transposons. In gram-negative bacteria, β-lactamase enzymes are secreted into the periplasmic space while in gram-positive bacteria, these enzymes are bound to the cytoplasmic membrane or excreted to the medium. Class A, C and D β-lactamases have a serine residue in the active site, but class B enzymes require zinc ions for catalytic activity (Majidudin et al., 2002). Among these enzymes, the prevelant type has always been the class A β-lactamases such as TEM-1 and SHV-1 which became model enzymes for extensive studies (Orencia et al., 2001; Matagne et al., 1995).

II.3. STRUCTURE OF TEM-1 AND SHV-1 β-LACTAMASES

Class A β-lactamase members TEM-1 and SHV-1 represent the major source of bacterial resistance. These enzymes constitute an important threat to human health (Matagne et al. 1998).

TEM-1 β-lactamase consists of two domains, an α/β and an all α domain (Jelsch et al. 1993] (Figure II.4). The α/β domain includes a five-stranded antiparallel β-sheet onto which three helices (h1, h10 and h11) are packed. The α domain, composed by eight helices (h2–h9), is placed on the other side of the β-sheet. The two domains are connected by two hinge regions. Three salt bridges (E37–R61, R43– E64, R61–E64) and one H-bond (E37–V44) in the first hinge region, the salt bridge (R222–D233) and one H-bond involving the aspartyl dyad (D214– D233) in the second hinge region, prevent local structural modifications to occur.

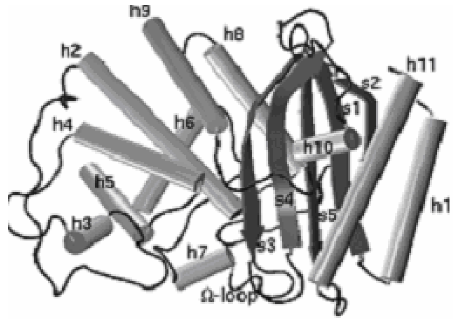

Figure II.4 Cartoon Representation of TEM-1 β-lactamase (Rocattano et al., 2005).

The active site is in a groove between the two domains and it is surrounded by conserved elements bearing the six residues S70, K73, S130, E166, N170, K234 and more involved in the catalytic process (Figure II.5). S70 and K73 are located on the NH_2-terminal of h2 helix, S130 on one side of the catalytic cavity, E166 and N170 on the Ω loop forming the bottom edge of the active site and K234 on the innermost strand (s3) of the β-sheet forming the other side of the catalytic cavity (Rocattano et al., 2005).

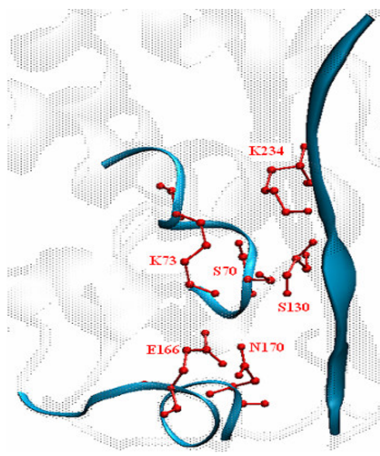

Figure II.5. Representation of active site residues of TEM-1 β-lactamase.

The 28.9 kDa SHV-1 β-lactamase, first described by Pitton in 1972 as Pit-2 (19), has been identified in several species of enterobacteria and is generally considered a plasmid-encoded enzyme (Bush et al., 1995). Nevertheless, this β-lactamase is found at a higher frequency (up to 80 to 90 %) in *Klebsiella pneumonie* (Babini et al., 2000). The SHV-1 β-lactamase is 68 % identical to TEM-1 β-lactamase and occurs also in gram negative bacteria. SHV-1 β-lactamase exhibits a substrate hydrolysis profile similar to TEM-1 β-lactamase (Lee et al., 1991). The consensus numbering for class A β-lactamases result in deletions in both enzymes at positions 239 and 253

(Barthelemy et al., 1988; Ambler, 1991; Strynadka et al., 1994; Du Bois et al., 1995). The detailed sequence alignment of SHV-1 and TEM-1 β-lactamases is given in Figure II.6.

TEM-1	H***P***ET***L***VKV***K***DA***E***D***QL***GA***RVG***Y***IE***L***DL***N***SG***KI***L***ESF***R***PE***ERFPMMSTFKV***L***LC GAVL***SRI***D***	**85**
SHV-1	S***P***QP***L***EQI***K***LS***ES******QL***SG***RVG***M***IE***M***DL***A***SG***RT***L***TAW***R***AD***ERFPMMSTFKVVLCGAVL***A***R***V***D***	**85**
TEM-1	***AG***Q***EQL***G***R***R***IHY***S***Q***N***DLV***E***YSPV***T***EKHL***T***DGMTV***R***ELC***S***AAITMSDN***T***AANLLL***TT***I***GGP***	**145**
SHV-1	***AG***D***EQL***E***R***K***IHY***R***Q***Q***DLV***D***YSPV******SEKHL***A***DGMTV***G***ELC***A***AAITMSDN***S***AANLLL***A***T***V***GGP***	**145**
TEM-1	KE***LTAFL***HNM***GDHVTRLDRWE***P***ELNEA***I***P***N***D***E***RDTT***M***P***V***A***MA***T***TLRKLLT***GEL***L***TLA***S***RQ	**205**
SHV-1	AG***LTAFL***RQI***GDNVTRLDRWE***T***ELNEA***L***P***G***D***A***RDTT***T***P***AS***MA***A***TLRKLLT***SQR***L***SAR***S***QR	**205**
TEM-1	***QL***ID***WM***EA***D***K***VAGPL***L***RS***A***LPAGWFIADK***S***GAGERG***S***RGI***IAA***LGP***DG***K***PS***RIVVIY***TTG	**266**
SHV-1	***QL***LQ***WM***VD***D***R***VAGPL***I***RS***V***LPAGWFIADK***T***GAGERG***A***RGI***VAL***LGP***NN***K***AE***RIVVIY***LRD	**266**
TEM-1	SQ***A***T***M***D***ERN***R***QIA***E***IGA***S***LI***K***HW***--	**292**
SHV-1	TP***A***S***M***A***ERN***O***OIA***G***IGA***A***LI***E***HW***OR	**292**

Figure II.6. Sequence alignment of TEM-1 and SHV-1 (Ambler Numbering System). Conserved residues are shown in bold and italic.

Followed by the crystal structures of TEM-1 β-lactamase reported by Strynadka et al. (1992) and Jelsch et al. (1993), Kuzin et al. (1999) determined the crystal structure of SHV-1 β-lactamase. Mutagenesis studies (Wang et al., 2009) as well as structural studies helped to elucidate the residues that are important for catalytic activity and for binding of SHV-1 β-lactamase. Critical residues of TEM-1 and SHV-1 β-lactamases and their functions are listed in Table II.1.

Table II.1 Important residues of TEM-1 and SHV-1 β-lactamases

REGION	FUNCTION
Catalytic Site (S70, K73, S130, E166, N170,K234)	Substrate Catalysis (Jelsch et al., 1993)
Omega (Ω) Loop (Residues 160 to 181)	Forms the bottom wall of the catalytic site (Strynadka et al., 1992)
H10 Helix (Residues 218 to 224)	Forms above the substrate binding site (Reynolds et al., 2006)
$E104_{TEM-1}/D104_{SHV-1}$, Y105	Substrate Binding (Petit et al., 1995 ; Doucet et al., 2004)

II.4. β-LACTAMASE INHIBITORY PROTEIN (BLIP)

The disparity between clavulanic acid quantification and β-lactamase inhibitory activity of *Strepomyces clavuligerus* cell lysates enabled the detection of β-lactamase inhibitory protein (BLIP). BLIP is the first protein based inhibitor of β-lactamases (Doran et al., 1990).

The BLIP crystal structure exhibits a novel fold with two similar domains. Each domain consists of a helix-loop-helix motif that packs against a four-stranded antiparallel β-sheet (Figure II.7). BLIP is the first example of a protein inhibitor having two similarly folded domains that interact with and inhibit a single target enzyme. The two domains of BLIP can be defined from Ala 1 to Leu 76 and from Ala 80 to Val 165, connected by a short tripeptide, Ala 77 to Ser 79 (Strynadka et al., 1994).

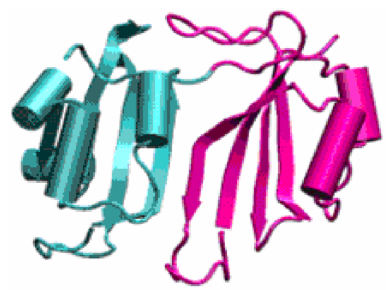

Figure II.7. The crystal structure of BLIP. The first domain (Residues 1 to 76) (green), the second domain (Residues 80 to 165) (pink).

BLIP is known to bind to a diverse set of class A β-lactamases with a wide range of affinities (Strynadka et al., 1994; Zhang et al., 2004). For instance, it binds to TEM-1 β-lactamase with a K_i of 0.5nM but it binds to SHV-1 β-lactamase with a K_i of 1.1 μM. This is one enigma of BLIP inhibition since TEM-1 and SHV-1 β-lactamases are 68% identical in amino acid sequence.

The interacting residues on BLIP and TEM-1 and SHV-1 β-lactamases are listed in Table II.2

Table II.2 Residues on TEM-1 and SHV-1 β-lactamases that interact with BLIP**.**

BLIP	TEM-1 and SHV-1 β-LACTAMASES	REFERENCE
Asp 49	Ser 130, Lys 234, Ser 235, Arg 244	Petrosino et al.,1999
Tyr 50	Pro 107, Val 216,Met 129	Zhang et al.,2003
Patch 1 of BLIP	Ser 106, Pro 107, Val108	Zhang et al.,2004
Patch 2 of BLIP	Interacts with 99QNDLV103 of TEM	Zhang et al.,2004

Alanine-scanning mutagenesis was employed to determine the functional epitopes of BLIP for binding to β-lactamase. Two patches of residues (patch 1: residues F36, H41, D49, Y53 and patch 2: H148, W150, R160, W162), one from each domain of BLIP, were shown to dominate binding affinity (Zhang et al. 2003) (Figure II.8). The residues including F36, H41, D49, Y53 and W150 comprise the functional epitope of BLIP for binding to β-lactamase. Four of the critical residues are from the first domain, whereas W150 is the only critical residue from the second domain. It is clear that the second domain of BLIP, including residues in patch 2, do not contribute as much energy for binding to β-lactamase (Zhang et al. 2004).

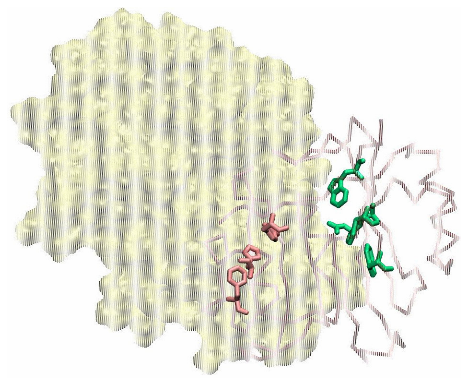

Figure II.8 Representation of Patch1 (pink) and Patch 2 (green) of BLIP (red) on SHV-1 β-lactamase (yellow).

The ability of BLIP to bind such a variety of class A β-lactamases is believed to be due in part to an extensive layer of water molecules that are trapped between the inhibitor and the 99–112 loop-helix region of the enzyme (Strynadka et al., 1996).

The three-dimensional structures of BLIP alone and BLIP in complex with the SHV-1 β-lactamase have been determined to high resolution and the structure of the complex indicates that a type II' β turn encompassing residues 46 to 51 of BLIP (Figure II.9) makes critical interactions with the active site of the β-lactamase (Rudgers et al., 2001)

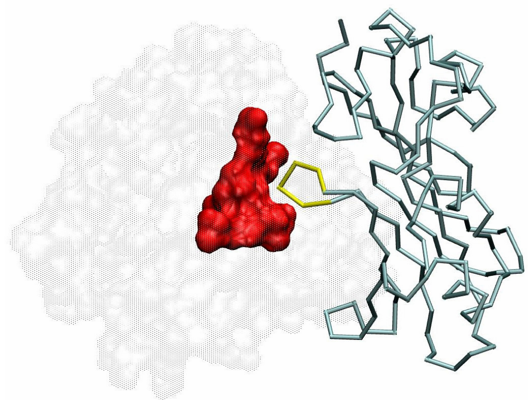

Figure II.9 Representation of BLIP (blue) binding to SHV-1 β-lactamase (gray). The region of BLIP from residues 46 to 51 is shown in green and the active site of SHV-1 is red.

$D49_{BLIP}$ is an important interface hot-spot residue for SHV-1 β-lactamase inhibition (Reynolds et al., 2006; Petrosino et al., 1999). Mutation of the aspartic acid (D) to alanine (A) removes the carboxylate moiety, which serves as a hydrogen bond acceptor for the active site residues of SHV-1. Elimination of the carboxylate reduces the inhibitory activity of BLIP approximately 100-fold, indicating that residue D49 makes significant contribution to BLIP inhibition of TEM-1 β-lactamase which shares 68% sequence identity with SHV-1 (Petrosino et al., 1999). To this purpose, $D49_{BLIP}$ was mutated to alanine, to be able to see the contribution of $D49_{BLIP}$ to β-lactamase binding.

II.5. PEPTIDE INHIBITORS OF β-LACTAMASE

The rise of resistant bacterial pathogens brings about the urgent need to develop novel classes of antibiotics and inhibitors. In this respect peptide inhibitors display a significant advantage over small organic molecules since β-lactamase has acquired resistance against most of the small organic molecules.

Development of peptide inhibitors was also extended to β-lactamase inhibition. Huang et al. (2003) reported that a linear 6-mer peptide with the sequence RRGHYY binds to the class A β-lactamase, TEM-1 using phage display. This peptide which is 50% identical with a type II β-turn sequence of BLIP was found to inhibit TEM-1 β-lactamase with a K_i of 136 μM.

Rudgers et al. (2001) reported the inhibition potential of peptides based on the 46 to 51 region of BLIP. The cyclic peptide with cysteine residues at both ends inhibits TEM-1 and SHV-1 with a K_i of 603 and 680 μM, while in reduced form, the peptide binds to TEM-1 and SHV-1 with a K_i of 488 and 420μM, respectively. On the other hand the same peptide with an N-terminal biotin binds to TEM-1 and SHV-1 with a K_i of 359 and 458μM, respectively. Biotin can be linked to the N-terminus of peptides or to the side chains of lysine (Lys) or glutamic acid (Glu) to enhance cellular uptake. The 244.31Da coenzyme Biotin is a water-soluble member of the B-complex group of vitamins and is commonly referred to as Vitamin H (Figure II.10). It is well documented that large biotinylated peptides can readily be transported into gram (-) bacteria such as *E. coli* (Walker and Altman, 2005).

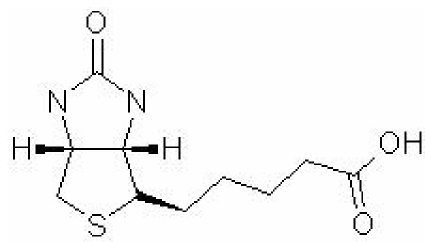

Figure II.10. The Chemical Structure of Biotin.

II.6. *In-vitro* β-LACTAMASE-LIGAND RECOGNITION

In kinetic studies of β-lactamase, mostly spectrophotometric methods are employed. CENTA (Figure II.11), a chromogenic cephalosporin structurally resembling nitrocefin, cephaloridine and cephalotin, can efficiently be used as a substrate in kinetic studies of β-lactamase (Jones et al., 1982). It undergoes a detectable color change from faint yellow (λ maximum 340 nm) to chrome yellow (λ maximum 405 nm) concomitant with enzymatic hydrolysis of the β-lactam ring, arising from the elimination of the 2-nitrothiobenzoate chromaphore from the hydrolytic product, cephalosphoroic acid.

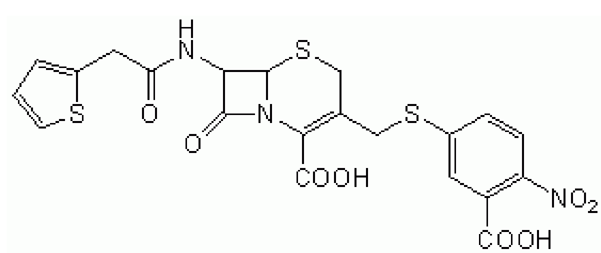

Figure II.11 The structure of CENTA.

CENTA can also be easily used in high-throughput screening tests for the selection of new β-lactamase inactivators. Unfortunately, it is not sufficient for the direct detection of β-lactamase producing colonies on agar plates or for the localization of β-lactamases after gel isoelectric focusing (Jones et al., 1982 and Bebrone et al., 2001).

The kinetic constants of TEM-1 β-lactamase with CENTA as the substrate (Bebrone et al., 2001) are given in Table II.3.

Table II.3 Kinetic parameters for TEM-1 β-lactamase with CENTA

Enzyme	CENTA (mM)	Enzyme (nM)	Kcat (s^{-1})	Km (μM)	Kcat/Km ($\mu M^{-1}s^{-1}$)
TEM-1	0.025-0.3	11.5	110	70	1.6

II.7. MOLECULAR DYNAMICS (MD) SIMULATIONS

Molecular dynamics simulations are used to calculate atomic trajectories by direct integration of the equations of motion. Newton's second law (Equation II.1) for classical particles is used with an appropriate specification of an inter-atomic potential and suitable initial and boundary conditions

$$F_i = m_i a_i \quad \text{or} \quad \frac{F_i}{m_i} = \frac{d^2 x_i}{dt^2} \tag{II.1}$$

where F_i is the force exerted on the particle i, m_i is its mass and a_i is its acceleration.

Simulations can provide the atomistic detail concerning individual particle motions as a function of time. Thus, they can be used to address specific questions about the properties of a model system, sometimes more easily than experiments on the actual system. For many aspects of biomolecular function, it is these details that are of interest. Experiments play an essential role in validating the simulation methodology: comparisons of simulation and experimental data serve to check the accuracy of the calculated results and to provide criteria for improving the methodology.

Another significant aspect of simulations is that, although the potentials used in simulations are approximate, user has control over the potential, so that by removing or altering specific contributions, the role of a particular interaction or energy in determining a given property can be examined. This is best demonstrated by the use of "computer alchemy" in the calculation of free energy differences, such as that used in computational alanine scanning (Karplus and McCommon, 2002).

A MD simulation requires the definition of a potential function or description of the terms by which the particles in the simulation will interact. The application of mathematical equations to describe the relationship of chemical structure to energy in combination with statistical mechanics, allows for all properties of a system to be calculated in theoretical chemistry. However, this is limited by the inability to calculate the energy of all possible conformations of a chemical system. One way to overcome this limitation is the use of simple mathematical functions to treat the structure-energy relationship. This type of approach is referred to as molecular mechanics or empirical force field calculations. However, the equation alone does not allow for computation of structure-energy relationships. In addition, parameters must be included in the mathematical equation. The empirical force field used in this study is CHARMM22 (Kale et al., 1998).

Bonded terms of the potential are:

$$\sum_{bonds} K_b (b - b_o)^2 + \sum_{angles} K_\theta (\theta - \theta_o)^2 + \sum_{torsions} K\phi(1 + \cos(n\phi - \delta)) +$$
$$\sum_{impropers} K_\varphi (\varphi - \varphi_o)^2 + \sum_{Urey-Bradley} K_{UB} (r_{1,3} - r_{1,3,o})^2 \qquad \text{(II.2)}$$

While nonbonded terms are:

$$\sum_{electrostatics} \frac{q_i q_j}{r_{ij}} + \sum_{VDW} \left[\left(\frac{R_{\min,ij}}{r_{ij}} \right)^{12} - 2\left(\frac{R_{\min,ij}}{r_{ij}} \right)^{6} \right] \qquad \text{(II.3)}$$

The first term in the energy function accounts for the covalent bond strecthing interaction between two atoms linked by a harmonic potential where b_o is the minimum energy bond length, hence b-b_o is the distance from equilibrium that the atom has moved and K_b is the bond force constant. The second term in the equation accounts for the bond angles where K_θ is the angle force constant and θ-θ_o is the deviation of the angle from the equilibrium value between 3 bonded atoms. The third term is used for the dihedral angle interaction where $K\phi$ is the dihedral force constant, n is the multiplicity of the function, ϕ is the dihedral angle and δ is the phase shift. The fourth term accounts for the impropers, where K_φ is the force constant and φ-φ_o is the out of plane angle. The Urey-Bradley component (cross-term accounting for angle bending using 1, 3 nonbonded interactions) comprises the fifth term, where K_{UB} is the respective force constant and r is the distance between the 1,3 atoms in the harmonic potential. Nonbonded interactions between pairs of atoms *(i,j)* are represented by the last two terms. By definition, the nonbonded forces are only applied to atom pairs separated by at least three bonds. The van der Waals (vdW) energy is calculated with a standard 12-6 Lennard-Jones potential and the electrostatic energy with a Coulombic potential. In the Lennard-Jones potential above, the $Rmin,_{ij}$ term is not the minimum of the potential, but rather where the Lennard-Jones potential crosses the x-axis (*i.e.* where the Lennard-Jones potential is zero). Nonbonded forces decrease as the distance between atoms increases. Many simulations use a cutoff radius to save computation time (Kalé et al., 1999).

NAMD2 (Kalé et al, 1999), is one of the new parallel programs aimed at utilizing large parallel machines in a scalable manner. The nonbonded force computations, which constitute the dominant component of the overall computational cost, require calculation of pairwise interactions between atoms. In most common methods, a cutoff distance is used. Nonbonded interactions between atoms beyond this cutoff radius are either not calculated or calculated less often.

NAMD2 allows the force field to be divided into three parts based on their variation frequency. All bonded forces (bonds, angles, dihedrals, and impropers) are considered quickly varying, nonbonded forces (electrostatics and Lennard-Jones) within a cutoff are slower, and long-range electrostatics vary on the slowest time scale.

NAMD2 is written using Charm++ (Kale et al., 1998), a parallel C++ extension that supports message-driven execution. NAMD2 uses CHARMM force fields and X-PLOR coordinate and molecular structure files. In addition to non-periodic simulations, NAMD2 can use periodic boundary conditions over any combination of the three coordinate axes. It performs cutoff simulations or full-electrostatic simulations. NAMD2 can be used with VMD (Humphrey et al., 1996) which is a computer package used for monitoring of and interaction with ongoing simulations (Kalé et al., 1999).

CHAPTER III

THE STUDY

III.1. COMPUTATIONAL MATERIALS

Workstations (HPxw8600 and HPxw6600)

NAMD program was used to perform MD Simulations.

VMD program was used to analyze and visualize simulation trajectories.

MATLAB™ was used to analyze simulation trajectories.

III.2. COMPUTATIONAL METHODS

III.2.1. Simulation System for SHV-1 β-lactamase

The three-dimensional crystal structures are available for SHV-1 (pdb code: 1shv) and SHV-1: BLIP complex (pdb code: 2g2u). BLIP was also extracted from this complex. These structures were used as the initial coordinates for the simulations. It has been shown that residues 46 to 51 of BLIP make critical interactions with the active site of the SHV-1 β-lactamase (Rudgers *et al.,* 2001). Since the peptide formed from the residues 46 to 51 of BLIP moved out from the boundary water box throughout the MD simulation, residues 45 to 52 of BLIP (NH_2-HAAGDYYA-COOH) was used as the inhibitory peptide in this study. The effect of alanine mutation on D49, Y50 and Y51 of peptide (NH_2-HAAG<u>A</u>YYA-COOH, NH_2-HAAGD<u>A</u>YA-COOH, NH_2-HAAGDY<u>A</u>A- COOH) was also investigated for binding.

III.2.2. Molecular Dynamics Simulation Protocols

The initial coordinates for the protein atoms and the crystallographic water molecules were obtained from the crystal structure of the SHV-1 β-lactamase at 1.98 Å resolution (1shv.pdb) and SHV-1:BLIP complex structure at 1.60Å resolution (2g2u.pdb). Hydrogen atoms were added and the structure was immersed in a TIP3 water rectangular box, the walls of which extend a specified distance, typically 9-12 Å buffer from the protein to the periodic boundary in each direction. Sodium and chloride ions were added to neutralize the total box charge. The calculation of long range interactions was performed by the Particle Mesh Ewald (PME) Method (Darden et al., 1993), using a grid size of 72 Å x 80 Å x 72 Å. A nonbond pairlist cutoff 12 Å was used by using conjugate gradients. The potential energy of the complete structure was minimized for 3000 steps. Water molecules were allowed to relax with constraints on the proteins. Then the whole simulation system of SHV-1 β-lactamase was gradually heated from 50 K to 300 K during 2400 ps. The MD simulations were performed with the NAMD program using the CHARMM22 force field and carried out for ten nanoseconds with the SHAKE algorithm using a 1 fs (10^{-15}s) time step. Snapshots from the trajectory were saved every 500 fs. A typical benchmark for the 25727 atom system was 0.8 day per nanosecond of simulation. The same protocol was used for SHV-1:peptide structures. The peptides were modified such that the N-terminal was acethylated and the C-terminal was amidated.

III.2.3. Trajectory Analysis

III.2.3.1. Root Mean Square Deviations (RMSD)

Calculation of the root-mean square distance between equivalent atoms of the two superimposed structures is the most common method for measuring structural similarity. The root mean square deviations were calculated as the deviations from the initial structure of the C_α coordinates throughout the MD simulations (Equation III.1). The alignment was performed on the same set of atoms unless otherwise stated.

$$rmsd = \frac{\sqrt{\sum_{i=1}^{N}(d_i^2)}}{N} \qquad \text{(III.1)}$$

N: number of atoms

d: the distance between each of the N pairs of equivalent atoms in two optimally superimposed structures.

III.2.3.2. Mean Square Fluctuations (MSF) of Atomic Positions

The conformations were aligned before calculation of MSF. Then mean square fluctuations were calculated by C_α backbone fluctuations of each residue according to the deviation from the average structure through the whole trajectory of the simulations (Equation III.2). The conformations were aligned before calculation of fluctuations.

$$MSF_i = \langle (R_i(t) - R_i^o)^T (R_i(t) - R_i^o) \rangle \quad \text{(III.2)}$$

$R_i(t)$=Vector of Cartesian coordinates of the C_α atom of i^{th} residue at time t.

R_i^o= Vector of coordinates of the average structure of i^{th} residue.

$\langle\ \rangle$ = Time average

III.2.3.3. Principal Component Analysis (PCA)

Principal Component Analysis is used to reduce large dimensional data sets to data sets with a few dimensions, which still retain most of the information in the original data matrix (Amadei et al., 1993).

Given a data matrix X with n cases and p variables (i.e., $X_1, X_2 ..., X_p$ variables) a linear transformation to a new set of variables $Y_1, Y_2 ..., Y_p$ can be calculated with Equations III.3-5.

$$Y_1 = a_{11}X_1 + a_{21}X_2 + \ldots + a_{p1}X_p \quad \text{(III.3)}$$

$$Y_2 = a_{21}X_1 + a_{22}X_2 + \ldots + a_{p2}X_p \quad \text{(III.4)}$$

$$Y_p = a_pX_1 + a_pX_2 + \ldots + a_pX_p \quad \text{(III.5)}$$

The first principal component explains the largest percentage of the variation in the original *p*-dimensional data set (and the second principal component explains the second largest percentage and so on). Typically the first few principal components account for most of the variation while the remaining principal components make a negligible contribution. By reducing the dimensionality of the original data, principal components can often simplify many analyses.

Principal components reduce to the problem of finding the eigenvalues and eigenvectors of the covariance (or correlation matrix) of the data matrix. The i^{th} column of the A matrix is the eigenvector corresponding to the i^{th} eigenvalue of the covariance (or correlation) matrix. Also, the proportion of the variance in the original data matrix explained by the i^{th} principal component is the i^{th} eigenvalue divided by the sum of all *p* eigenvalues. Covariance matrix is preferred when the original data have reasonably comparable scales. If this is not the case, the correlation matrix is preferred.

III.3 EXPERIMENTAL MATERIALS

III.3.1. Bacterial Strains and The Plasmid

In this study, *Escherichia coli* K12 and *Escherichia coli* XL-1 strains were used from our laboratory stocks. β-lactamase expression was obtained from pUC18 plasmid carrying the gene for R-TEM-1.

III.3.2. Chemicals

All chemicals and solutions used in this study were purchased from MERCK (Germany) and SIGMA (USA).

III.3.3. Growth Media for *Escherichia coli*

M9 Minimal medium (Yamamoto, 1982) and Luria Broth (LB) Medium (Yamamoto, 1982) were used throughout this study. For selective media, 100 mg/ml ampicillin was added.

Per Liter of growth media completed to one liter with deionized and distilled water:

<u>M9 Minimal Medium</u>

5X M9 Salts	200 ml
1M $MgSO_4$	2 ml
1M $CaCl_2$	100 μl
20% Glucose	40 ml

<u>M9 salts</u>

Na_2HPO_4	33.9 g
KH_2PO_4	15 g
NaCl	2.5 g
NH_4Cl	5 g

<u>LB Medium</u>

Yeast Extract	5 g
Tyrptone	10 g
NaCl	10 g

M9 Minimal and LB media were supplemented with 15 g/L of agar to prepare solid medium.

III.3.4. Buffers and Solutions

III.3.4.1. SDS-PAGE Buffers and Solutions

Solution A (Acrylamide/Bis; 30:0.8):

Per 100 ml of solution, completed with deionized and distilled water:

Acrylamide	29.2 g
N'N'-bis-methylene-acrylamide	0.8 g

Stored in dark and at 4 °C

Solution B (4X Seperating Gel Buffer, 1.5M Tris-HCl, pH 8.8):

Per 100 ml of solution, completed with deionized and distilled water:

Tris-base	18.5 g

pH was adjusted to 8.8 with 3N HCl and stored at 4 °C.

Solution C (4X Stacking Gel Buffer, 0.5M Tris-HCl, pH 6.8):

Per 50 ml of solution, completed with deionized and distilled water:

Tris-base	3 g

pH was adjusted to 6.8 with 5N HCl and the solution was stored at 4°C.

Solution D (%10 SDS):

Per 100 ml of solution, completed with deionized and distilled water:

SDS	10 g

Stored at room temperature.

%10 APS:

Per 5 ml of solution, completed with deionized and distilled water:

Amonnium persulfate	0.5 g

2X SDS Gel Loading Buffer

Per 10 ml of solution, completed with deionized and distilled water:

0.5 M Tris-HCl, pH 6.8	1 ml
10 % SDS	1.6 ml
Glycerol	0.8 ml
β-mercaptoethanol	0.4 ml
Bromophenol blue	0.4 ml

stored at -20 °C

10X SDS-PAGE Running Buffer (g/L) :

Glycine	154 g
Tris-base	30 g
SDS	10 g

Electrophoresis separating gel (10 %)

Solution A	4 ml
Solution B	2.5 ml
10% APS	50 µl
TEMED	5µl
dH_2O	3.5 ml

Electrophoresis stacking gel (5 %)

Solution A	2.5 ml
Solution C	0.67 ml
10% APS	30 µl
TEMED	5 µl
dH_2O	2.5 ml

Solution1 (Fixing Solution)

50 % Ethanol

2 % Phosphoric acid

Solution 2 (Wash Solution)

34 % Methanol

17 % Ammoniumsulfate

2 % Phosphoric acid

Stain

Commassie Brillant Blue -G250

III.3.4.2. SDS-PAGE Molecular Weight Markers

Fermentas #SM0441 is used as a marker in the SDS-PAGE.

Protein (≈0.2mg/ml)	Source	Molecular Wight (kDa)
β- galactosidase	*E. coli*	117
Bovine serum albumin	bovine plasma	84
Ovalbumin	chicken egg white	49
Carbonic anhydrase	bovine erythrocytes	34
β- lactoglobulin	bovine milk	25
Lysozyme	chicken egg white	19

III.3.4.3 Buffers and Solutions Used for Matrix Assisted Laser Desorption/Ionization-Time of Flight Analysis

<u>Trypsin Solution</u>

6 ng/µl trypsin

50 mM Ammonnium Carbonate

<u>Matrix solution</u>

0.5 mg/ml α-cyano-4-hydroxycinnamic acid (CHCA) dissolved in 49.5 % ethanol (or acetonitrile), and 0.1% TFA

III.3.4.4. Buffers Used in Enzyme Activity Measurements

<u>K^+PO_4 Buffer (1M, pH 7.0) (g/L):</u>

1M K_2HPO_4	450 ml
1M KH_2PO_4	550 ml

<u>Preparation of Substrate Solution</u>

25 mg CENTA was dissolved in 1 ml 50 mM K^+PO_4 Buffer and aliquoted and maintained at -20 °C. The concentration of the stock solution was 4.7 mM.

III.3.5 Peptides

Peptide 1: Biotinyl-NH-AAGDYY-COOH	100 mg
Peptide 2: Biotinyl-NH-CETGGSFGDSIHCRGHAAGD-COOH	54.5 mg

The peptides were >50 % purity. Peptide 1 and peptide 2 were dissolved 4 ml and 2.18 ml 50 mM K^+PO_4 Buffer respectively and the 28.2 mM and 11 mM stock solutions respectively were aliquoted and maintained at -20 °C.

III.3.6 Enzyme

E. coli R-TEM-1 (Sigma, P-3553)

III.3.7 Laboratory Equipment

Autoclaves	Systec 3870 ELV Steam Strilizer,Germany Nüve OT 032, Turkiye
Balances (0.1, 1, 10 mg)	Ab204-S, Pg403-S, Pg4002-S, Mettler Toledo, Sweden
Centrifuge	3K30 Sigma, Germany
Deep Freezer (-20 °C)	Hlf585, Heto Holten, Denmark

Deep Freezer (-86 ˚C)	Uf4420, Heto Holten, Denmark
Ice Machine	Arttex Bar Line, Italia
Magnetic Stirrer	MSH 300 BIOSAN
MALDI-TOF	Waters-Micromass,
Microcentrifuge	1-15k, Sigma, Germany
Micropipets	Finnpipet, Finland
No Frost Refigrator	Arçelik, Turkiye
Orbital Shaker	Certomat Bs1, B. Braun, Germany
Safety Thermostat	Nüve FN500, Türkiye
pH Meter	Mp220k, Mettler Toledo, USA
Power Supply	Heidolph MR3001, Germany
SDS-PAGE Electrophoresis System	Mini Protean, BIORAD, Canada
Spectrophotometer	Lambda 35, Perkin Elmer, USA
Safety Cabinet	Labculture ESCO, USA
Vortex	Heidolph, Germany
Water Purification Systems	ELGA LabWater, England

III.4. EXPERIMENTAL METHODS

In all experiments strerilized equipment were used. Glassware, pipetman tips, eppendorf tubes, petri dishes etc. were either bought sterile or were sterilized in an autoclave at 1.02 atm and 121 ˚C for 15 minutes. Glucose was filter sterilized using membranes of 45 µM pore size.

III.4.1. Preparation of Frozen Stocks

A single colony from a master plate was inoculated into LB media and grown overnight at 37 ˚C and 180 rpm. 500 µl from the grown cells were mixed one to one with 50 % sterile glycerol and stored at -80 ˚C.

III.4.2. Preparation of Preculture

Five ml of sterile liquid medium was inoculated from a frozen stock culture kept at -80 ˚C and the cells were grown overnight at 37 ˚C and 180 rpm.

III.4.3. Plasmid Transformation into *E. coli* K12 Cells

$CaCl_2$ protocol was used to transform *E. coli* K12 cells with the pUC18 plasmid. Preculture of *E. coli* K12 cells, was grown overnight in LB broth, was used for inoculation into fresh LB broth at a 1:100 dilution (OD_{600} was kept below 0.05). Cells were grown at 37 ˚C with vigorous shaking in flasks to facilitate aeration. When the cells reached the optical density of 0.6 at 600 nm, they were centrifuged at 3,000 rpm for ten minutes at 4 ˚C in sterile tubes. The supernatant was discarded and the cells were resuspended in 100 µl of sterile, ice-cold 0.1 M $CaCl_2$. The cells were incubated on ice for 30 minutes. The tube was mixed gently every ten minutes to allow a homogenous mixture. 1-2 ng pUC18 was added to the cells. The cells were then incubated on ice for one hour to allow the plasmid DNA to enter the cells. Following a heat shock at 42 ˚C for 60 seconds, the cells were further incubated on ice for ten more minutes. Following the addition of 800 µl of LB broth without any antibiotics, the cells were incubated at 37 ˚C for one hour. The transformed cells were centrifuged at 3000 rpm for one-five minutes and then plated on selective plates containing 100 mg/ml ampicillin. The plates were incubated overnight at 37 ˚C. This protocol is summarized in Figure III.1.

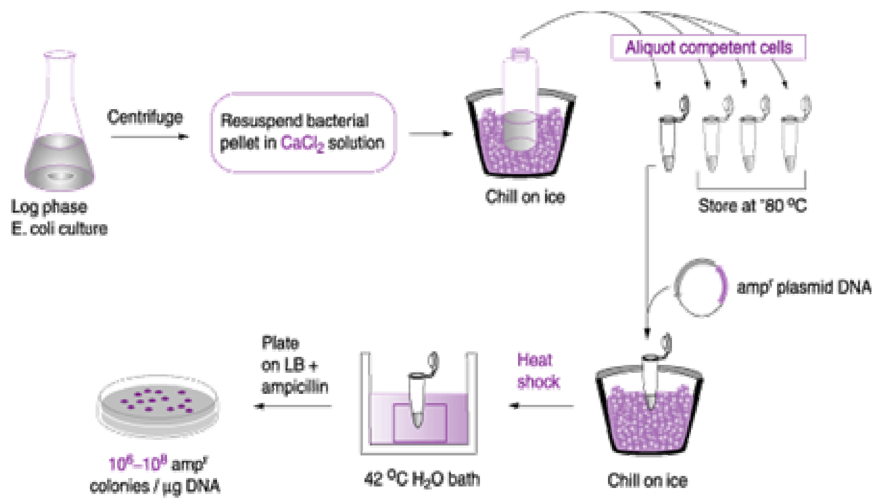

Figure III.1. Representation of plasmid transformation to *E. coli* cells by $CaCl_2$. (http://www.biochem.arizona.edu/classes/bioc471/pages/Lecture4/Lecture4.html)

III.4.4. Monitoring Cell Growth and Determination of Colony Forming Units

Preculture of *E. coli* cells, grown overnight in liquid broth, was used for inoculation into fresh liquid broth at a 1:100 dilution (OD_{600} was kept below 0.05). 0.5-1 ml samples were taken every hour (every half hour during exponential phase) to monitor growth by measuring the optical density at 600 nm.

Bacterial samples were plated to determine the colony forming units. For a ten fold dilution, 100 µl of the bacterial sample taken at each time interval was transferred to a glass tube containing 0.9 ml of fresh liquid medium and was vortexed to get a homogeneous mixture. For another ten-fold dilution 100 µl from this mixture was taken and placed in a new glass tube containing 0.9 ml fresh liquid medium. This process continued until the desired dilution was obtained. 100 µl of the appropriate dilution was spread on LB or M9 Minimal agar plates, in triplate, and incubated overnight at 37 °C.

This procedure is summarized in Figure III.2.

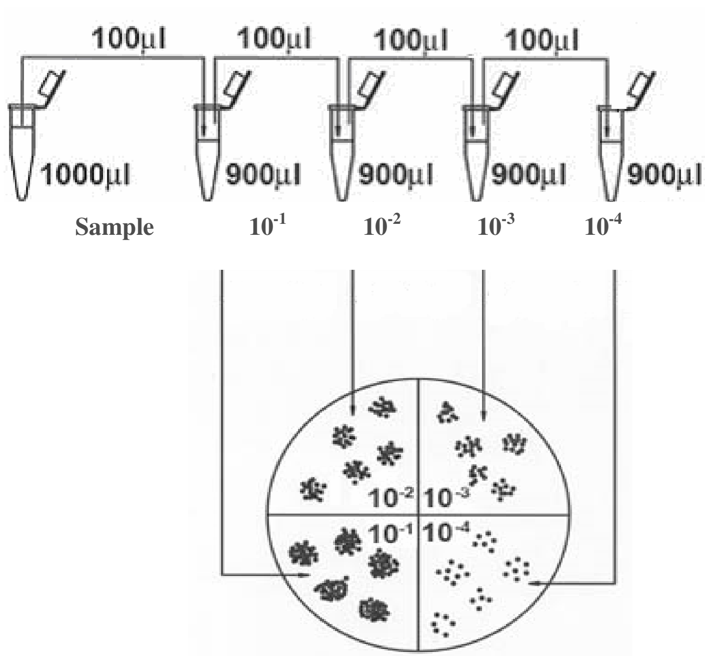

Figure III.2. Dilution of the cells on agar plate.
(http://www.biofilmbook.hypertextbookshop.com/public_version/artifacts/images/labExercises/alternate_method_v3.jpg)

The number of viable cells per culture was then calculated from the number of colonies counted and averaged over triplate plates, after the correction by the dilution factor.

III.4.5. Extraction of Periplamic Proteins

Osmotic shock procedure was used to extract periplasmic proteins from *E. coli* (Nossal et al, 1966). Fresh LB broth inoculated with a preculture at a 1:100 dilution (OD_{600} was kept below 0.05) was incubated at 37 °C and 180 rpm. When the cells reached the optical density of 0.8 at 600 nm, they were centrifuged at 7,000 rpm for ten minutes at 4 $^{\circ}$C. The supernatant was discarded and the cells were resuspended in 20 % sucrose in 30 mM Tris-HCl (pH 8.0) with 1 mM ethylenediaminetetraacetic acid (EDTA). The cells were gently incubated for ten minutes at room temperature. Following centrifugation of cells at 9000 rpm for 20 minutes, the pellet of sucrose-treated cells was rapidly resuspended in ice-cold 5 mM $MgCl_2$ which cause periplasmic proteins to be released. The cells were removed from the periplasmic extract by centrifugation at 9000 rpm for 20 minutes. The supernatant contained periplasmic proteins mixture including R-TEM-1 β-lactamase.

III.4.6. Determination of Protein Concentration

Protein concentration in the periplasmic protein extract was determined using the method described by Bradford (1976). Bovine Serum Albumin (BSA) was used as the standard for the preparation of the calibration curve. For this purpose, bradford samples with different BSA concentrations were prepared and absorbance at 595 nm was measured. The readings were used to relate protein concentration to absorbances using linear regression analysis. The calibration curve obtained is given in Appendix C.

III.4.7. SDS-PAGE Analysis of Periplasmic Proteins

Osmotic shock sample with a protein concentration of 1.95 μg/15 μl was mixed with 15 μl volume of sample buffer and boiled for five minutes for denaturation of the proteins. The sample was then loaded to the SDS polyacrylamide gel. When the electrophoretic separation was finished, the gels were gently removed from the plate and placed into the fixation solution overnight to fix proteins. The following day the gels were washed with solution 2 for an hour. Then the gels were stained with Commassie G-250 at least overnight and destaining solution was used to remove excess unbound stain. Finally the gels were dried. By comparing the protein bands of the samples against the standard, the presence of β-lactamase was verified.

III.4.8. Analysis of the β-Lactamase by Matrix Assisted Laser Desorption/ Ionization, Time Of Flight Mass Spectrometry

Matrix-assisted Laser Desorption/Ionization (MALDI) mass spectrometry was used for the analysis of the probable β-lactamase on the gel. The method was adopted from Shevchenko et al. (2006). Following destain, the SDS polyacrylamide gel was rinsed with water and then the protein band corresponding to β-lactamase on the gel was sliced with a sterile knife. The sliced band was carefully placed into a microcentrifuge tube and then spinned down in a bench-top microcentrifuge. After adding 100 μl of 100 mM ammonium bicarbonate/acetonitrile (1:1,v/v), the tube was incubated with occasional vortexing, until the pieces became white and schrank. Then acetonitrile was removed. Enough trypsin buffer (typically 50 μl or more depending on the volume of gel matrix) was added to cover the dried gel pieces. If after 30 min, all of this buffer was absorbed by the gel pieces, more trypsin buffer was added until the gel pieces were all covered and the gels were saturated with trypsin for another 90 min. 10-20 μl 100 mM ammonium bicarbonate buffer was added to cover the gel pieces and keep them wet during the overnight enzymatic cleavage at 37 °C for maximal peptide recovery. After the tube was chilled to room temperature, the gel pieces were spinned down using a microcentrifuge. 1-1.5 μl aliquots of the supernatant were withdrawn directly from the digest without further extraction. Each sample was mixed with 1 μl of saturated CHCA matrix solution in the tubes, and a droplet of the resulting mixture (1 μl) was placed on a metal MALDI plate. The solvent was vaporized leaving the recrystallized matrix containing the sample (sample and the matrix co-crystallized). A laser was fired at these remaining crystals, the MALDI spots. These resulting ions from the laser energy were then analyzed via the mass spectrometer to obtain spectral data. Using the Swisport 54.7 database, the spectral data was identified as β-lactamase.

III.4.9. *In-vitro* Enzyme Activity Measurement

Osmotic shock fluids from *E. coli* K12 cells harboring plasmid pUC18 were assayed for β-lactamase activity using CENTA as the substrate. All β-lactamase reactions were carried out in a total of 1 ml reaction mixture. 470 μM CENTA was mixed with the pre-determined amount of osmotic shock fluid the hydrolysis of CENTA was immediately monitored by following the change in the absorbance at OD_{405}nm with a spectrophotometer. Osmotic shock fluid from cells not harboring pUC18 was used as the control. For inhibition studies, β-lactamase was incubated with different concentrations of inhibitor peptide (100, 200, 400 μM) at 25 °C for one hour prior to activity analysis.

One Unit (U) of β-lactamase activity was defined as the amount of enzyme which hydrolyzed 1 μmol of substrate per minute at 25 °C and pH 7.0 (Equation III.6).

$$U = \frac{V_t \times d_A/d_t \times 1000 \times DF}{\varepsilon\lambda \times V_s \times d} \qquad \text{(III.6)}$$

V_t = Total reaction volume of (ml)

$\varepsilon\lambda$ = Extinction coefficient of the substrate ($cm^2.mol^{-1}$)

V_s = Volume of enzyme (ml)

d_A/d_t = Absorbance change per time (min^{-1})

DF = Dilution Factor

d = Light path (1 cm)

III.4.10. *In-vivo* β-lactamase Inhibition by Peptides

E. coli K12 cells harboring plasmid pUC18 were grown in M9 Minimal Medium at 37°C. The cells were treated with 25 μg/ml of peptide (A46-Y51 or C30-D49) in early logarithmic phase (OD_{600} nm ~ 0.2). Cell growth was monitored every hour at OD_{600}nm to examine the inhibitory effect of the peptides under these conditions. Bacterial samples grown in the absence of the peptide were also plated on M9 agar plates containing 25 μg/ml peptide for the measurement of colony forming units.

CHAPTER IV

RESULTS and DISCUSSION

IV.1 COMPUTATIONAL RESULTS

In this study, seven different MD simulation trajectories for SHV-1 enzyme in the presence and absence of ligand were calculated. In addition to this, six simulations on the free ligand were calculated to characterize the properties of the ligands in the unbound form. The simulation length was 10 ns for all simulations. The list of simulations is given in Table IV.1.

Table IV.1 Simulation systems examined in this study

RUN	SHV-1	BLIP	PEPTIDE*
1	Wild Type	-	-
2	Wild Type	Wild Type	-
3	Wild Type	D49A	-
4	Wild Type	-	Wild Type
5	Wild Type	-	D49A
6	Wild Type	-	Y50A
7	Wild Type	-	Y51A
8	-	Wild Type	-
9	-	D49A	-
10	-	-	Wild Type
11	-	-	D49A
12	-	-	Y50A
13	-	-	Y51A

* BLIP residues 45 to 52 (NH_2-HAAGDYYA-COOH).

IV.1.1. Root Mean Square Deviations (RMSD) from Initial Structure

RMSD of a conformation from the initial structure was calculated by aligning the Carbon alpha (Cα) backbone on the initial structure of the MD simulation and calculating the deviation of each Cα atom from its initial position as averaged over the same selection of atoms. For example, RMSD profile of SHV-1 in the simulations was determined by first aligning SHV-1 snapshots on the initial SHV-1 conformation and then by calculating the RMSD of the SHV-1 snapshots to the initial structure. RMSD profiles give information about the equilibration period of the simulations and also show the motions of the proteins throughout the simulation.

Apo SHV-1 β-lactamase and average SHV-1 β-lactamase structures were aligned and the average RMSD was calculated as 1.14 Å throughout the simulation (Figure IV.1). There was no important fluctuation in RMSD of apo SHV-1 β-lactamase. The system reached equilibrium after about 2ns.

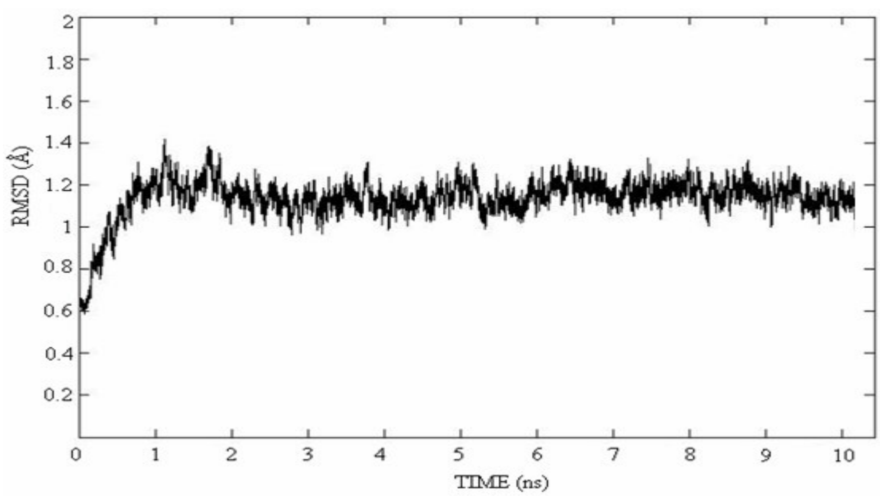

Figure IV.1.RMSD of Apo SHV-1 β-lactamase.

Simulations on free BLIP and free BLIP (D49A) were performed in order to observe their dynamics in the unbound form and for later comparison with the dynamics in the bound form. RMSD profiles of free BLIP (purple) and free BLIP (D49A) (gray) are shown in Figure IV.2. It was observed that both simulation systems reached equilibrium with an average RMSD of 0.89 Å and 0.99 Å respectively.

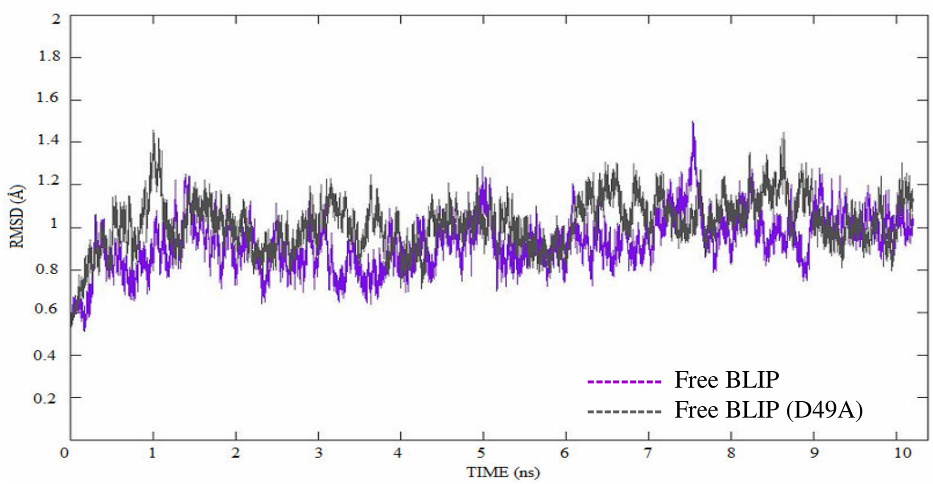

Figure IV.2 RMSD in free BLIP and BLIP (D49A) simulations with respect to the initial structure.

The RMSD profiles for SHV-1 from the SHV-1: BLIP complex and SHV-1: BLIP (D49A) complex simulations (Figure IV.3) showed that equilibrium was reached after about 4 ns. Both MD simulation trajectories exhibit approximately the same average RMSD value and reveal a stable behavior with low amplitude fluctuations during the time course of the simulation.

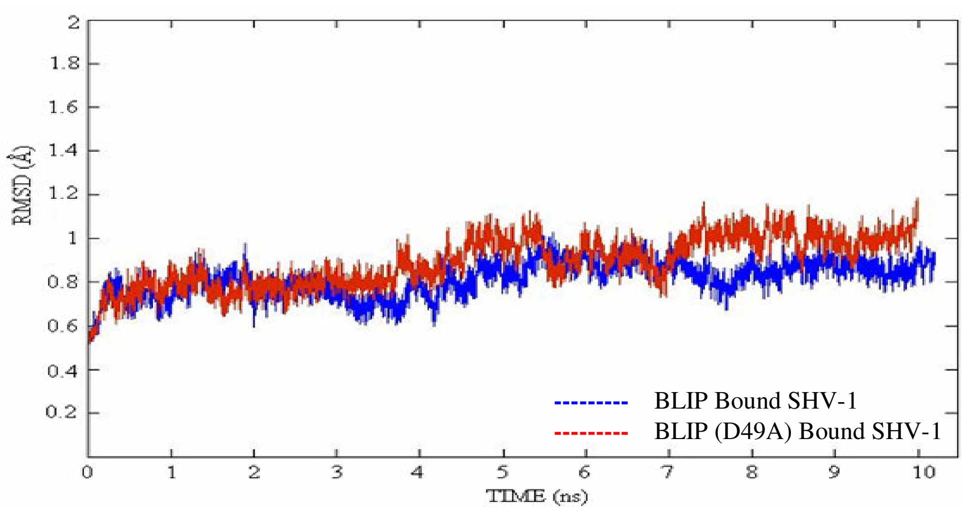

Figure IV.3 The RMSD of SHV-1 β-lactamase in the simulations on the SHV-1:BLIP and SHV-1:BLIP (D49A) complexes.

The RMSD values report changes in the internal structure of the substrate. The purpose of measuring substrate deviations is to elucidate the structural changes in the substrates upon binding. The RMSD values of BLIP and BLIP (D49A) fluctuate around 1 Å in the simulations performed on SHV-1: BLIP structure. The maximum RMSD value observed during the simulations was around 1.2 Å. The RMSD profile exhibited higher fluctuations in the SHV-1: BLIP complex form (Figure IV.4).

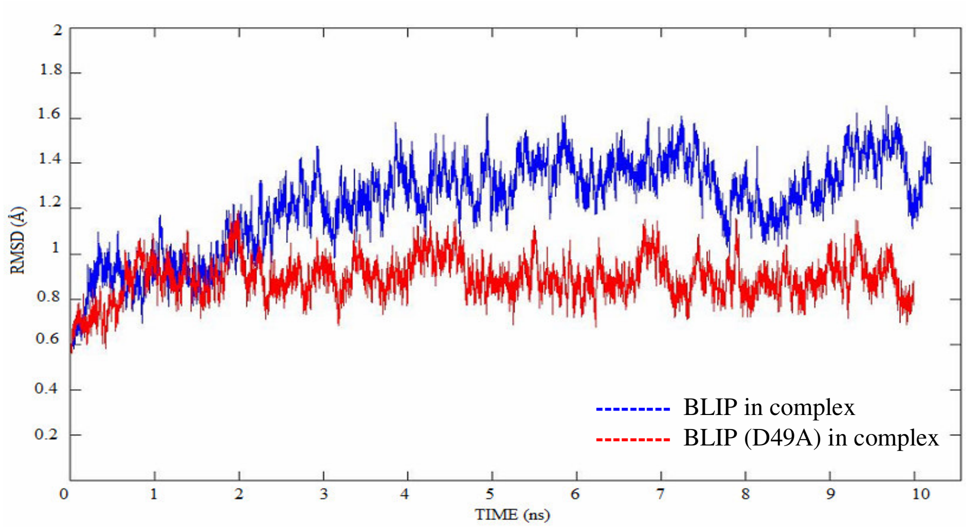

Figure IV.4 The RMSD of BLIP and BLIP (D49A) from the initial structure throughout the simulations on the SHV-1:BLIP and SHV-1:BLIP (D49A) complexes.

SHV-1:peptide simulations were performed using four different peptides based on the BLIP residues 45 to 52 (NH_2-HAAGDYYA-COOH). RMSD vs time profiles for the SHV-1 β-lactamase Cα atoms in the simulations performed on SHV-1: peptide complexes are shown in Figure IV.5. SHV-1 β-lactamase is stable in the SHV-1: wild type peptide complex simulation which is colored pink in all panels. SHV-1 β-lactamase showed low amplitude fluctuations during the simulation when D49A mutation was performed on the peptide (Figure IV.5.A) SHV-1 β-lactamase had a similar fluctuations with respect to the SHV-1: peptide structure when residues Y50 (Figure IV.5.B) and Y51 were mutated to alanine (Figure IV.5.C).

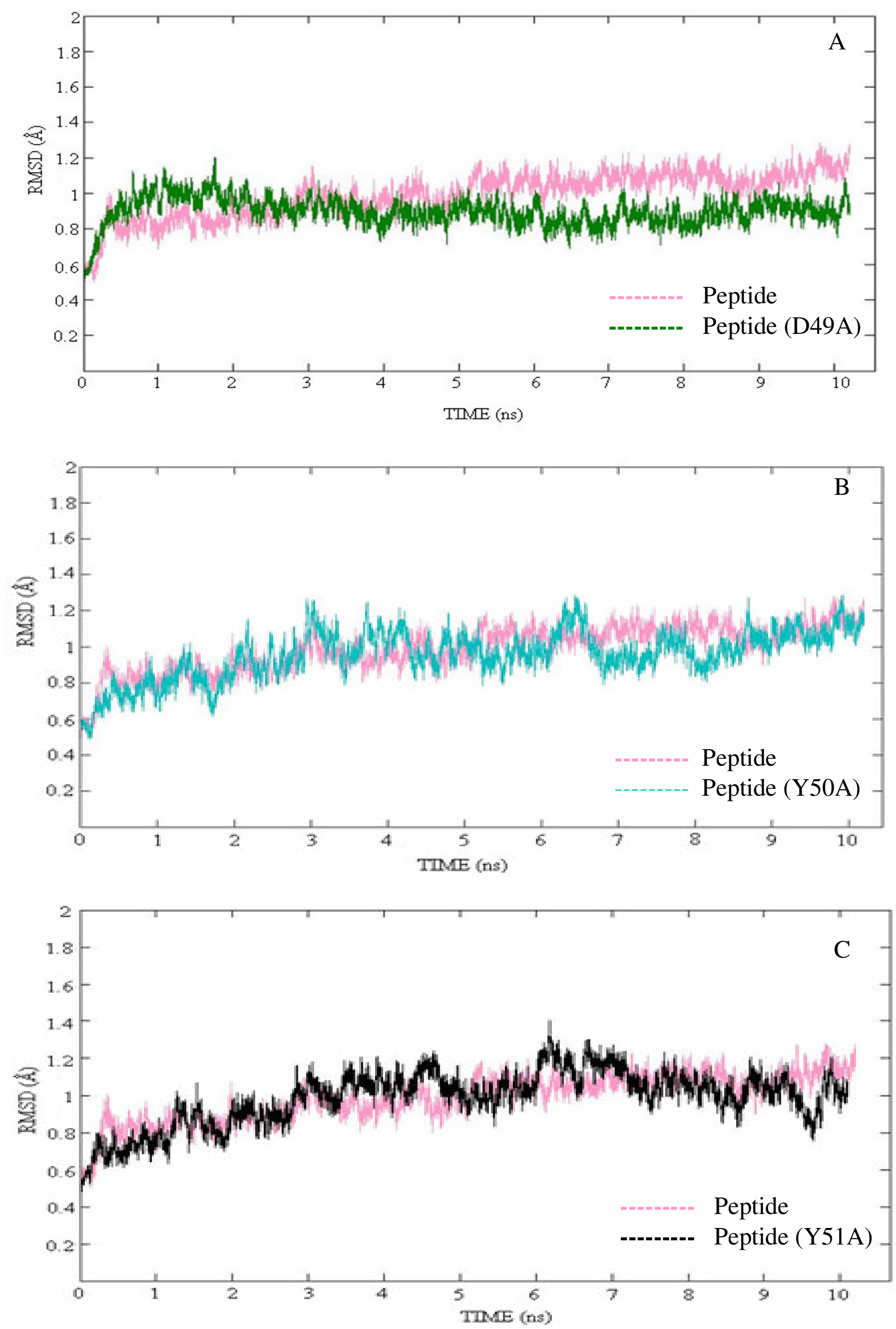

Figure IV.5 RMSD vs time profiles of the Cα atoms of SHV-1 β-lactamase in simulations on SHV-1:peptide complexes.

Internal RMSD vs time profiles of peptides were calculated in the complex simulations of SHV-1 with the peptides. These simulations reached equilibrium in the first 3 ns. However the internal RMSD profiles of peptides Y50A and Y51A exhibited high fluctuations even after 3 ns (Figure IV.6).

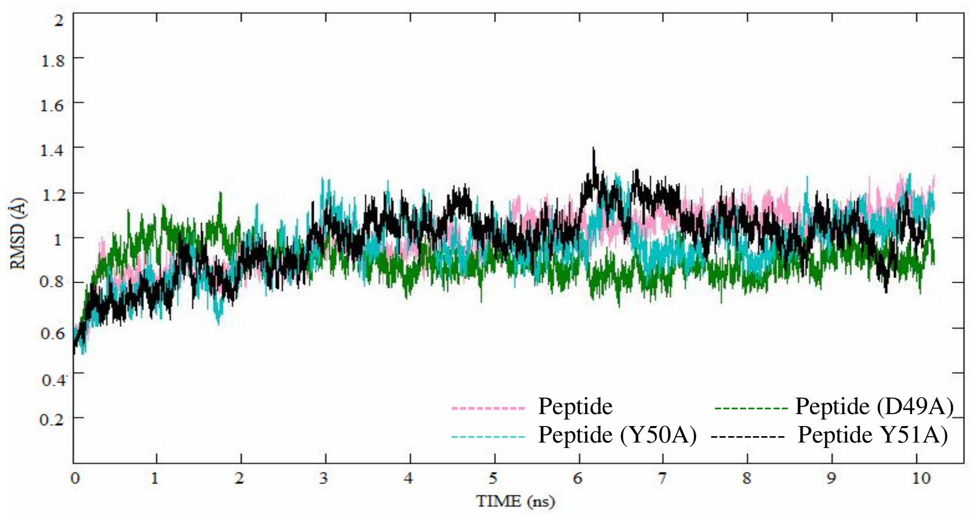

Figure IV.6 RMSD vs time profiles of the peptides with respect to their initial structure.

The average RMSD values obtained for the enzyme and ligand from their initial conformations are given in Table IV.2.

Table IV.2 Average RMSD Values of SHV-1 β-Lactamase and its ligands with respect to the initial conformation.

Simulation	**Average RMSD(Å) for SHV-1**	**Average RMSD(Å) for the Ligand**
SHV-1	1.14	-
SHV-1:BLIP	0.73	0.90
SHV-1:Mutant BLIP (D49A)	0.89	1.23
SHV-1:Peptide	0.99	1.27
SHV-1:Mutant Peptide (D49A)	0.90	0.91
SHV-1:Mutant Peptide (Y50A)	0.95	0.97
SHV-1:Mutant Peptide (Y51A)	0.98	0.99

IV.1.2. Mobility of Structures During MD Simulations

IV.1.2.1. Apo SHV-1 β-Lactamase

The MSF for each residue of SHV-1 β-lactamase was calculated by aligning Cα atoms of structures for the equilibration period. In Figure IV.7, the peaks in the MSF per residue graph represent the mobile regions of the structure. It was observed that residue $G175_{SHV-1}$ (located in the Ω-loop) forming one edge of the active site had the highest mobility. Figure IV.8 shows the free SHV-1 β-lactamase structure colored according to mobility. Red denotes the most rigid regions during the simulation, green shows more mobile regions than red ones and blue indicates the most flexible residues (Figure IV.8.A).

PCA was performed on the simulation trajectories to determine the concerted motions in the protein. The trajectory was projected along the first principal component (PC) obtained from the apo SHV-1 β-lactamase simulation to show the collective motions of the enzyme (Figure IV.8.B).

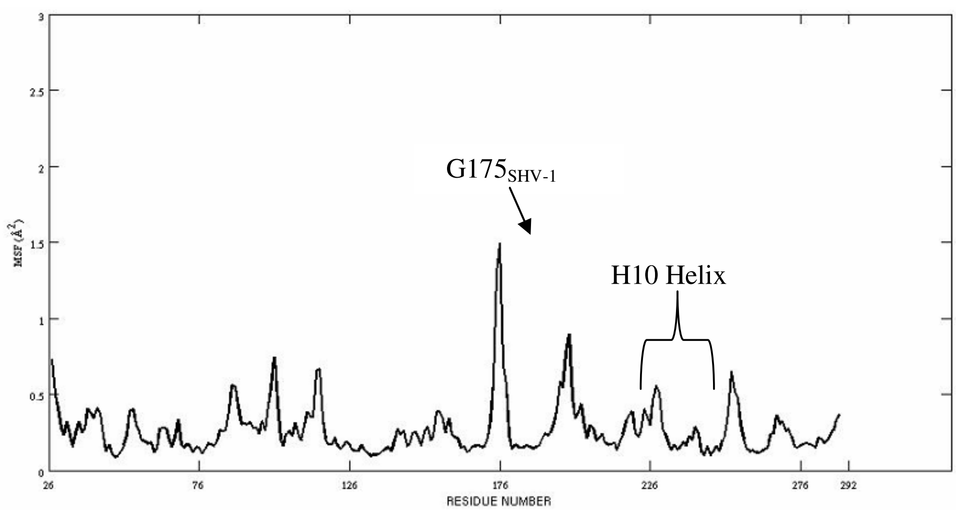

Figure IV.7 MSF of SHV-1 β-lactamase residues during the simulations performed on SHV-1 β-lactamase.

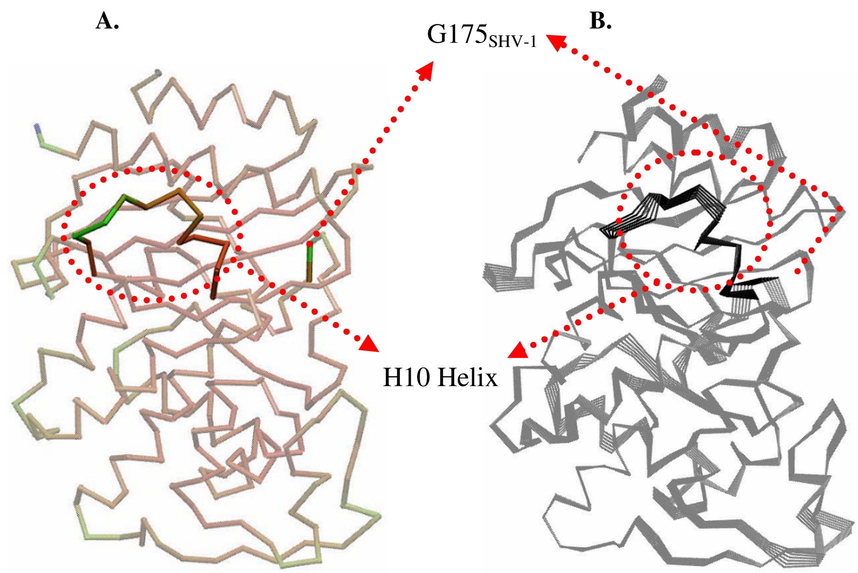

Figure IV.8 A. SHV-1 β-lactamase colored according to the MSF values obtained from apo SHV-1 simulation. **B**. Projections along the first PC of apo SHV-1 simulation.

IV.1.2.2. SHV-1 β-lactamase and BLIP Complexes

Comparison of the residue based MSF plots for the simulations on the SHV-1: BLIP complex with that on the SHV-1: BLIP (D49A) complex showed that residue $G175_{SHV-1}$ mobility maintained. On the other hand, mutation on BLIP caused H10 helix mobility to increase from 0.5 Å^2 to 1.5 Å^2 (Figure IV.9). The residue mobility of SHV-1 in SHV-1:BLIP simulation (Figure IV.10) and SHV-1 in SHV-1:BLIP (D49A) simulation (Figure IV.11) is shown by coloring the residues according to the MSF values (left panels) and by projections along the first principal component (right panels). It was observed that in the BLIP (D49A) bound SHV-1, H10 helix region is more flexible than BLIP bound form.

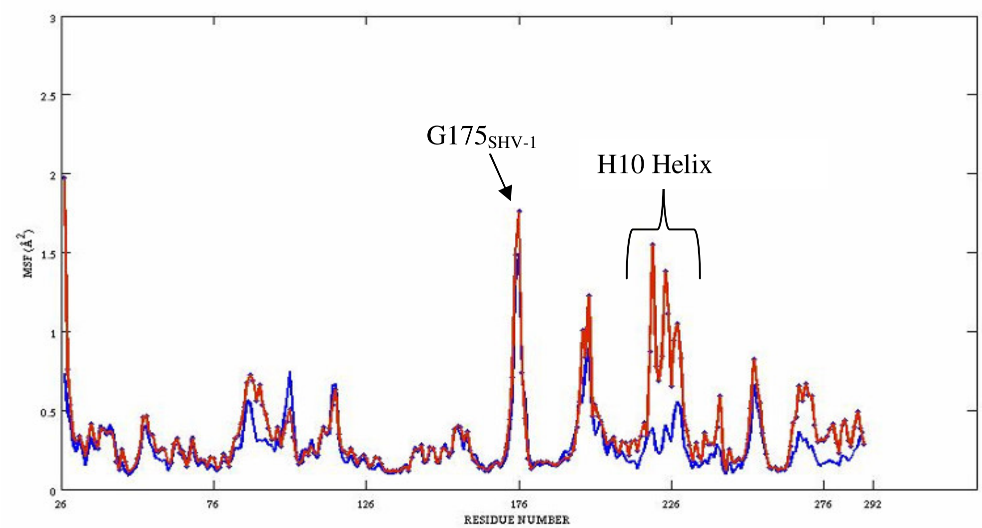

Figure IV.9. Residue based MSF of SHV-1 β-lactamase in SHV-1:BLIP (blue) and SHV-1:BLIP (D49A) (red) simulation.

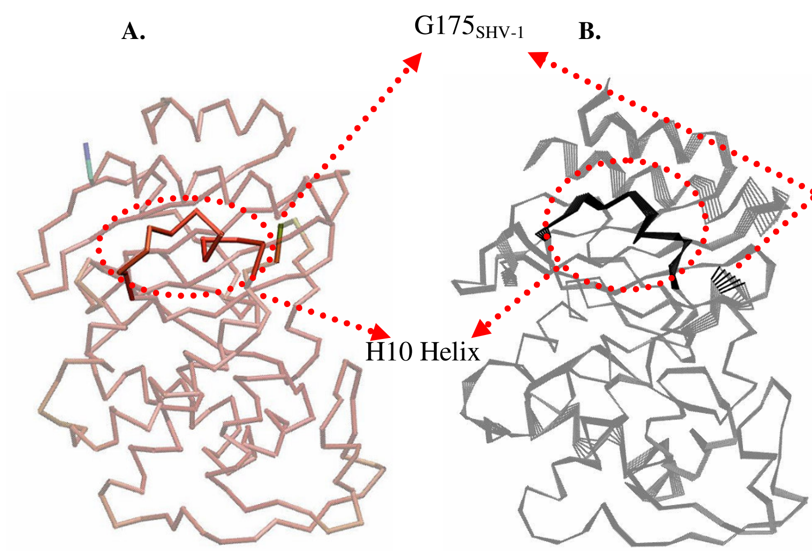

Figure IV.10. A. SHV-1 β-lactamase in SHV-1:BLIP complex structure colored according to the MSF values obtained from SHV-1:BLIP simulation**. B.** Projections along the first PC of SHV-1:BLIP simulation.

A. B.

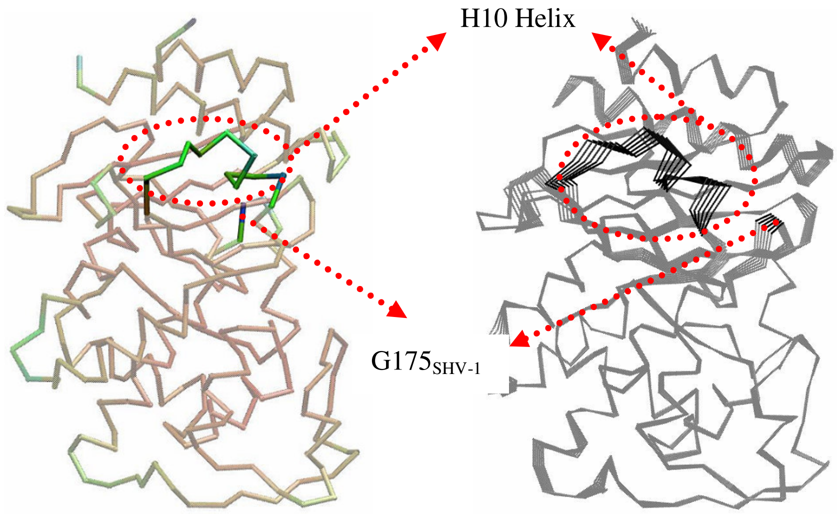

Figure IV.11. A. SHV-1 β-lactamase in SHV-1:BLIP (D49A) complex structure colored according to the MSF values obtained from SHV-1:BLIP simulation**. B.** Projections along the first PC of SHV-1:BLIP (D49A) simulation.

IV.1.2.3. SHV-1 β-lactamase and Peptide Complexes

The residue based MSF plots for the simulations on the SHV-1: peptide complex and for the SHV-1: peptide (D49A) complex are compared in Figure IV.12. The results showed that D49A mutation on the peptide affected the mobility of $G175_{SHV-1}$ the MSF value of which increased approximately from 1.5 $Å^2$ to 2.2 $Å^2$. On the other hand, this mutation decreased the mobility of the H10 helix. This finding is in contrast with the MSF decrease in H10 helix observed upon BLIP D49A mutation. The residue mobility of SHV-1 in SHV-1: wild type peptide simulation (Figure IV.13) and SHV-1 in SHV-1: peptide (D49A) simulation (Figure IV.14) is shown by coloring the residues according to the MSF values (left panels) and by projections along the first principal component (right panels).

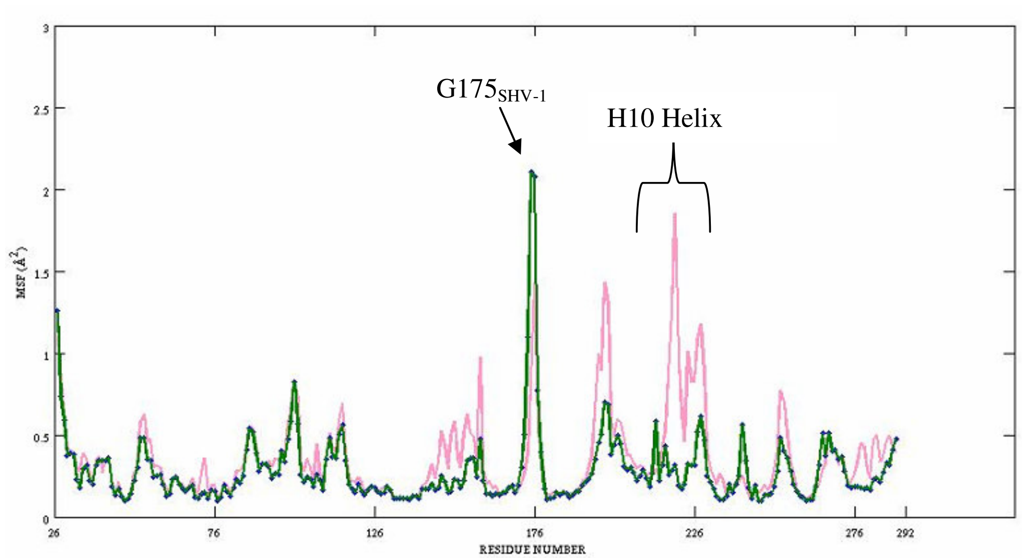

Figure IV.12. Residue based MSF of SHV-1 β-lactamase in SHV-1: peptide (pink) and SHV-1: peptide (D49A) (green) complex simulations.

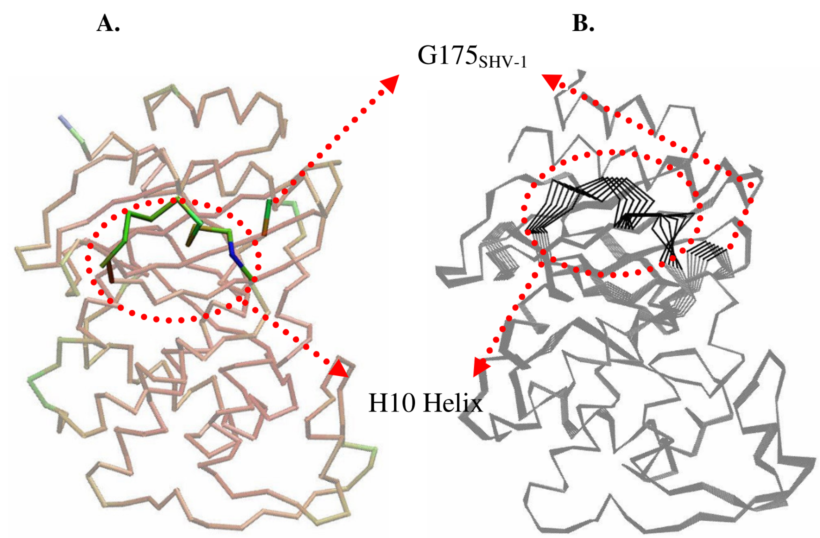

Figure IV.13. A. SHV-1 β-lactamase in SHV-1: peptide complex structure colored according to the MSF values obtained from SHV-1:peptide simulation**. B.** Projections along the first PC of SHV-1:peptide simulation.

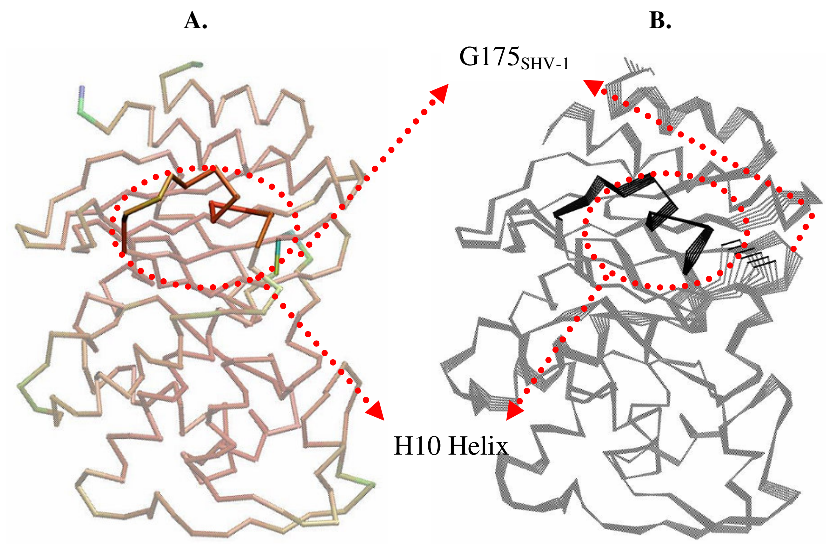

Figure IV.14. A. SHV-1 β-lactamase in SHV-1:peptide (D49A) complex structure colored according to the MSF values obtained from SHV-1:peptide (D49A) simulation**. B.** Projections along the first PC of SHV-1:peptide (D49A) simulation.

When $Y50_{peptide}$ was mutated to alanine, the MSF value of $G175_{SHV\text{-}1}$ resembled that the wild type peptide bound form. Besides, it was observed that in peptide (Y50A) bound SHV-1, H10 helix region is less mobile than the peptide bound SHV-1 (Figure IV.15). However, the mobility of H10 helix increased with respect to peptide (D49A) bound complex. The residue mobility of SHV-1 in SHV-1: peptide (Y50A) simulation (Figure IV.16) is shown by coloring the residues according to the MSF values (left panels) and by projections along the first principal component (right panels).

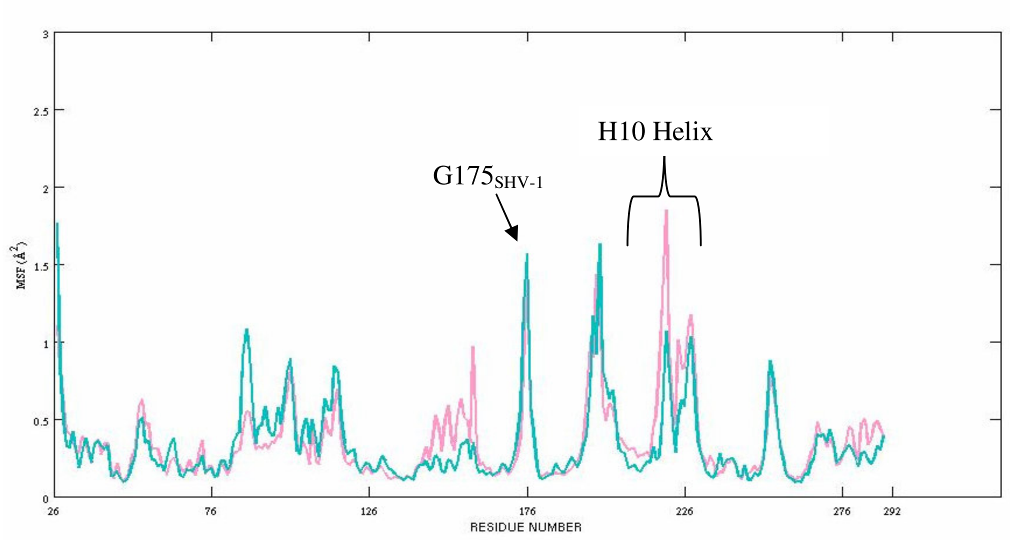

Figure IV.15 Residue based MSF of SHV-1 β-lactamase in SHV-1:peptide (pink) and SHV-1:peptide (Y50A) (cyan) complex simulations.

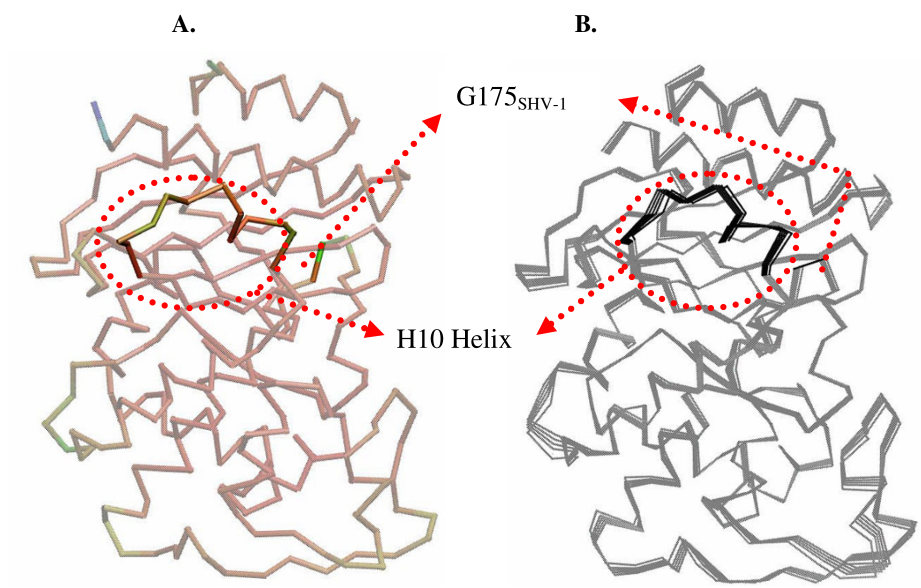

Figure IV.16. A. SHV-1 β-lactamase in SHV-1:peptide (Y50A) complex structure colored according to the MSF values obtained from SHV-1: peptide (Y50A) simulation. **B.** Projections along the first PC of SHV-1: peptide (Y50A) simulation.

When $Y51_{peptide}$ was mutated to alanine, $G175_{SHV\text{-}1}$ and H10 helix on SHV-1 behaved similar to the other mutant peptide bound forms. There was a slight change in the mobility of $G175_{SHV\text{-}1}$ between the wild type peptide and peptide (Y51A) bound forms. In addition to this, the mobility of the H10 helix region of SHV-1 decreased in the mutant bound form (Figure IV.17). The residue mobility of SHV-1 in SHV-1:peptide (Y51A) simulation (Figure IV.18) is shown by coloring the residues according to the MSF values (left panels) and by projections along the first principal component (right panels).

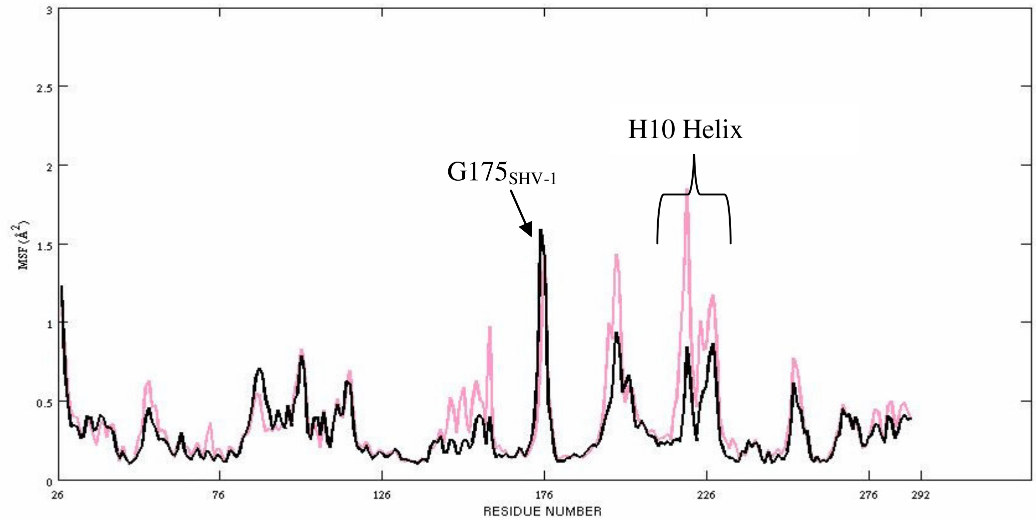

Figure IV.17. MSF of SHV-1 β-lactamase in SHV-1: peptide (pink) and SHV-1:peptide (Y51A) (black) complex simulations.

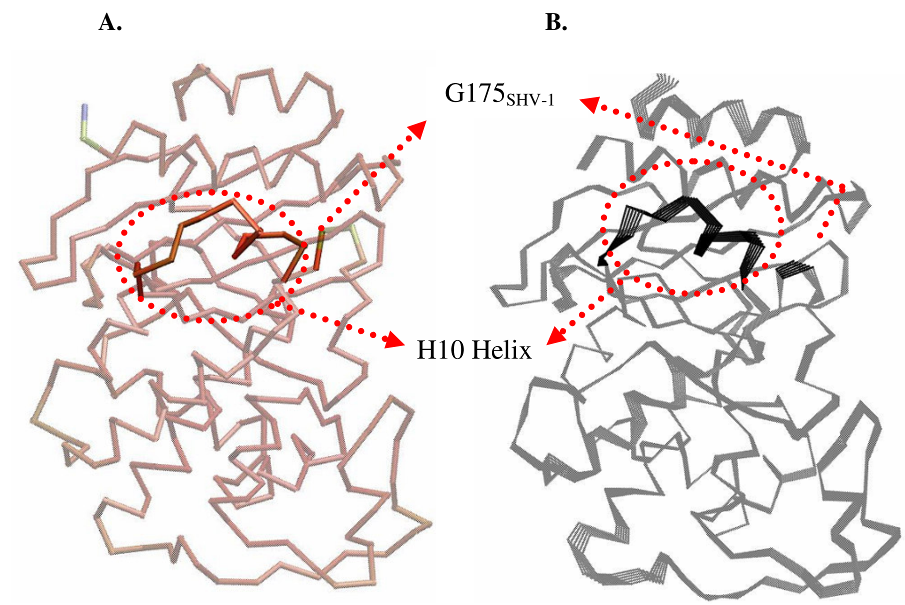

Figure IV.18. A. SHV-1 β-lactamase in SHV-1:peptide (Y51A) complex structure colored according to the MSF values obtained from SHV-1:peptide (Y51A) simulation. **B.** Projections along the first PC of of SHV-1: peptide (Y51A) simulation.

IV.1.3. Active-Site Residue Interactions

In this section the distances between active site residues (S70, K73, S130, E166, N170 and K234) were examined. Residue distances were calculated using the terminal heavy atom on the side chains. Distance trajectories in between active site residues are given in Appendix B. Final snapshots of the 10 ns simulations were taken as representative structures in all structure figures.

Molecular modeling studies have suggested that S70-OG group can attack the β-lactam carbonyl carbon (Lamotte-Brasseur et al., 1991). In addition to this, Imtiaz et al., (1993) suggested that the carboxylate moiety in β-lactam molecules interacts with the side chains of K234 of class A β-lactamases. Because of the importance of these two residues, the distance between OG atom of S70 and the NZ atom of K234 was examined during the simulations on apo SHV-1, BLIP and peptide bound SHV-1 β-lactamases. Representative snapshots of the two residues from the simulations on apo SHV-1 (yellow), BLIP bound SHV-1 (blue) and BLIP (D49A) bound SHV-1 (red) are shown (Figure IV.19). While the distance between S70 and K234 was maintained in BLIP bound form; however when $D49_{BLIP}$ was mutated to alanine, the distance increased approximately 1.20 Å relative to apo SHV-1 β-lactamase.

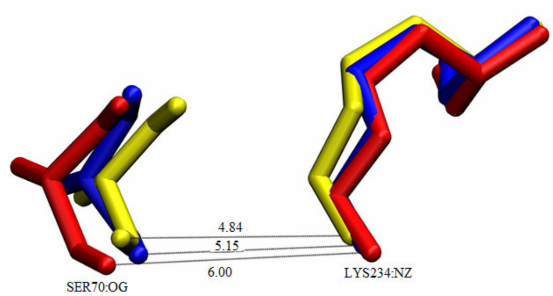

Figure IV.19 Distance between $S70_{SHV\text{-}1}$ and $K234_{SHV\text{-}1}$ in the simulations on apo SHV-1 β-lactamase (yellow), SHV-1 in SHV-1:BLIP complex structure (blue) and SHV-1:BLIP (D49A) structure (red).

The distance of active site residues S70-OG and K234-NZ were compared for the simulations on apo SHV-1 and SHV-1 complexes with peptide or mutant peptides (Figure IV.20). SHV-1 from the simulations of SHV-1 complexes with wild type peptide is colored pink in all panels. SHV-1 in SHV-1: peptide (D49A) simulation is shown in green. Cyan denotes SHV-1 in SHV-1: peptide (Y50A) simulation and SHV-1 in SHV-1: peptide (Y51A) simulation is colored in black. When wild type peptide was bound to SHV-1, this interaction increased by about 1 Å with respect to apo SHV-1. This interaction decreased by about 1Å in the peptide (D49A) bound SHV-1 (Figure IV.20.A). In the peptide (Y50A) bound SHV-1 these two significant residues move away by about 1.65Å from each other compared to apo SHV-1 (Figure IV.20.B). The S70-OG and K234-NZ distance is maintained in simulations on the peptide (Y51A) bound SHV-1 with respect to apo SHV-1 (Figure IV.20.C).

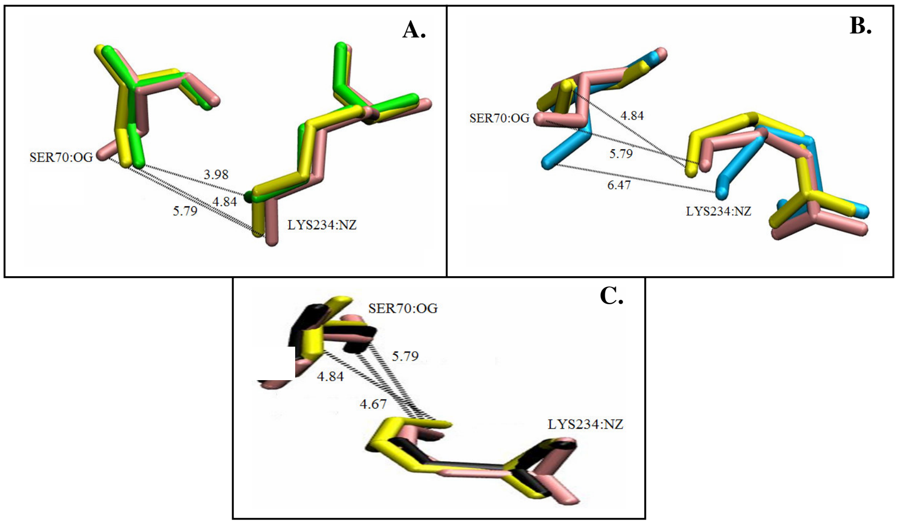

Figure IV.20. Distance between $S70_{SHV-1}$ and $K234_{SHV-1}$ in the simulations on apo SHV-1 β-lactamase (yellow) and peptide bound SHV-1 (pink) **A.** peptide (D49A) bound (green), **B.** peptide (Y50A) bound (cyan) and **C.** Y51A peptide bound SHV-1 (black).

The active site residues E166 and S130 are conserved in class A β-lactamases. E166 is located in the Ω-loop. Site directed mutagenesis experiments suggested that E166 might play the role of general base in the acylation reaction (Gibson et al., 1990 and Lamotte-Brasseur et al., 1991). The hydroxyl group of S130 has a role in substrate binding and catalysis and in TEM-1 and SHV-1, mutations of S130 confer resistance to inactivation by the β-lactamase inhibitors such as clavulanic acid (Helfand et al., 2003). The distance between E166-CD and S130-OG was measured for the simulations on the apo SHV-1 (yellow), on the SHV-1 in the BLIP (blue) and on the BLIP (D49A) bound (red) forms (Figure IV.21). The distance between E166 and S130 was 7.92Å in the apo SHV-1 β-lactamase. When BLIP was bound to SHV-1, these residues moved slightly away from each other to 0.6 Å. This distance and the orientation of E166 and S130 were maintained in BLIP bound or BLIP (D49A) bound complex simulations.

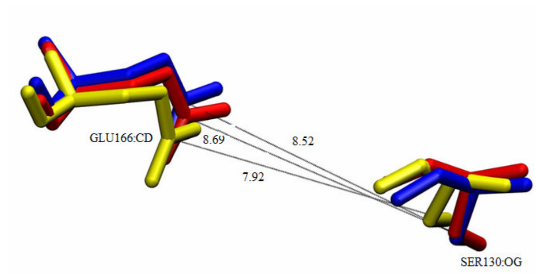

Figure IV.21 The distance between E166 and S130 for the simulations on the apo SHV-1 (yellow), BLIP bound SHV-1 (blue) and BLIP (D49A) bound SHV-1 (red).

The important active site residues S130 and K234 interactions were measured in the apo and peptide and mutant peptides bound SHV-1 (Figure IV.22). The distance between S130-OG and K234-NZ is 2.87 Å in apo SHV-1(yellow). There were little changes in the peptide bound (pink), peptide (D49A) bound (green) and peptide (Y51A) bound (black) SHV-1. However, in the Y50A peptide bound SHV-1, this two residues moved away from each other by 2.43Å compared to apo SHV-1. Therefore, Y50 of peptide may play a significant role on the distance between S130 and K234 of SHV-1.

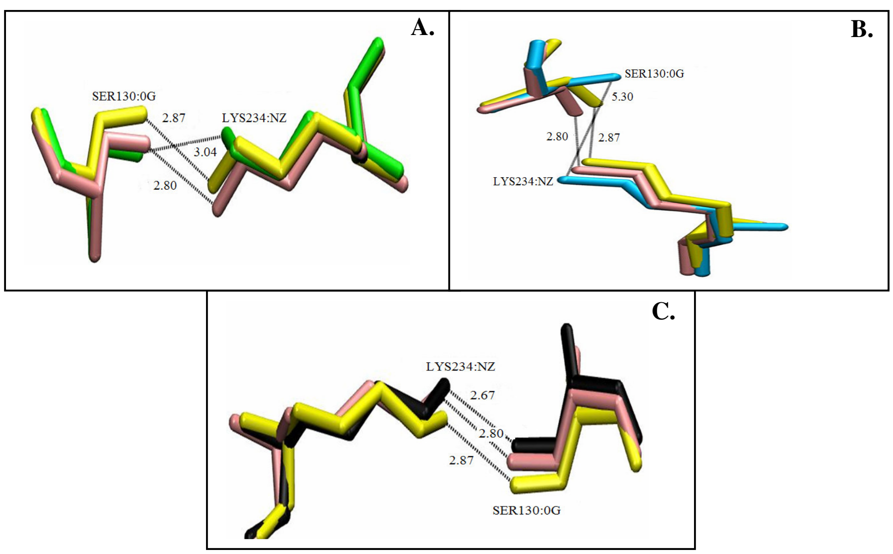

Figure IV.22. The distance between S130 and K234 of SHV-1 in the simulations on apo SHV-1 (yellow in all panels), peptide bound (pink, in all panels), **A.** peptide (D49A) bound (green), **B.** peptide (Y50A) bound (cyan) and **C.** peptide (Y51A) bound SHV-1 (black).

IV.1.4. Effect of Mutations on BLIP and Peptide on SHV-1 Structure and Binding

Examining the SHV-1: BLIP structure shows that there are 5 residues and 2 regions on SHV-1 within 5Å of BLIP. These SHV-1 residues include S70, M129, S130, T167, N170 and residues 99 to 111 loop and residues 235 to 241 region (Figure IV.23).

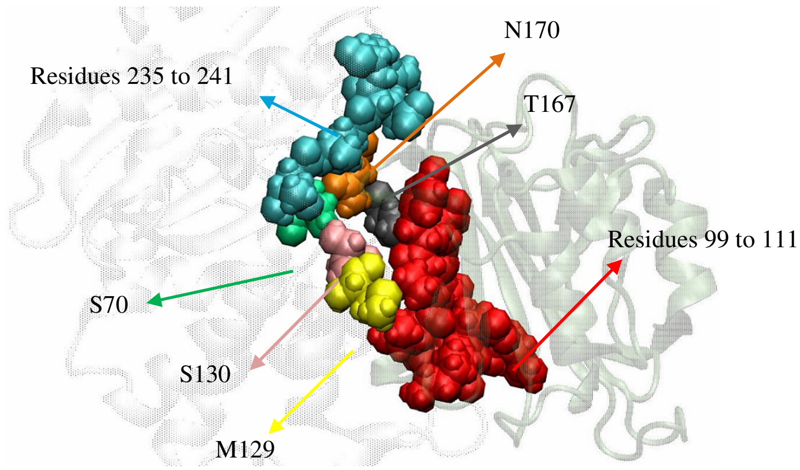

Figure IV.23 Residues of SHV-1 β-lactamase (red) within 5Å of BLIP (green) in the SHV-1:BLIP complex simulation.

In this section, residue-residue distances were measured in all structures by aligning the active site residues of both SHV-1 structures.

Inhibitors that interact with the active site cavity near the 99 to 114 loop of β-lactamase blocks substrate binding (Petrosino et al., 1996). $Y105_{SHV-1}$, which is on this loop, delineates one of the edges of the active site cavity and plays a significant role in substrate binding and/or stabilization (Doucet et al., 2004; Doucet et al., 2007). Tyr 105 does not change its orientation in any of the apo or ligand bound simulations. When the D49 residue was mutated to alanine on BLIP, the distance between residue 49_{BLIP} and $Y105_{SHV-1}$ changed. Figure IV.24 shows the distance between D49-CA or A49-CA and Y105-CZ. Active site residues were aligned on both structure and the distance between CA atom of $D49_{BLIP}$ and CZ atom of $Y105_{SHV-1}$ was measured at 5.78 Å in the simulations on SHV-1: BLIP complex (blue). Residue 49_{BLIP} moved 0.5 Å toward $Y105_{SHV-1}$ in the BLIP (D49A) bound SHV-1 (red) simulations.

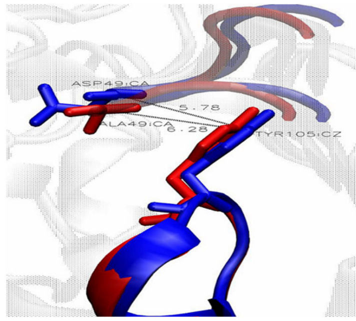

Figure IV.24. Effect of D49A Mutation on residue Y105 of SHV-1 β-lactamase. Snapshot from the simulation on SHV- 1:BLIP complex (blue) and snapshot from the simulation on SHV-1:BLIP (D49A) complex (red).

The distance between CA atom of residue 49_{BLIP} and CZ atom of $Y105_{SHV-1}$ was measured in SHV-1: peptide (pink), SHV-1: peptide (D49A) (green), SHV-1: peptide (Y50A) (cyan) and SHV-1: peptide (Y51A) (black) simulations. (Figure IV.25). D49A mutation on peptide had a little effect on the interaction between these residues with respect to wild type peptide bound SHV-1. However, Y50A mutation on peptide caused 49_{BLIP} to move toward 1 Å $Y105_{SHV-1}$ relative to SHV-1:peptide structure (Figure IV.25.A and B). On the other hand, 49_{BLIP} moved away from $Y105_{SHV-1}$ by 2Å in SHV-1:peptide (Y51A) simulations (Figure IV.25.C) compared to wild type peptide bound SHV-1.

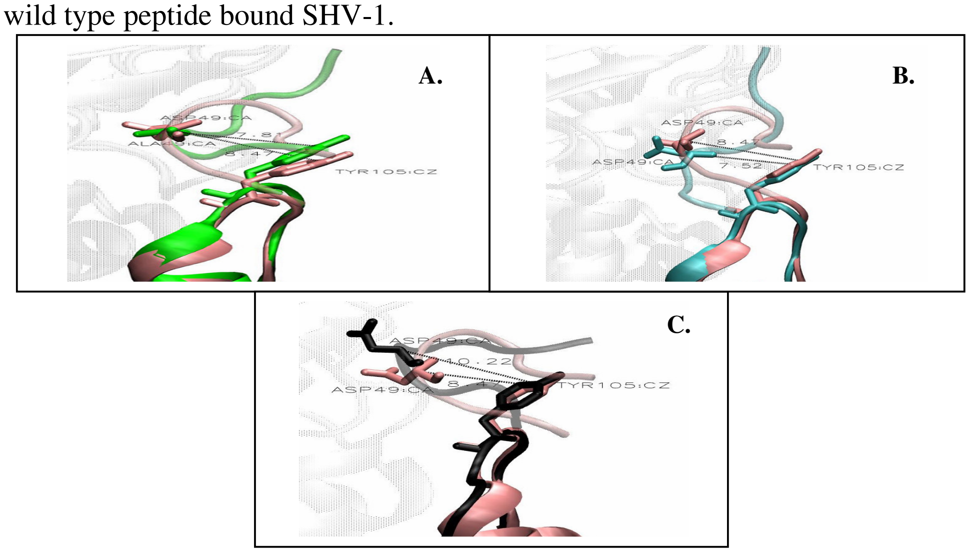

Figure IV.25. Interactions between residue 49_{BLIP} and $Y105_{SHV-1}$ in the simulations on SHV-1: peptide (pink) **A.** SHV-1: peptide (D49A) (green), **B.** SHV-1:peptide (Y50A) (cyan) and **C.** SHV-1: peptide (Y51A) (black).

Reynolds et al. (2006) have shown that $D104_{SHV-1}$ plays a key role in mediating BLIP affinity and has a hydrogen bond with $N132_{SHV-1}$ which may influence the positioning of the 130-132 loop (Petit et al., 1995). The distance between the CG atom of $D104_{SHV-1}$ and ND2 atom of $N132_{SHV-1}$ was measured (Figure IV.26). The distance between $D104_{SHV-1}$ and N132 was around 7Å for the simulation on the SHV-1:BLIP complex (blue). In the simulation on SHV-1:BLIP (D49A) (red) $D104_{SHV-1}$ moved toward $N132_{SHV-1}$ by about 1.67Å in the simulation on BLIP (D49A) bound SHV-1 (red).

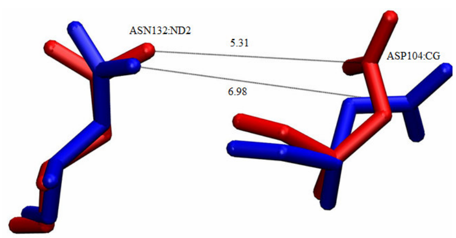

Figure IV.26 The interaction between D104 and N132 of SHV-1 β-lactamase in the BLIP bound SHV-1 (blue) and BLIP (D49A) bound SHV-1 (red) complex simulations.

The distance between CG atom of $D104_{SHV-1}$ and ND2 atom of $N132_{SHV-1}$ was also calculated in the peptide bound simulations. $D104_{SHV-1}$ maintained its conformation and contacts in the SHV-1: peptide (pink in all panels), SHV-1:peptide (D49A) (green) (Figure IV.27.A), SHV-1:peptide (Y50A) (cyan) (Figure IV.27.B) and SHV-1: peptide (Y51A) (black) (Figure IV.27.C) simulations.

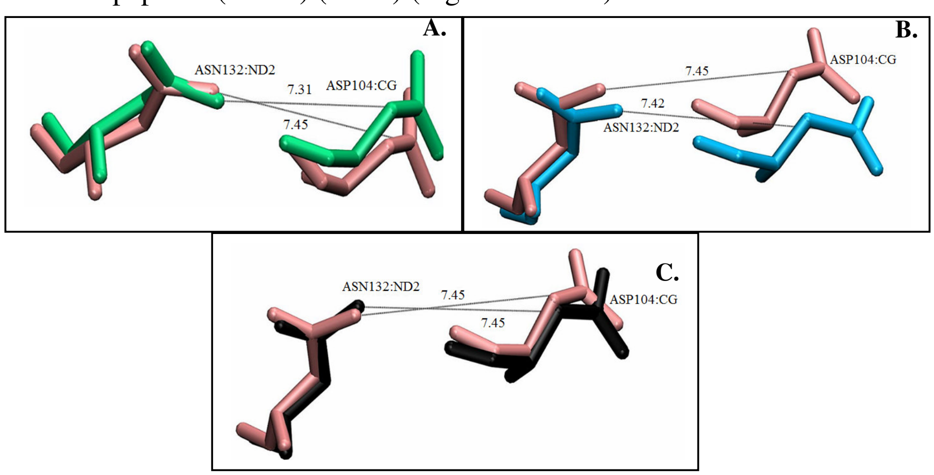

Figure IV.27. Interaction between residues $D104_{SHV-1}$ and $N132_{SHV-1}$ in the simulations on SHV-1: peptide (pink) **A.** SHV-1: peptide (D49A) (green), **B.** SHV-1:peptide (Y50A) (cyan) and **C.** SHV-1: peptide (Y51A).

The crystal structure of BLIP with SHV-1 β-lactamase showed that $D49_{BLIP}$ forms two salt bridges with $R244_{SHV-1}$ and $K234_{SHV-1}$, as well as making two hydrogen bonds with $S130_{SHV-1}$ and $T235_{SHV-1}$ (Reynolds et al., 2006). Representative snapshots from the simulations on SHV-1:BLIP (blue) and SHV-1:BLIP (D49A) (red) were aligned with respect to active site residues and residue 49_{BLIP} and the four critical SHV-1 residue interactions are shown in Figure IV.28. It was observed that the orientation and the distance between residue 49_{BLIP} and R244 (Figure IV.28.A), K234 (IV.26.B), T235 (Figure IV.28.C) and S130 (Figure IV.28.D) were maintained in the BLIP bound or BLIP (D49A) bound SHV-1 structures.

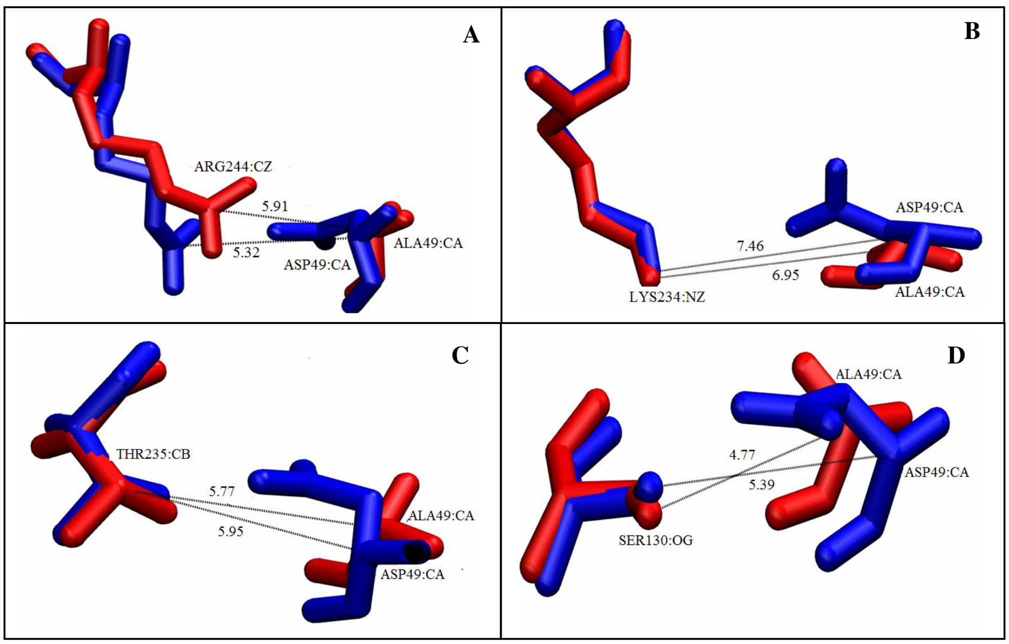

Figure IV.28 The interaction between residue 49_{BLIP} and the four critical residues of SHV-1 in the SHV-1:BLIP (blue) and SHV-1 in SHV-1:BLIP (D49A) (red) complex simulations.

The distance between CA atom of residue 49_{BLIP} and CZ atom of $R244_{SHV-1}$ was measured in the simulations on the SHV-1 bound to the peptides (Figure IV.29). When peptide (D49A) was bound to SHV-1 (green), residue $49_{peptide}$ moved toward 1.20Å to $R244_{SHV-1}$ relative to wild type peptide bound SHV-1 (Figure IV.29.A). On the other hand, Y50A (cyan) mutation on peptide caused the break down of the salt bridge between residue $49_{peptide}$ and $R244_{SHV-1}$ (Figure IV.29. B). However, Y51A (black) mutation on peptide had a little effect on the distance between residue 49_{BLIP}

and residue R244$_{SHV-1}$ with respect to the SHV-1: peptide (pink in all panels) structure (Figure IV.29. C).

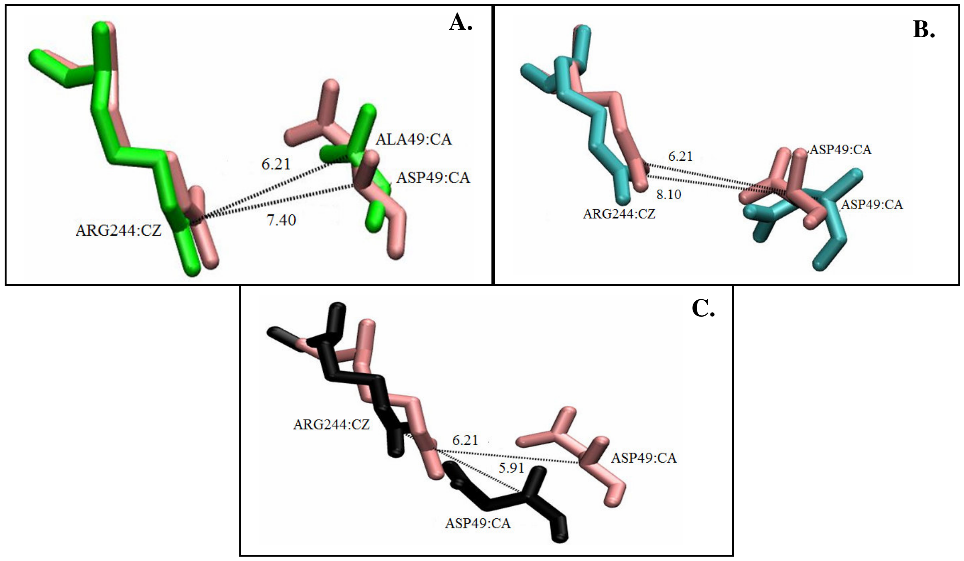

Figure IV.29. Interactions between residue 49$_{BLIP}$ and R244$_{SHV-1}$ in the simulations on SHV-1: peptide (pink) **A.** SHV-1: peptide (D49A), **B.** SHV-1:peptide (Y50A) (cyan) and **C.** SHV-1: peptide (Y51A) (black).

The distance between CA atoms of residue 49$_{BLIP}$ and NZ atom of K234$_{SHV-1}$ was measured in SHV-1: peptide (pink in all panels) and SHV-1: mutant peptides (D49A is green, Y50A is cyan and Y51A is black). Comparison of SHV: peptide and SHV-1: mutant peptides structures showed that D49A mutation on peptide caused residue 49$_{BLIP}$ to move toward approximately 1.00Å to K234$_{SHV-1}$ relative to SHV-1:peptide structure (Figure IV.30.A). However, Y50A mutation on peptide had no effect on the interactions between these residues (Figure IV.30.B). Y51A mutation on peptide caused residue 49$_{BLIP}$ to move about 1.00 Å from K234$_{SHV-1}$ compared to peptide bound SHV-1 (Figure IV.30.C).

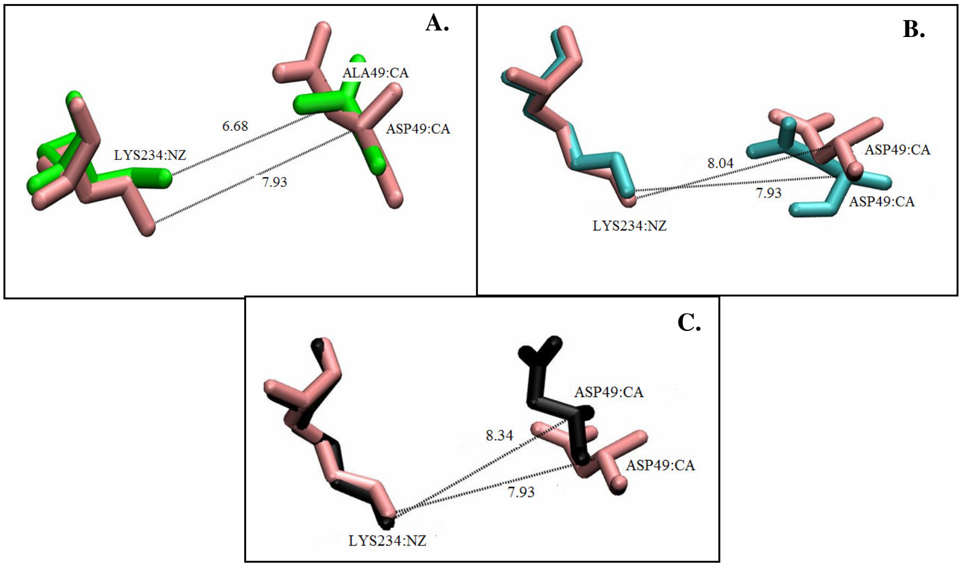

Figure IV.30. Interactions between residue 49_{BLIP} and $K234_{SHV-1}$ in the simulations on SHV-1:peptide (pink) **A.** SHV-1:peptide (D49A) (green), **B.** SHV-1:peptide (Y50A) (cyan) and SHV-1:peptide (Y51A) (black).

The distance between CA atoms of residue 49_{BLIP} and CB atom of $T235_{SHV-1}$ was measured in Figure IV.28. SHV-1: peptide is colored pink in all panels, SHV-1: peptide (D49A) is green (Figure IV.31.A), SHV-1: peptide (Y50A) is cyan (Figure IV.31.B) and SHV-1: peptide (Y51A) is shown in black (Figure IV.31.C). D49A mutation on peptide caused residue 49_{BLIP} moved away approximately 1 Å from $T235_{SHV-1}$. Y50A mutation on peptide had no effect on the interactions between 49_{BLIP} and $T235_{SHV-1}$. Y51A mutation on peptide caused residue 49_{BLIP} moves toward by about 1.00 Å to $T235_{SHV-1.}$

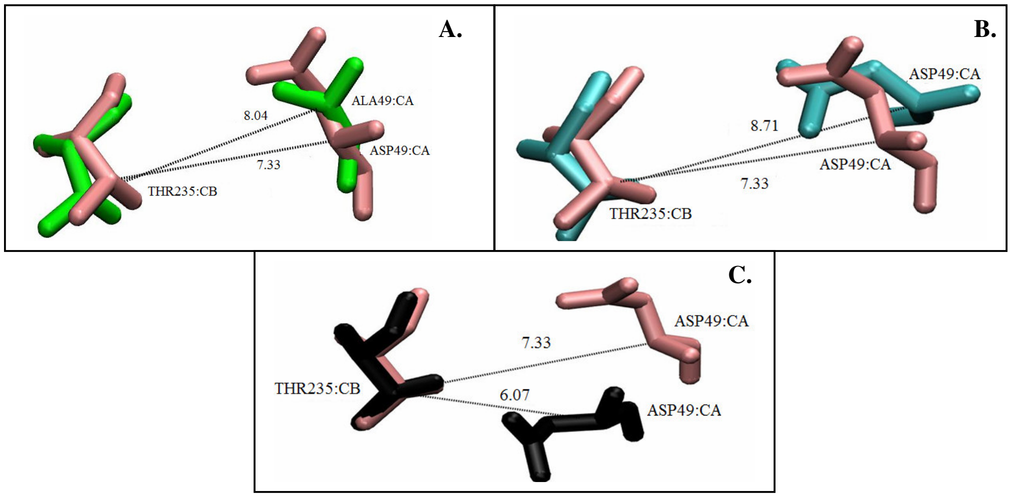

Figure IV.31. Interactions between residue 49_{BLIP} and $T235_{SHV-1}$ in the simulations on SHV-1: peptide (pink) **A.** SHV-1: peptide (D49A) (green), **B.** SHV-1:peptide (Y50A) (cyan) and **C.** SHV-1: peptide (Y51A) (black).

Residue 49_{BLIP} forms hydrogen bond with $S130_{SHV-1}$, a catalytic site residue. The distance between CA atoms of residue 49_{BLIP} and OG atom of $S130_{SHV-1}$ was measured in Figure IV.32. SHV-1:peptide is colored pink in all panels, SHV-1: peptide (D49A) is shown green (Figure IV.32.A), SHV-1:peptide (Y50A) is cyan (Figure IV.32.B) and SHV-1:peptide (Y51A) is colored black (Figure IV.32.C). It was observed that D49A mutation had a little effect on these interaction compared to SHV-1:peptide structure. On the other hand, Y50A mutation on peptide caused residue 49_{BLIP} moved toward by about 0.40Å to $S130_{SHV-1}$ relative to peptide bound SHV-1. However, Y51A mutation on peptide affected that 49_{BLIP} moved away approximately 2.00 Å from $S130_{SHV-1}$ with respect to peptide bound SHV-1.

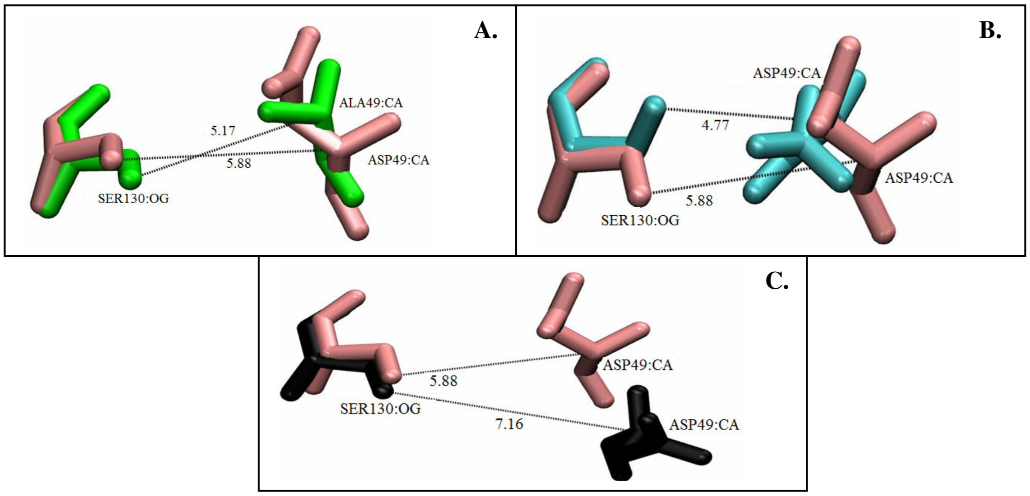

Figure IV.32 Interactions between residue 49_{BLIP} and $S130_{SHV-1}$ in the simulations on SHV-1: Peptide structure is pink in all panels. **A.** the SHV-1: peptide (D49A) (green) **B.** SHV-1: peptide (Y50A) (cyan) and **C.** SHV-1: peptide (Y51A) (black).

In the SHV-1: BLIP complex, there was a strong salt bridge between residues $K234_{SHV-1}$, $D214_{SHV-1}$ and $R222_{SHV}$ which may affect the mobility of H10 helix of SHV-1. When $D49_{BLIP}$ was mutated to alanine, salt bridge between $D214_{SHV-1}$ and $R222_{SHV-1}$ was broken (Figure IV.33). This finding may be one of the reason of H10 helix mobility.

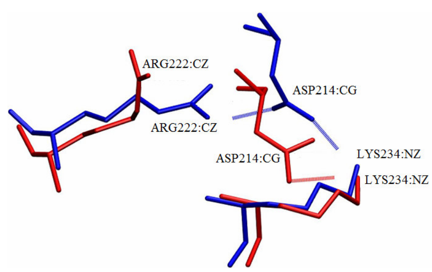

Figure IV.33 The salt bridge between $D214_{SHV-1}$ and $R222_{SHV-1}$ of the H10 Helix is maintained in simulations on SHV-1:BLIP complex (blue) which this salt bridge is broken in the SHV-1:BLIP (D49A) complex simulations (red).

$Y50_{BLIP}$, which forms extensive van der Waals interactions with $M129_{SHV-1}$ (Zhang et al.,2003; Potapov et al., 2008), has a significant role in binding BLIP and also shown that mutation of this residue to alanine results in ~ 50 fold increase in binding affinity (Zhang et al. 2003). Active site residues of both structures were aligned and CE atom of $M129_{SHV-1}$ and CZ atom of $Y50_{BLIP}$ distance was measured

(Figure IV.34). D49A mutation on BLIP has a little effect on the interactions between these two residues.

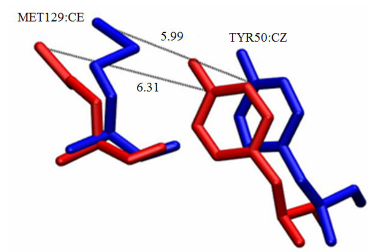

Figure IV.34 The distance between $M129_{SHV\text{-}1}$ and $Y50_{BLIP}$ in a snapshot from the simulations on BLIP bound (blue) and BLIP (D49A) bound SHV-1 (red).

The interactions between CE atom of $M129_{SHV\text{-}1}$ and CZ atom of $Y50_{BLIP}$ was measured in Figure IV.35. SHV-1:peptide is colored pink in all panels, SHV-1: peptide (D49A) is shown green (Figure IV.35.A), SHV-1:peptide (Y50A) is cyan (Figure IV.35.B) and SHV-1:peptide (Y51A) is colored black (Figure IV.35.C). D49A and Y50A mutations on peptide caused the breakdown of the interactions between $M129_{SHV\text{-}1}$ and residue 50_{BLIP} with respect to wild type peptide. On the other hand, when $Y51_{BLIP}$ mutated to alanine on peptide, $M129_{SHV\text{-}1}$ and residue 50_{BLIP} moved toward to each other about 1.00Å relative to peptide.

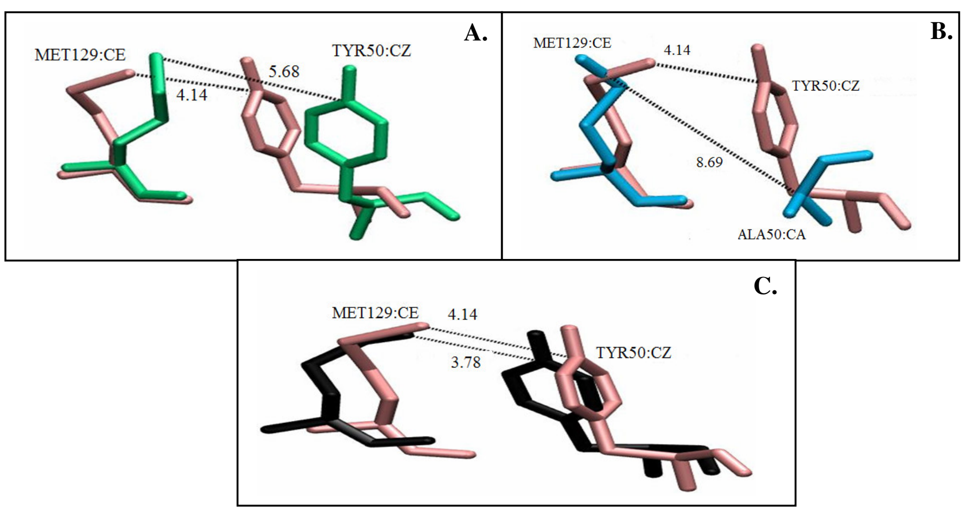

Figure IV.35. Interactions between residue $M129_{SHV\text{-}1}$ and 50_{BLIP} in the simulations on SHV-1: Peptide (pink in all panels). **A.** the SHV-1: peptide (D49A) (green) **B.** SHV-1: peptide (Y50A) (cyan) and **C.** SHV-1: peptide (Y51A) (black).

IV.2 EXPERIMENTAL RESULTS

IV.2.1. Selection of Microorganisms

High amounts of pUC18 mediated β-lactamase production requires growth in rich media supplemented with ampicillin. On the other hand, peptide uptake with a biotin tag can be monitored effectively in minimal media. The details of the uptake experiments are explained in Section III.4.10. For this reason, in the experiments of this study *E. coli* growth needed to be supported in both rich and minimal media.

LB Medium, with a rich context of vitamins and amino acids, and M9 minimal medium with only growth essential elements were used in this study. The growth of *E. coli* K12 and *E. coli* XL1 strains were monitored in both the complex and the minimal media and the growth profiles of the two *E. coli* strains are given in Figure IV.36.

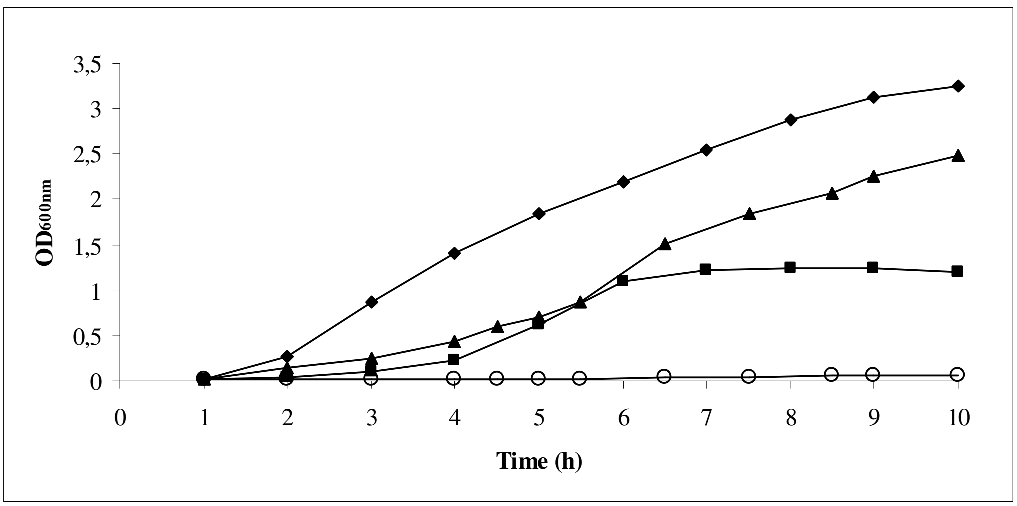

Figure IV.36. Growth profiles of *E. coli* K12 cells in LB medium (♦), in M9 minimal medium (■), of *E. coli* XL1 cells in LB medium (▲) and M9 minimal medium (○)

Based on the results on Figure IV.36, both LB and M9 minimal media could support *E. coli* K12 growth whereas *E. coli* XL1 could not grow in M9 minimal media. Therefore further experiments were carried out with *E. coli* K12 only.

IV.2.2. Transformation of plasmid pUC18 into *E. coli* cells

pUC18 plasmid carrying the gene for R-TEM-1 β-lactamase was transformed into *E. coli* K12 cells using $CaCl_2$ method. In order to verify that the transformed *E. coli* K12 cells harbored the pUC18 plasmid, both *E. coli* K12 cells (Figure IV.37.A) and *E. coli* K12 cells harboring plasmid pUC18 (Figure IV.37.B) were plated on LB agar media with 100 μg/ml ampicillin. It was clearly seen on the Figure IV.37 that selective media supported the growth of only plasmid harboring cells. R-TEM-1 β-lactamase expression by these cells rendered the bacteria resistant to ampicillin.

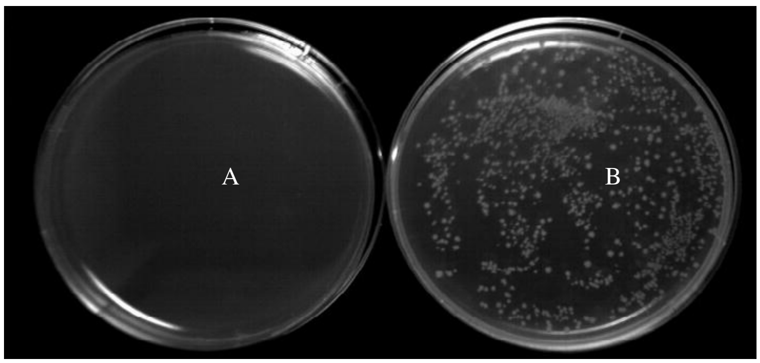

Figure IV.37. Growth of *E. coli* K12 cells **A.** without pUC18 **B.** with pUC18 on selective plates.

IV.2.3. Growth of *E. coli* K12 cells Harboring Plasmid pUC18

β-lactamase production is expected to be maximum during exponential phase when the amount of ampicillin is still high in the growth media. As the growth media is depleted of ampicillin through its hydrolysis by β-lactamase, the production of β-lactamse is expected to drop. It was found that *E. coli* cells consumed ampicillin (100 μg/ml) supplied in the growth medium in the first ten hours (Utkur et al., 2006). For this reason, it is important to determine the growth profile of the cells for selecting the appropriate time to harvest the cells for sufficient β-lactamase production. The cells were grown in M9 minimal and LB media supplemented with 100 μg/ml ampicillin and the growth profiles are plotted in Figure IV.38.

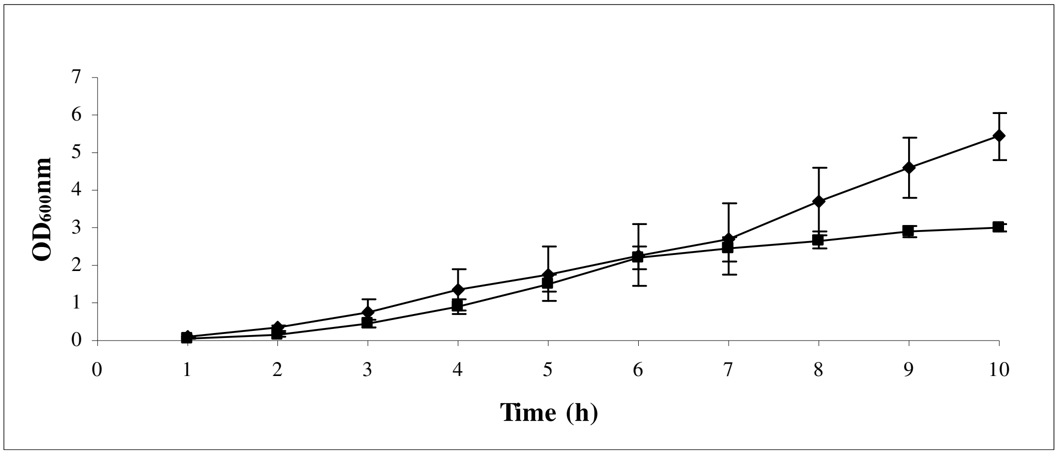

Figure IV.38 Growth profiles of *E. coli* K12 cells harboring plasmid pUC18 in M9 Minimal (■) and LB (♦) media.

Cells growing in minimal media entered stationary phase at about 6 hours of growth whereas cells were still exponential phase in LB media at the end of 10 hours.

The absorbance readings were also correlated to viable cell number by counting the colony forming units (CFU) on agar plates. The average values for three independent experiments are given in Table IV.3.

Table IV.3. Relation of Absorbance to CFU.

OD_{600}nm	Dilution Rate	CFU/Plate	CFU / 100 µl
0.03	10^{-4}	70	700000
0.1	10^{-4}	144	1440000
0.2824	10^{-4}	173	1730000
0.4516	10^{-5}	36	3600000
0.5576	10^{-5}	52	5200000
0.6193	10^{-5}	63	6300000
0.7556	10^{-5}	116	11600000
0.8408	10^{-6}	32	32000000

The details of the plating procedure are given in methods section III.4.4.

IV.2.4. Extraction of the Osmotic Shock Fluid and Electrophoretic Analysis

β-lactamase is a periplasmic protein. Therefore *E. coli* K12 cells harboring plasmid pUC18 were subjected to osmotic shock to extract the periplasmic proteins. Following determination of the protein concentration, the two samples one of which was control were loaded to SDS-polyacrylamide gels with the same amount of protein and the proteins were analyzed after Commassie G-250 staining (Figure IV.39).

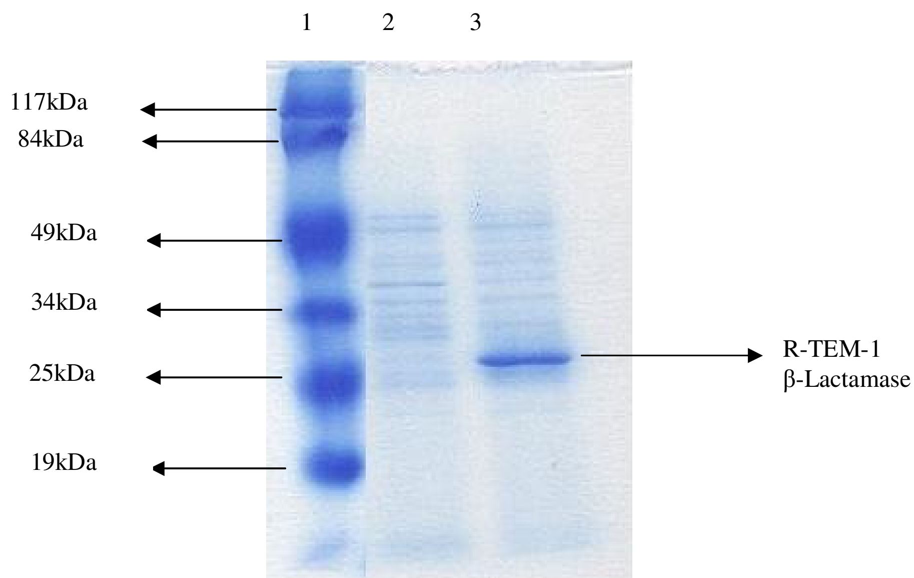

Figure IV.39. Electrophoretic analysis of the osmotic shock fluids from *E. coli* K12 cells. Lane 1: Marker, Lane 2: *E. coli* K12, Lane 3: *E. coli* K12 haboring pUC18.

In Figure IV.39 Lane 3, the protein band appeared between 25 kDa and 34 kDa from the extract of the plasmid harboring cells suggested that there should be significant β-lactamase production when cells were subjected to osmotic shock as OD_{600}nm of growing cells reached ~ 0.8.

IV.2.5. Analysis of β-Lactamase by Matrix Assisted Laser Desorption/Ionization, Time Of Flight Mass Spectrometry

A band corresponding to R-TEM-1 β-lactamase was apparent on the SDS-polyacrylamide gel. In order to verify this protein, the band was analyzed with the mass spectrometry.

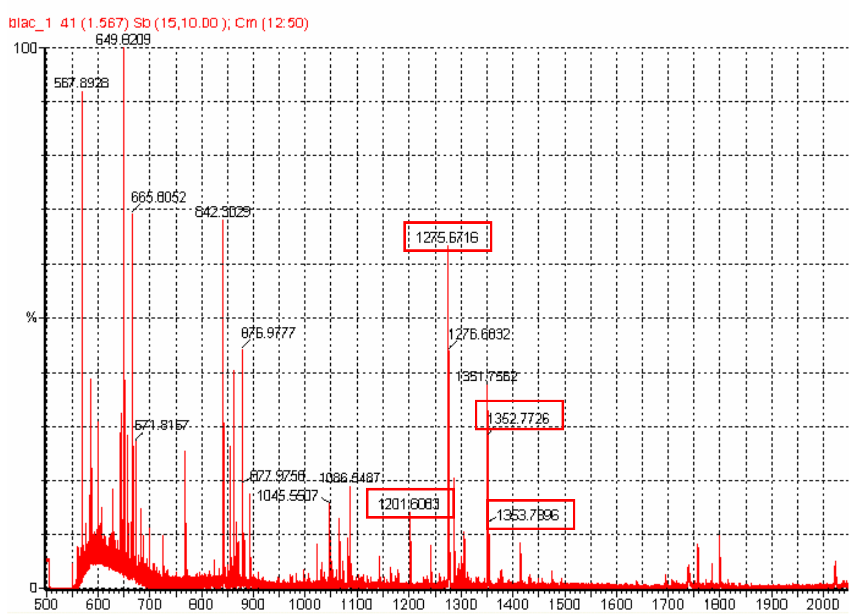

Figure IV.40 Mass spectral analysis of *E. coli* R-TEM-1 β-lactamase.

Using Swisport 57.4 database, the monoisotopic peptide masses obtained matched 92% to *E. coli* R-TEM-1 β-lactamase (Figure IV.40).

IV.2.6. *In-vitro* β-Lactamase –Ligand Recognition

Spectrophotometric method was used for the *in-vitro* β-lactamase activity measurements for which the initial concentrations of the substrate and the enzyme were adapted from published data found in literature (Rudgers *et al.,* 2001). In their experiments, nitrocephin was used as the common substrate. However, in this study a more recently proposed substrate, CENTA, was used. This is a chromogenic substrate for β-lactamase. Since the absorbance values obtained with CENTA using the procedure adopted from Jones et al (1982) were too low for an accurate measurement, optimization of the CENTA concentration was necessary.

IV.2.6.1. Determination of CENTA Concentration

R-TEM-1 enzyme (SIGMA P-3553) was used for the optimization of the CENTA concentration in the reaction mixture. Reaction mixtures with various CENTA concentrations (94, 235, 376, 470 μM) were prepared. The absorbance values of the reaction mixture at 405 nm as CENTA was hydrolyzed by β-lactamase were plotted in Figure IV.41.

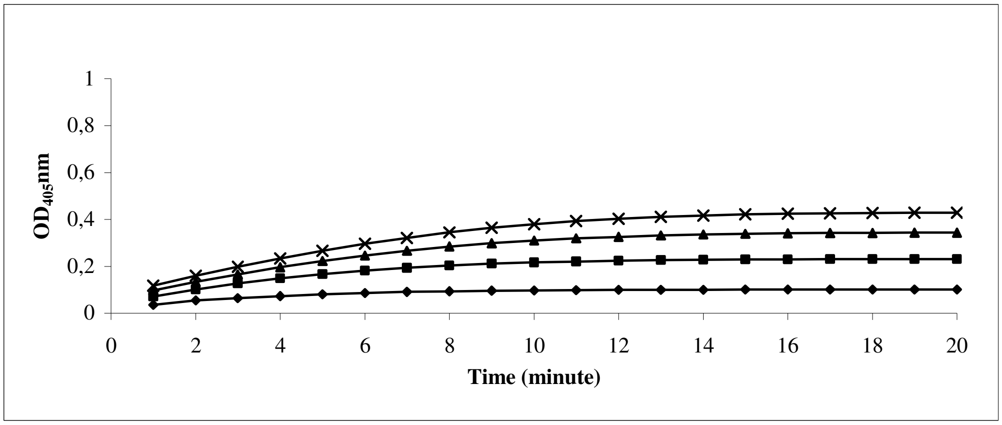

Figure IV.41. Monitoring CENTA hydrolysis with various CENTA concentrations: 94 μM (♦), 235 μM (■), 376 μM (▲), 470 μM (x)

As the CENTA product formed a significant difference in the absorbance value was observed with the 470 μM CENTA concentration and the reaction was completed in 12 minutes. Therefore, further experiments involving activity measurement were carried out with this substrate concentration.

IV.2.6.2. Determination of the Amount of Osmotic Shock Fluid

The aim of this study was to propose peptides that would be effective within the cell. Since the osmotic shock fluid is a mixture of the periplasmic proteins, which will be in the vicinity of the inhibitor peptide within the cell, in order to mimic the *in-vivo* conditions, osmotic shock fluid rather than purified β-lactamase was used in further reactions. The disadvantage in using the osmotic shock fluid as the source of β-lactamase is that the exact amount of β-lactamase is unknown. In addition to this, in each periplasmic protein extract, the amount of total proteins and β-lactamase amount may vary. This is mainly due to the slight differences in growth conditions, e.g. duration, and extraction protocol. For this reason, prior to measurement of activity, the amount of osmotic shock fluid to be added to the reaction mixture should be determined. Initial experiments were carried out with 750 μl (97.5 μg) osmotic shock fluid. The CENTA hydrolysis, monitored as the change in absorbance at 405 nm for 5 minutes, is given in Figure IV.42.

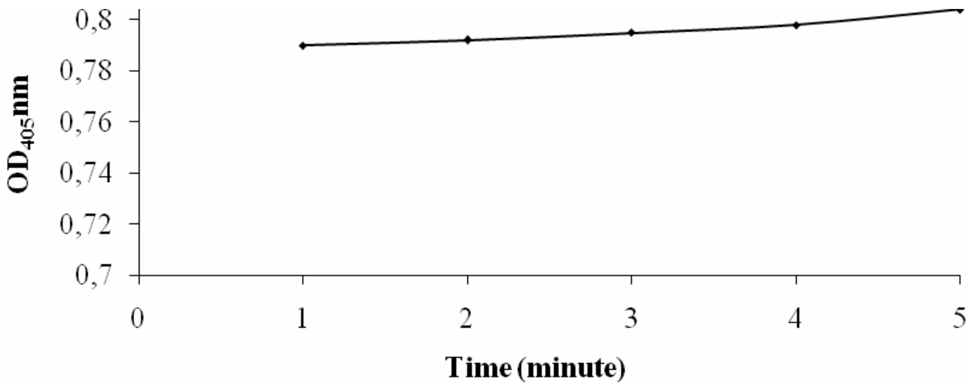

Figure IV.42 CENTA product formation using 750 µl osmotic shock fluid.

Since the differences in the absorbance readings taken every minute were not significant enough, as given in Figure IV.42, the reaction was probably already finished within a minute. This may be due to the high amount of β-lactamase in the osmotic shock fluid. Therefore the amount of osmotic shock fluid was reduced to 5 µl (0.65 µg), 10 µl (1.30 µg), 20 µl (2.60 µg), and 40 µl (5.20 µg) and CENTA hydrolysis was monitored at 405 nm for one minute. The absorbance readings are given in Figure IV.43.

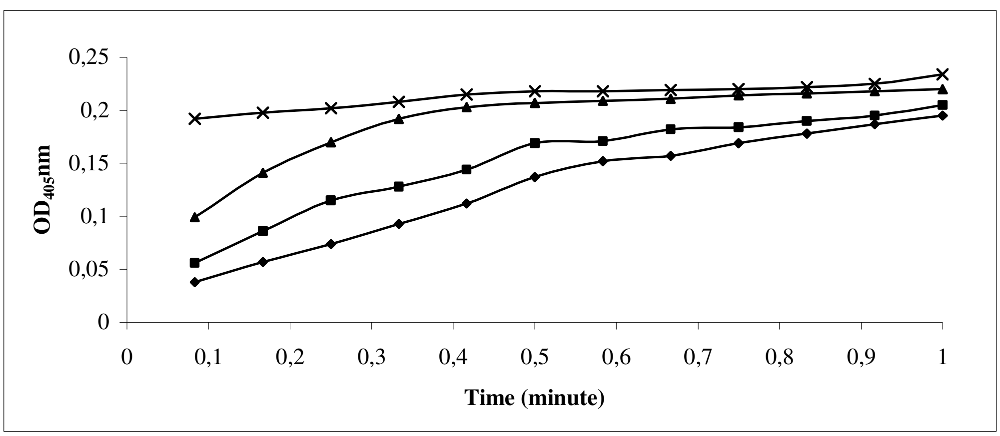

Figure IV.43. CENTA hydrolysis by 5 µl (♦),10 µl (■), 20 µl (▲), and 40 µl (x) osmotic shock fluid.

From the results of Figure IV.43, it was concluded that 5 µl osmotic shock fluid (0.65 µg/5 µl) was sufficient for the reaction mixture. However, as already stated, protein concentration in the osmotic shock fluid may vary. The amount of protein in this sample was taken as the standard in further experiments.

IV.2.6.3. Determination of Peptide Concentrations to Inhibit β-Lactamase

Peptides derived from BLIP have been shown to inhibit β-lactamase (Rudgers *et al.,* 2001). Since the two peptides of this study were very similar in sequence to the already investigated peptides, it was expected that these peptides would also inhibit β-lactamase even in the osmotic shock fluid. β-Lactamase inhibition was performed with 100, 200 and 400 μM concentrations of the two different N-terminal biotinylated peptides; 6 amino acids (A46-Y51 residues of BLIP) and 20 amino acids (C30-D49 residues of BLIP). Osmotic shock fluid without incubation with the peptides was used as a control. The results are given in Figure IV.44 and IV.45.

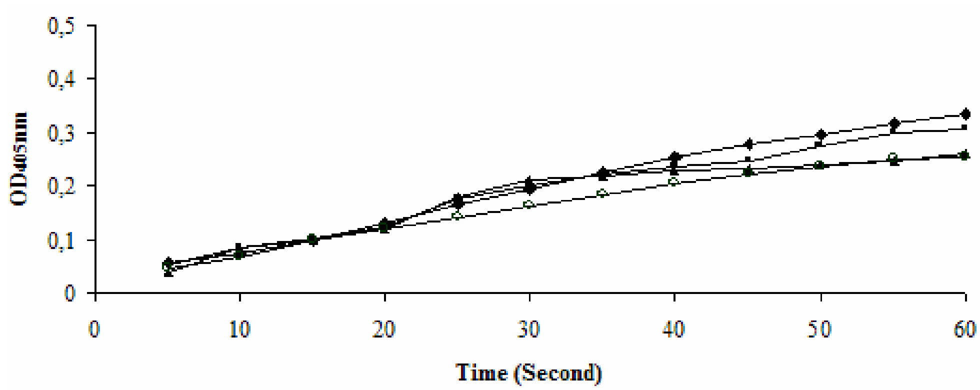

Figure IV.44. *in-vitro* β-lactamase inhibition by the 6-mer peptide with inhibitor concentrations of 0 μM (♦), 100 μM (■), 200 μM (▲), and 400 μM (◦) monitored by CENTA hydrolysis

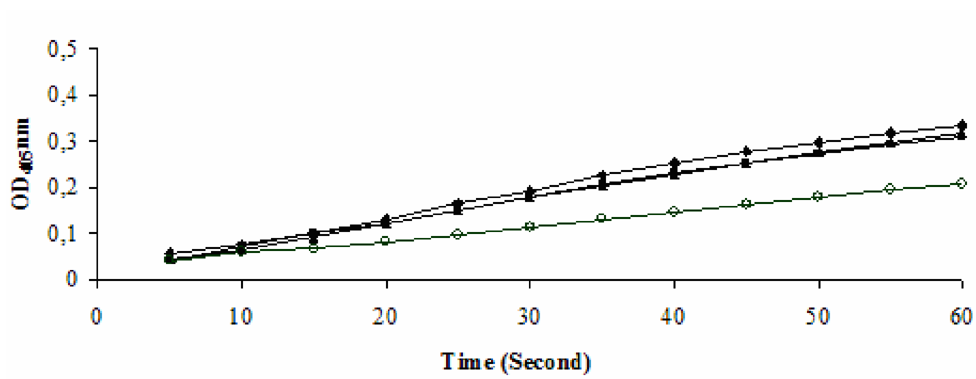

Figure IV.45. *in-vitro* β-lactamase inhibition by the 20-mer peptide with inhibitor concentrations of 0 μM (♦), 100 μM (■), 200 μM (▲), and 400 μM (◦) monitored by CENTA hydrolysis.

The slope of absorbance readings gives the rate of CENTA hydrolysis. Therefore the decrease in the slope in these figures indicates that β-lactamase was indeed inhibited by both peptides. The rate of CENTA hydrolysis droped when the enzyme was incubated with the peptide prior to its reaction with CENTA. Both peptides, the 6-mer and the 20-mer, at concentrations of 100 µM and 200 µM, had only slight inhibition on β-lactamase activity. On the other hand when the concentration of the 6-mer and the 20-mer peptides were raised to 400 µM, hydrolysis rate was reduced by 1.41 and 1.79 fold respectively. From these results, it can be concluded that the peptides at 400 µM concentration are effective in inhibition.

Using this concentration of the inhibitor, CENTA hydrolysis rate was calculated. First the absorbance values were converted to the hydrolysis of CENTA in nmoles using the calibration curve given in Appendix D. Values calculated with 400 µM peptide are plotted in Figure IV.46 and the rate of CENTA hydrolysis is given in Table IV.4.

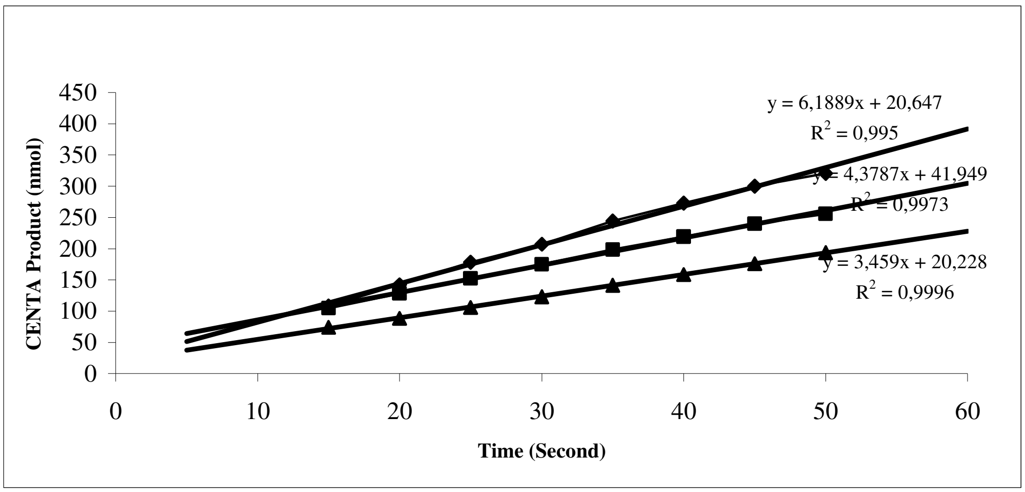

Figure IV.46 CENTA hydrolysis in nmoles, in the absence of the peptide (♦), in the presence of the 400 µM 6-mer peptide (■), and in the presence of the 400 µM 20-mer peptide (▲).

Table IV.4. The rate of CENTA hydrolysis

Inhibitor Concentration (µM)	CENTA Hydrolysis Rate (nmoles/sec)
-	6.19
400 (6-mer peptide)	4.38
400 (20-mer peptide)	3.46

The slopes of the different reaction mixtures were compared for the following conclusions: When β-lactamase was incubated with the 6-mer peptide, rate was reduced by 33 % and when β-lactamase was incubated with the 20-mer peptide, rate was reduced by 44 %.

The rate of CENTA hydrolysis was used to calculate total enzyme Units using Equation III.6. The detailed calculation of the corresponding slopes (d_A/d_t) for each hydrolysis reaction is given in Appendix E. Using the extinction coefficient, $\Delta\varepsilon$, of TEM-1 as 6.4 cm^2mol^{-1} at OD_{405} nm for CENTA (Bebrone *et al.,* 2001) the calculated total enzyme Units are given in Table IV.5.

Table IV.5. The total of β-lactamase activity Units.

SAMPLE incubate with	UNIT (U/L)
No inhibitor	560.4
400µM peptide (A46-Y51)	380.2
400µM peptide (C30-D49)	300.6

IV.2.7. *In-vivo* β-Lactamase Inhibition by Peptides

Peptides used in this study were synthesized with N-terminal biotinylation, specifically for *in-vivo* studies. Biotin is an essential vitamin for many microorganisms. There is biotin biosynthetic pathway in *E. coli* K12, but when this vitamin is supplied in the growth media, cells uptake the vitamin from the culture broth instead of synthesizing it. Biotin biosynthetic pathway is turned on as biotin is finished. The main reason for using biotinylated peptides for the peptide uptake experiments was to force the cells to utilize biotin available in the minimal growth medium, which was covalently attached to the peptide. The M9 minimal medium is composed of only salts and minerals, in addition to the basic carbon and nitrogen sources for growth. Therefore uptake of biotinylated peptide was expected to be triggered under these conditions. Upon entry into the cell, if the peptide binds β-lactamase, the cells should lose their resistance to ampicillin and die in this selective medium.

Two different approaches were used to investigate *in-vivo* binding and inhibition potential of the peptides. In the first approach, In the first approach, cells in their early logarithmic phase were exposed to the peptide (25 µg/ml) in the liquid medium and cell growth was monitored. When the results for the 6-mer and 20-mer peptide supplemented cells were compared with the control groups in Figures IV.47 and IV.48, it was seen that growth was only slightly affected in either case.

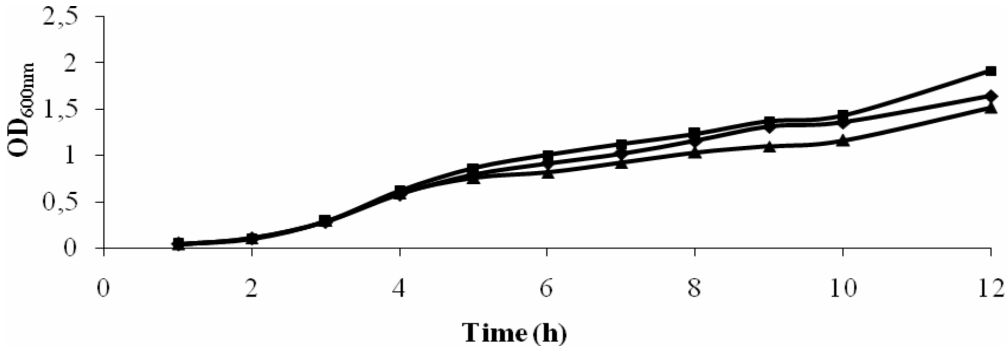

Figure IV.47. Growth Profile of plasmid harboring cells upon exposure to the distilled water (♦), potassium phosphate buffer (▲) and 6-mer peptide (■), at early logarithmic phase.

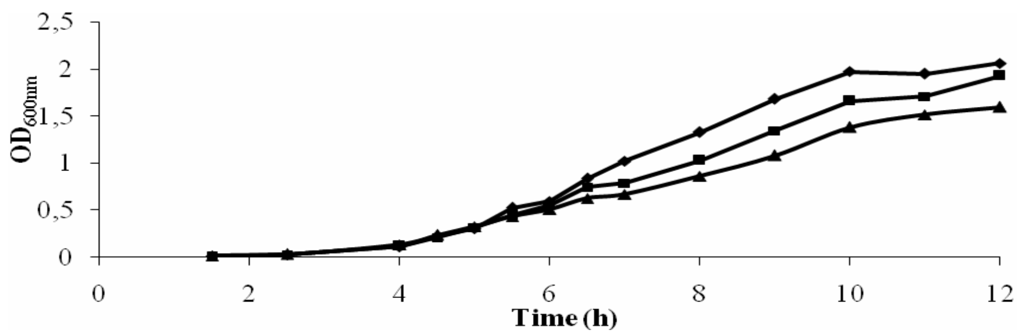

Figure IV.48. Growth Profile of plasmid harboring cells upon exposure to the distilled water (♦), potassium phosphate buffer (▲) and 20-mer peptide (■), at early logarithmic phase.

In the second approach, cells at different stages of growth were plated on solid media containing 25 μg/ml 6-mer peptide and the colony forming units were counted. The results given in Table IV.6 showed that only about 10 % of the cells died upon exposure to the inhibitory peptide.

Table IV.6. Change in CFU with respect to the potassium phosphate buffer supplemented cells.

OD_{600}nm	Remaining CFU upon exposure to the peptide (%)
0.2	87
0.4	93
0.6	96
0.8	88

These findings are consistent with the *in-vitro* experiments. Under *in-vitro* conditions, effective inhibition was recorded for 400 µM peptide concentration. However peptide supplement in the growth media was only 28 µM. Therefore higher concentrations of the peptide in the growth media, solid or liquid, can be more effective in terms of β-lactamase inhibition.

CHAPTER V

CONCLUDING REMARKS and RECOMMENDATIONS

V.1. CONCLUDING REMARKS

The aim of this research was to propose BLIP based peptide inhibitors for β-lactamase using computational methods and to verify the inhibition potential of peptides using *in-vitro* and *in-vivo* methods.

MD simulations on the apo-enzyme crystal structure of SHV-1 β-lactamase as well as SHV-1 bound to BLIP and to BLIP based peptides in different mutant forms were carried out for 10 ns. The RMSD trajectories of the simulations showed that all simulation systems reached equilibrium within the simulation time.

In all simulations, on apo or inhibitor bound SHV-1 β-lactamase, the active site structure and the interactions between key residues were maintained.

When the residue mobility of SHV-1 β-lactamase in all simulations was investigated, the mobility of the H10 helix was similar in BLIP and peptide (D49A) bound SHV-1 complexes relative to apo SHV-1. On the other hand, the H10 helix mobility was noticeably high in the BLIP (D49A), wild type peptide, peptide (Y50A) and peptide (Y51A) bound SHV-1 simulations compared to apo SHV-1.

The salt bridge between $D214_{SHV-1}$ and $R222_{SHV-1}$ of the H10 Helix was maintained in simulations on SHV-1:BLIP complex structure. When D49 was mutated to alanine, this salt bridge was broken. It is possible that this finding may be one of the reasons of H10 helix mobility.

A significant region on β-lactamase is the Ω-loop where $G175_{SHV-1}$ is located. The MSF values of $G175_{SHV-1}$ showed little variation in apo SHV-1, SHV-1:BLIP, SHV-1:peptide, SHV-1:peptide (Y50A) and SHV-1:peptide (Y51A) simulations. On the other hand, D49A mutation on BLIP and peptide caused the MSF value of $G175_{SHV-1}$ to decrease suggesting that residue D49 on BLIP is in long range communication with $G175_{SHV-1}$.

Petrosino et al. (1999) and Reynolds et al. (2006) showed that $D49_{BLIP}$ is an important hot-spot residue for SHV-1 β-lactamase inhibition. $D49_{BLIP}$ interacts with four significant residues of SHV-1 β-lactamase (R244, K234, S130 and T235). In all simulations, $D49_{BLIP}$ maintained its contact with the $R244_{SHV-1}$, $K234_{SHV-1}$, $S130_{SHV-1}$ and $T235_{SHV-1}$.

It was found that $Y105_{SHV-1}$ plays an important role in substrate binding and/or stabilization to SHV-1 β-lactamase (Doucet et al., 2004; Doucet et al., 2007). In all simulations, the interaction between $Y105_{SHV-1}$ and $D49_{BLIP}$ was examined. The distance between these residues was slightly changed in the simulations on BLIP, BLIP (D49A), wild type peptide, peptide (D49A) and peptide (Y50A) bound SHV-1 β-lactamase simulations while these residues moved toward each other from about 4.50 Å in the peptide (Y51A) bound SHV-1 β-lactamase. This suggests that residue Y51 may be required to maintain the interaction between $Y105_{SHV-1}$ and $D49_{BLIP}$.

$D104_{SHV-1}$ which has a hydrogen bond with $N132_{SHV-1}$, plays a key role in binding BLIP to SHV-1 β-lactamase (Reynolds et al., 2006). In this study, the interaction between $D104_{SHV-1}$ and $N132_{SHV-1}$ was investigated in all simulations. It was observed that this interaction was maintained in all simulations.

$Y50_{BLIP}$ forms van der Waals interactions with $M129_{SHV-1}$ which has a significant role in binding of BLIP to β-lactamase (Zhang et al., 2003). In all simulations, the distance between $Y50_{BLIP}$ and $M129_{SHV-1}$ was similar.

In the experimental part of the study, *in-vitro* and *in-vivo* binding of BLIP based peptides BLIP and RTEM-1 β-lactamase was examined. Both peptides (A46-Y51, C30-D49) inhibit RTEM-1 β-lactamase at a concentration of 400 μM under *in-vitro* conditions. When β-lactamase was incubated with the 6-mer (A46-Y51) and 20-mer (C30-D49) peptides, total activity units decreased by 33 and 44 %, respectively.

The two peptides effectively inhibit RTEM-1 β-lactamase in the osmotic shock fluid. Osmotic shock fluid contains all periplasmic proteins and therefore inhibition of the β-lactamase in the osmotic shock fluid constitutes a preliminary step toward examining *in vivo* inhibitory properties of the peptides. However, incubation of the β-lactamase producing cells with the inhibitory peptides did not result in any significant retardation in cell growth. Small peptide concentration in growth media was too low (28 μM). This concentration should be increased to at least 400 μM to see effective *in-vivo* β-lactamase inhibition.

V.2. RECOMMENDATIONS

Different BLIP based peptides should be investigated to find the best SHV-1 β-lactamase inhibitors and mutations on these new peptides can be performed to elucidate the contribution of these residues to β-lactamase binding.

Free Energy calculations, which provide clues on the affinity of binding, can be performed. The simulation length should be increased to get more accurate information on the SHV-1:Ligand binding dynamics.

The K_m and K_i values should be determined for the different peptides by a detailed kinetic investigation.

In this study, *in-vivo* inhibition effect of biotinylated peptides could not be observed due to the low concentration of peptides. The reason for this should further be investigated by gradually increasing the peptides concentration.

The question of whether the peptides are actually taken up by the cell or not remains to be answered. The location of the biotinylated peptide can be determined by chromatography methods using the high affinity between avidin and biotin.

REFERENCES

Ambler, R.P.; Coulson, A.F.; Frere,J.M.; Ghuysen, J.M.; Jaurin, B.; Jouris,B.; Levesque, R.; Tiraby, G.; Waley, S.G.A.: “Standart numbering scheme for the class A β-Lactamases”, *Biochem. J.* 276 **(1991)** 269-272.

Babini, G.S.; Livermore D.M.: “Antimicrobial resistance amongst Klebsiella spp. collected from intensive care units in Southern and Western Europe in 1997-1998.”, *J. Antimicrobial Chemother,* 45 **(2000)** 183-189.

Barthelemy, M.; Peduzzi, J.; Yaghlane, H. B.; Labia, R.: “Single Amino Acid Substitution between SHV-1 beta-lactamase and Cefotaxime-hydrolyzing SHV-2 enzyme”, *FEBS Lett,* 231 **(1988)** 217-220.

Bayles, K.W.: “The bactericidal action of penicillin: new clues to an unsolved mystery.” , *Trends Microbiol., 8* **(2000)** 274-278.

Bebrone, C.; Moali, C.; Mahy, F.; Rival, S.; Docquier, J.D.; Rossolini, G.M.; Fastrez, J.; Pratt, R.F.; Frère, J.M.; Galleni,M.: “CENTA as aChromogenic Substrate for Studying β-Lactamases”, *Antimicrobial Agents and Chemotherapy,* 45 **(2001)** 1868-1871.

Bush, K.: “Functional classification scheme for β-Lactamases and its correlation with molecular structure”, *Antimicrobial Agents and Chemotherapy,* 39 **(1995)** 1211-1233.

Coates, A.; Hu, Y.; Bax, R.; Page, C.: “The future challanges facing the development of new antimicrobial drugs”, *Nat. Rev. Drug Disco.,* 1 **(2002)** 895-910.

Cunningham, B. C.; Wells, J. A.: “Minimized Proteins.”, *Curr. Opin. Struct. Bio.,* 7 **(1997)** 457-462.

Doran, J.L.; Leskiw, B.K.; Aippersbach, S.; Jensen, S.E.: “Isolation and Characterization of a β-Lactamase-Inhibitory Protein from *Streptomyces clavuligerus* and Clonning and Analysis of the Corresponding Gene.”, *Journal of Bacteriology,* 172 **(1990)** 4909-4918.

Doucet, N.; De Wals, P.Y.,; Pelletier, J.N.: “Site-saturation Mutagenesis of Tyr-105 Reveals Its Importance in Substrate Stabilization and Discrimination in TEM-1 β-lactamase”, *The Journal of Biological Chemistry,* 279 **(2004)** 46295-46303.

Doucet N., Savard P.Y., Pelletier J.N., Gagne S.M.: “NMR Investigation of Tyr105 mutants in TEM-1 β-Lactamase”, *The Journal of Biological Chemistry* 282 **(2007)** 21448-21459.

Du bois, S. K.; Marriott, M. S.; Amyes, S. G.: “TEM and SHV-derived extended-spectrum beta-lactamases: Relationship between Selection, Structure and Function”, *J. Antimicrobial Chemother,* 35 **(1995)** 7-22.

Fisher, J.F.; Meroueh, S.O.; Mobashery, S.: “Bacterial resistance to beta-lactam antibiotics: compelling opportunism, compelling opportunity”, *Chem. Rev.*105 **(2005)** 395-424.

Gibson, R.M.; Christensen H.; Waley, S.G.: “Site-directed mutagenesis of beta-lactamase I. Single and double mutants of Glu-166 and Lys-73.”, *Biochem. J.* 272 (**1990)** 613-619.

Helfand, M.S.; Bethel, C.R.; Hujer, A.M.; Hujer, K.M.; Anderson, V.E.; Bonomo, R.A.: “Understanding Resistance to β-Lactams and β-Lactamase Inhibitors in the SHV-1 β-Lactamase”, *The Journal of Biological Chemistry,* 278 **(2003)** 52724-52729.

Huang ,W.; Beharry, Z.; Zhang, Z.; Pazkill, T.: "A broad spectrum peptide inhibitor of β-lactamase identified using phage display and peptide arrays", *Protein Engineering*, 16 **(2003)** 853-860.

Humphrey, W.; Dalke, A.; Schulten, K.: "VMD: visual molecular dynamics.", *J. Mol Graph.* 14 **(1996)** 33-38.

Imtiaz, U.; Manavathu, E.K.; Lerner, S.A.; Mobashery, S.: "Critical Hyrogen Bonding By Serine 235 for Cephlosporine Activity of TEM-1 β-lactamase", *Antimicrobial Agents and Chemotheraphy,* 37 **(1993)** 2438-2442.

Jelsch, C.; Mourey, L.; Masson, J. M.; Samama, J. P.: "Crystal structure of Escherichia coli TEM1 beta-lactamase at 1.8 Å", *Proteins*, 16 **(1993)** 364-383.

Jones, R.N.; Wilson, H.W.; William, J.; Novick, J.R.; Barry, A.L.; Thornsberry, C.: "In vitro Evaluation of CENTA, a New Beta-Lactamase-Susceptible Chromogenic Cephalosporin Reagent.", *Journal of Clinical Microbiology,* 15 **(1982)** 954-958.

Kaiser, G.E.: " Biol 230 Microbiology Lecture E-Text", **2004**.

Kale, L.V.; Bhandarkar, M.; Brunner, R.; Krawetz, N.; Phillips, J.; Shinozaki, A.; "NAMD : A case study in multilingual parallel programming" *Lecture notes in Computer Science,* 1366 **(1998)** 367-381.

Kalé, L.; Skeel, R.; Bhandarkar, M.; Brunner, R.; Gursoy, A.; Krawetz, N.; Phllips, J.; Shinozaki, A.; Varadarajan, K.; Schulten, K.: "NAMD2: Greater scalability for paralel molecular dynamics" , *Journal of Computational Physics*, 151 **(1999)** 283-312.

Kuzin,A.P.; Nukaga, M.; Nukaga, Y.; Hujer, A.M.; Bonomo R.A.; Knox, J.R.: "Structure of the SHV-1 β-Lactamase", *Biochemistry,* 38 **(1999)** 5720-5727.

Lamotte-Brasseur, J.; Dive, G.; Dideberg, O.; Charlier, P.; Frere, J. M.; Ghuysen, J. M.: " Mechanizm of acyl transfer by the class A serine β-lactamase of *Streptomyces albus* ", *G. Biochem. J.,* 279 **(1991)** 213-221.

Lapan, K.A.; Chapple, J.P.; Galcheva-Gargova, Z.; Yang, M.; Tao J.Lee, K. Y.; Hopkins, J. D.; "Peptide ligands in antibacterial drug discovery: use as inhibitors in target validation and target-based screening.", *Expert Opin Ther Targets.* 6 **(2002)** 507-516.

Livermore, D.M.; Yuan, M.: "Antibiotic resistance and production of extended-spectrum beta-lactamases amongst Klebsiella spp. from intensive care units in Europe.", *J Antimicrob Chemother.* 38 (**1996**) 409-24.

Majiduddin, F. K.; Materon, I. C.; Palzkill, T. G.: "Molecular anaylsis of beta-lactamase structure and function", *International Journal of Medical Microbiology*, 292 **(2002)** 127-137.

Massova, I.; Mobashery, S.: "Kinship and Diversification of Bacterial Penicillin-binding Proteins and Beta-Lactamases", *Antimicrob. Agents Chemother,* 42 **(1998)** 1-17.

Matagne, A.; Frere, J. M.: "Contribution of mutant analysis to the understanding of enzyme catalysis : the case of class A beta-lactamases", *Biochimica et Biophysica Acta*, 1246 **(1995)** 109-127.

Nossal, N.G.; Heppel, L. A.: "The Release of Enzymes by Osmotic Shock from Escherichia coli in Exponential Phase", *The Journal of Biological Chemistry,* 241 **(1966)** 3055-3062.

O'Brien, T. F.; Syvanen, M.: "Gly-238-Ser Substitution Changes the Substrate Specificity of the SHV Class A beta-lactamases", *Proteins,* 11 **(1991)** 45-51.

Orencia, M.C.; Yoon, J.S.; Ness J.E.; Stemmer, W.P.; Stevens, R.C.: "Predicting the emergence of antibiotic resistance by directed evolution and structural analysis.", *Nat Struct Biol.,* 8 **(2001)** 238-242.

Page, M. I.; Laws, A. P.: "The mechanizm of catalysis end the inhibition of β-lactamases ", *Chen. Commun.,* **(1998)** 1609-1617.

Palumbi, S. R.: "Humans as the world's greatest evolutionary force", *Science,* 293 **(2001)** 1786-1790.

Petit, A.; Maveyraud, L.; Lenfant, F.; Samama, J.P.; Labia, R.; Masson, J.M.: "Multiple substitutions at position 104 of beta-lactamase TEM-1: assessing the role of this residue in substrate specificity.", *Biochem J.* 305 **(1995)** 33-40.

Petrosino, J.F.; Palzkill T.: "Systematic Mutagenesis of the Active Site Omega Loop of TEM-1 β-lactamase", *Journal of Bacteriology,* 178 **(1996)** 1821-1828.

Petrosino, J.; Rudgers, G. W.; Gilbert, H.; Palzkill, T.: "Contributions of Aspartate 49 and Phenylalanine 142 Residues of a Tight Binding Inhibitory Protein of beta -Lactamases", *Journal of Biological Chemistry*, 274 **(1999)** 2394-2400.

Potapov V., Reichmann D., Abramovich R., Filchtinski D., Zohor N., Halevy B.D., Edelman M., Sobolev V., Shreiber G.: "Computational Redesign of a protein-protein Interface for High Affinity and Binding Specificity Using Modular Architecture and Naturally Occuring Template Fragments", *Journal Mol. Biol.*384 **(2008)** 109-119.

Reichmann, D.; Rahat, O.; Albeck, S.; Meged, R.; Dym, O.; Schreiber, G.: **"**A The modular architecture of protein-protein binding interfaces", *Proc Natl Acad Sci,* 102 **(2005)** 57-62.

Reynolds,K.A.; Thomson, J.M.; Corbett K.D.; Bethel, C.R.; Berger, J.M:; Kirsch J.F.; Bonomo R.A.; Handel T.M.: "Structural and Computational Characterization of the SHV-1 β-lactamase- β-lactamase Inhibitor Protein Interface", *The Journal of Biological Chemistry,* 281 **(2006)** 26745-26753.

Roccatano, D.; Sbardella, G.; Aschi, M.; Amicosante, G.; Bossa, C.; Nola, A.D.; Mazza, F.: "Dynamical aspects of TEM-1 β-lactamase probed by molecular dynamics", *Journal of Computer-Aided Molecular Design*, 19 **(2005)** 329-340.

Rogers, H.J.; Forsberg, C.W.: "Role of autolysins in the killing of bacteria by some bactericidal antibiotics.", *J Bacteriol.,*108 **(1971)** 1235-43.

Rudgers, G. W.; Huang, W.; Palzkill, T.: "Binding Properties of a Peptide Derived from β-lactamase Inhibitory Protein", *Antimicrobial Agents and Chemotherapy*, 45 **(2001)** 3279-3286.

Shevchenko, A.; Tomas, H.; Havlis, J.; Olsen, J. V.; Mann, M.: "In-gel Digestion for Mass Spectrometric Characterization of Protein and Proteomes", *Nature Protocols,* 1 **(2006)** 2856-2860.

Strynadka, N. C. J.; Adachi, H.; Jensen, S. E.; Johns, K.; Sielecki, A.; Betzel, C.; Sutoh, K.; James, M. N. G.: "Molecular structure of the acyl-enzyme intermediate in β lactam hydrolysis at 1.7A° resolutions", *Nature*, 359 **(1992)** 700-705.

Strynadka, N. C. J.; Jensen, S.E.; Johns, K.; Blanchard, H.; Page M.; Matagne, A.; Frere, J.M.; James, M.N.G.: "Structural and Kinetic Characterization of a β-lactamase-inhibor protein.", *Nature,* 368 **(1994)** 657-660.

Strynadka, N. C.; Jensen, S. E.; Alzari, P. M.; James, M. N. G.: "A potent new mode of beta-lactamase inhibition revealed by the 1.7 Å X-ray crystallographic structure of the TEM-1-BLIP complex.", *Nature Structural Biology*, 3 **(1996)** 290-297.

Tomas, A.; Albino, A.; Zanati, E.: "Multiple antibiotic resistance in a bacterium with suppressed autolytic system.", *Nature.,* 227 **(1970)** 138-40.

Tipper, D.J.; Strominger, J.L.: "Mechanism of action of penicillins: a proposal based on their structural similarity to acyl-D-alanyl-D-alanine.", *Proc Natl Acad Sci*, 54 **(1965)** 1133-41.

Utkur O.: “Experimental Studies to Determine the Effect of Protein Characteristics On Translocation of Fusion Proteins in *Escherichia Coli*”, MSc Thesis, Boğaziçi University, Department of Chemical Engineering, Istanbul, Turkey, **(2006)** 48-49.

Walker, J.R.; Altman, E.: “Biotinylation Facilitates the Uptake of Large Peptides by *Escherichia coli* and Other Gram-Negative Bacteria”, *Applied and Environmental Microbiology,* 71 **(2005)** 1850-1855.

Wang J., Palzkill T., Chow D.C.: “Structural Insight into the Kinetics and Delta Cp of Interactions between TEM-1 Beta Lactamase and Beta Lactamase Inhibitory Protein (BLIP)” *The Journal of Biological Chemistry,* 284 **(2009)** 595-609.

Yamamoto, T.; Yamagata, S.; Horii, K.; Yamagishi, S.: “Comparison of transcription of beta-lactamase genes specified by various ampicillin transposons.”*, J Bacteriol.,* 150 **(1982)** 269-76.

Zhang, Z.; Palzkill, T.: “Determinants of binding affinity and specificity for the interaction of TEM-1 and SME-1 β-Lactamase with β-Lactamase inhibitory protein β-Lactamases”, *The Journal of Biological Chemistry*, 278 **(2003)** 45706–45712.

Zhang, Z.; Palzkill, T.: **“**Dissecting the protein-protein interface between β-lactamase inhibitory protein and Class A β-lactamases”, *The Journal of Biological Chemistry*, 279 **(2004)** 42860–42866.

APPENDIX A

INPUT FILES USED IN COMPUTATIONAL STUDIES

NAMD Configuration File

```
#############################################################
## JOB DESCRIPTION                                         ##
#############################################################
# Minimization and Equilibration of
# SHV1-BLIP in a Water Box
#############################################################
## ADJUSTABLE PARAMETERS                                   ##
#############################################################
structure          ../ionizedSHVBLIP.psf
coordinates        ../ionizedSHVBLIP.pdb
set temperature    300
set outputname     complex_wb_eq
set init_temp      50
firsttimestep      0
#############################################################
## SIMULATION PARAMETERS                                   ##
#############################################################
# Input
paraTypeCharmm          on
parameters          ../toppar/par_all27_prot_lipid.prm
temperature         $init_temp
# Force-Field Parameters
exclude             scaled1-4
1-4scaling          1.0
```

```
cutoff              12.
switching           on
switchdist          10.
pairlistdist        13.5
# Integrator Parameters
timestep            1.0  ;# 1fs/step
rigidBonds          all  ;# needed for 2fs steps
nonbondedFreq       1
fullElectFrequency  2
stepspercycle       10
# Constant Temperature Control
langevin            on    ;# do langevin dynamics
langevinDamping     5     ;# damping coefficient (gamma) of 5/ps
langevinTemp        $init_temp
langevinHydrogen    off    ;# don't couple langevin bath to hydrogens
# Periodic Boundary Conditions
cellBasisVector1    81.55100059   0.   0.
cellBasisVector2    0.   79.43899917  0.
cellBasisVector3    0.    0.  87.30799913
cellOrigin          15.4557247162 27.078086853 51.3710594177
margin              2.5
wrapAll             on
# PME (for full-system periodic electrostatics)
PME                 yes
PMEGridSizeX        90
PMEGridSizeY        80
PMEGridSizeZ        90
# Constant Pressure Control (variable volume)
useGroupPressure    yes ;# needed for rigidBonds
useFlexibleCell     no
useConstantArea     no
langevinPiston      on
langevinPistonTarget  1.01325 ;#  in bar -> 1 atm
```

```
langevinPistonPeriod  100.
langevinPistonDecay   50.
langevinPistonTemp    $init_temp
# Output
outputName          $outputname
restartfreq         500     ;# 500steps = every 1ps
dcdfreq             250
xstFreq             250
outputEnergies      100
outputPressure      100
#############################################################
## EXTRA PARAMETERS                                        ##
#############################################################
constraints on
consexp 2
consref   ../ionizedSHVBLIP.pdb
conskfile ../ionizedSHVBLIP_cons.pdb
conskcol B
constraintScaling 5
#############################################################
## EXECUTION SCRIPT                                        ##
#############################################################
# turn off until later
#langevinPiston                  off
# Minimization
minimize            1000
output mini.cons5
cnstraintScaling 3
minimize            1000
output mini.cons3
constraintScaling 0
minimize            1000
output mini.all
```

```
reinitvels      $init_temp
run          4000
for { set TEMP [expr ($init_temp + 10)] } { $TEMP < $temperature } { incr TEMP
10
} {
   langevinTemp         $TEMP
   LangevinPistonTemp   $TEMP
   run                  4000
}
langevinTemp         $temperature
#LangevinPistonTemp   $TEMP
run                  5000000
```

PGN File used to build the PSF file

```
package require psfgen
topology top_all27_prot_lipid.inp
pdbalias residue HIS HSE
pdbalias atom ILE CD1 CD
segment SHV {pdb shv.pdb}
coordpdb shv.pdb SHV
segment pep {pdb blip.pdb}
coordpdb blip.pdb pep
guesscoord
writepdb shvblip.pdb
writepsf shvblip.psf
```

Tk Scripting

Distance.tcl

```
proc distance {molid residue1 type1 residue2 type2} {
set a1 [atomselect $molid "chain B and resid $residue1 and name $type1"]
set a2 [atomselect $molid "chain A and resid $residue2 and name $type2"]
set ind1 [$a1 get index]
set ind2 [$a2 get index]
label add Bonds $molid/$ind1 $molid/$ind2 }
```

MATLAB SCRIPTS

Calculation of RMSD

```
X=readdcd ('shv.ca.dcd', 1:265);
X(:,end-5:end)=[];
x= bestfit(X);
r=findrmsd(x);
plot(r)
xlabel ('Time Step');
ylabel ('RMSD');
title ('RMSD vs Time Step of SHV-1 Beta Lactamase');
```

Calculation of MSF

```
X=readdcd ('shv.ca.dcd', 1:265);
X(:,end-5:end)=[];
x= bestfit(X);
size (x)
a b
y=x(b:a,:);
y=bestfit(y);
msf=findmsf(y);
plot(msf,'.-k')
```

Calculation of PCA

```
X=readdcd ('shv.ca.dcd', 1:265);
X(:,end-5:end)=[];
x= bestfit(X);
size (x)
a b
y=x(b:a,:);
```

```
y=bestfit(y);
[T,P,ssq]=pca(mncn(y),0);
plot (ssq (1;50,2), '.-')
plot(T(:,1))
plot(T(1:200,1), '.-')
plot(P(:,1))
expl=explainres(y, P(:,1:4),ssq(1:4,2),1:8)
```

APPENDIX B

ACTIVE-SITE RESIDUE INTERACTIONS

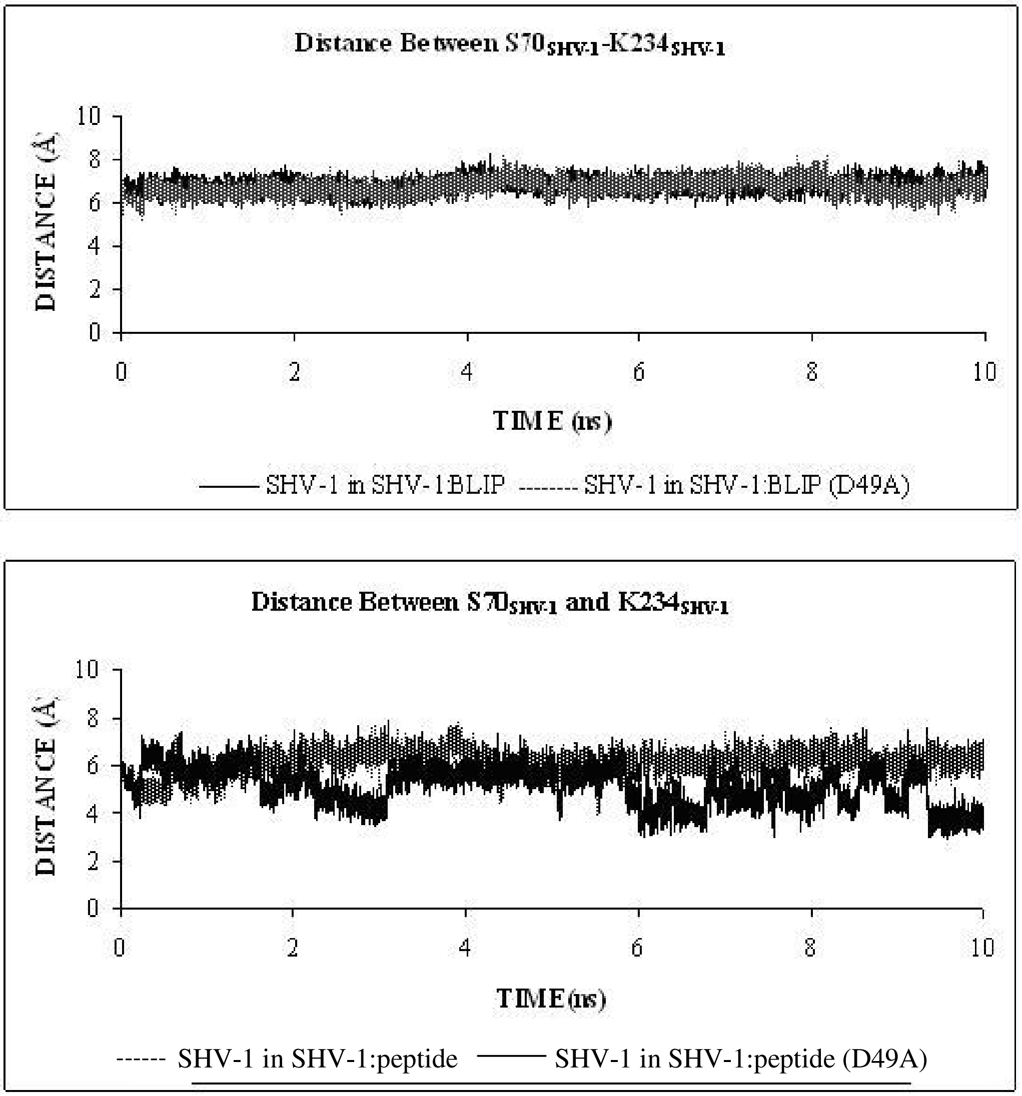

Figure B.1 Distance Between S70 and K234 of SHV-1 in all 10ns Simulations.

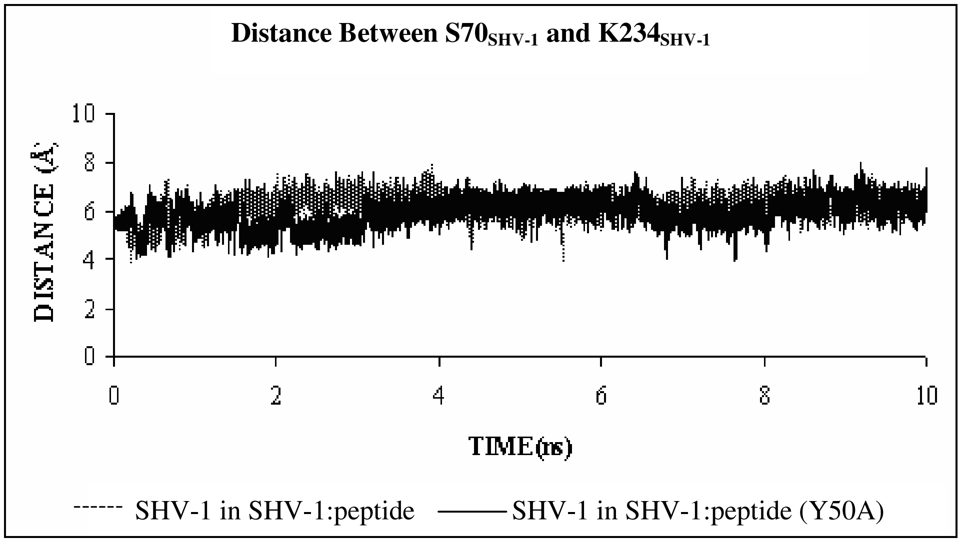

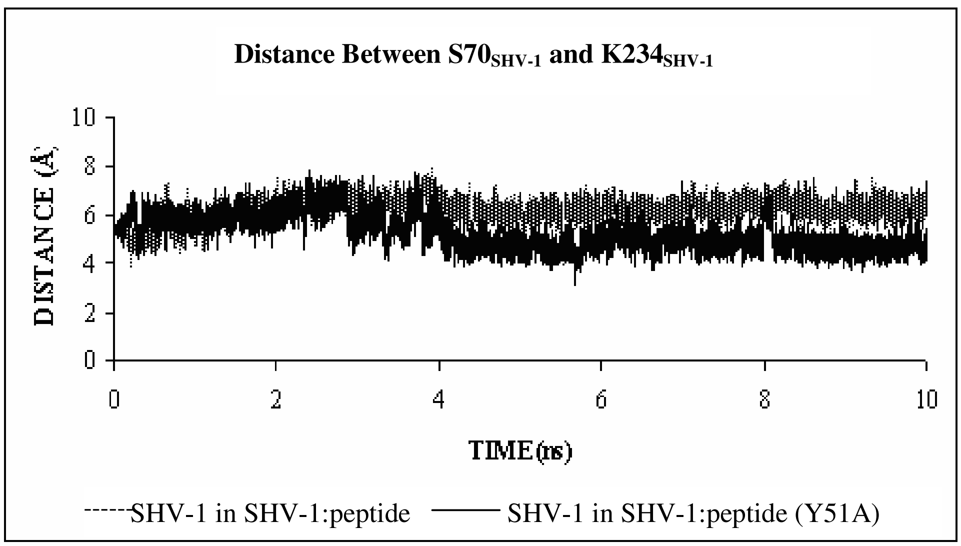

Figure B.1 Continued.

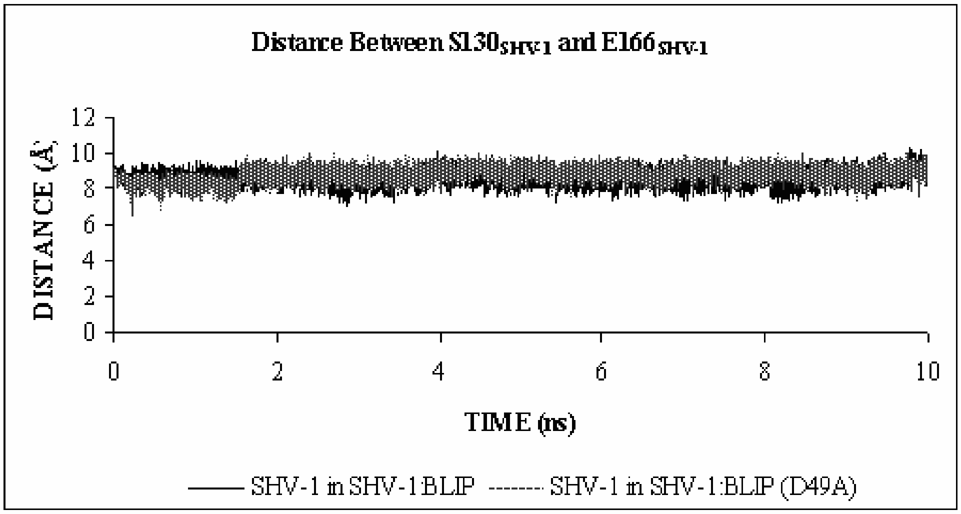

Figure B.2 Distance Between S130$_{SHV-1}$ and E166$_{SHV-1}$ in the simulations on SHV-1:BLIP and SHV-1:BLIP (D49A).

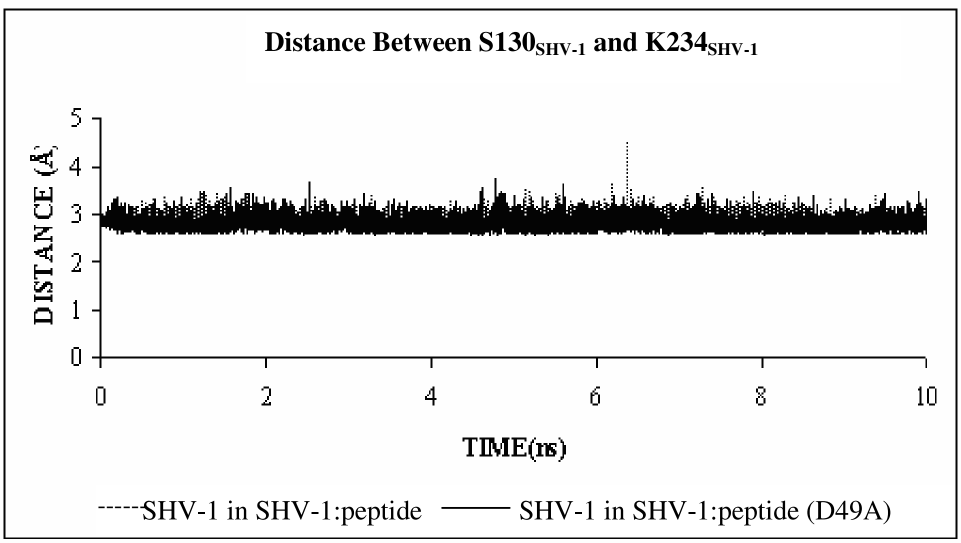

Figure B.3 Distance Between S130$_{SHV-1}$ and K234$_{SHV-1}$ in the simulations on SHV-1:peptide complexes.

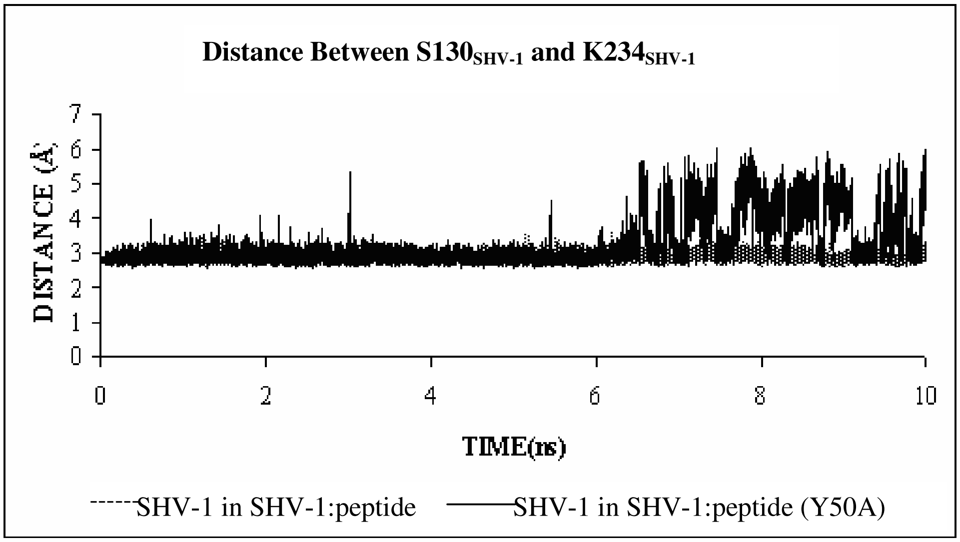

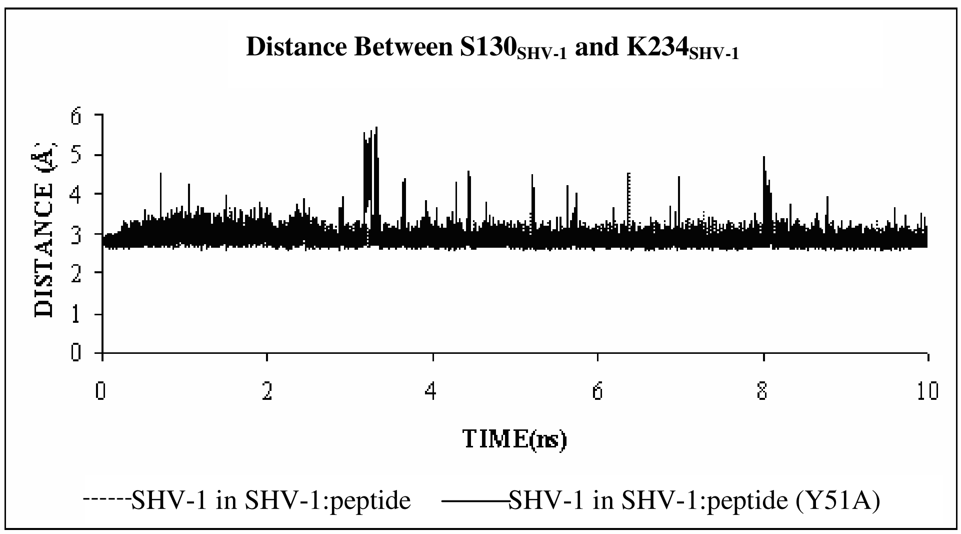

Figure B.3 Continued.

APPENDIX C:

BSA CALIBRATION CURVE

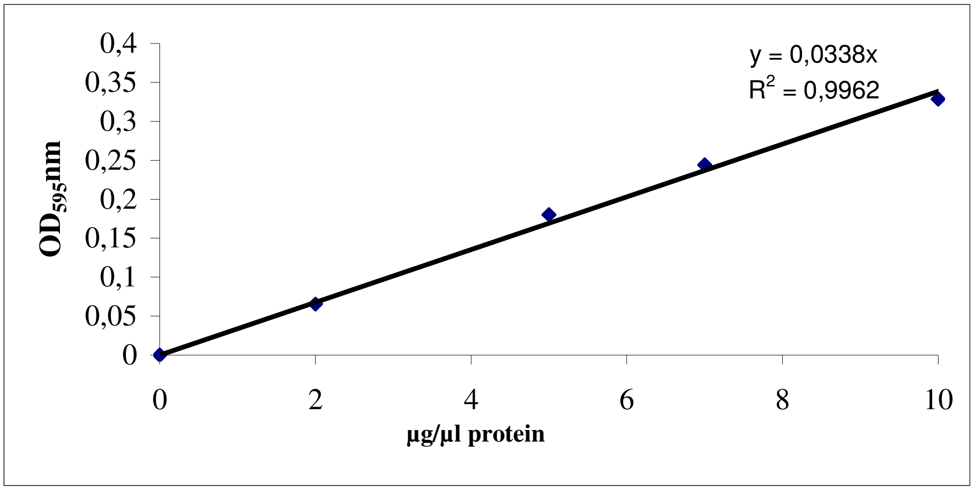

Figure C.1. BSA Calibration Curve

APPENDIX D:

CENTA CALIBRATION CURVE

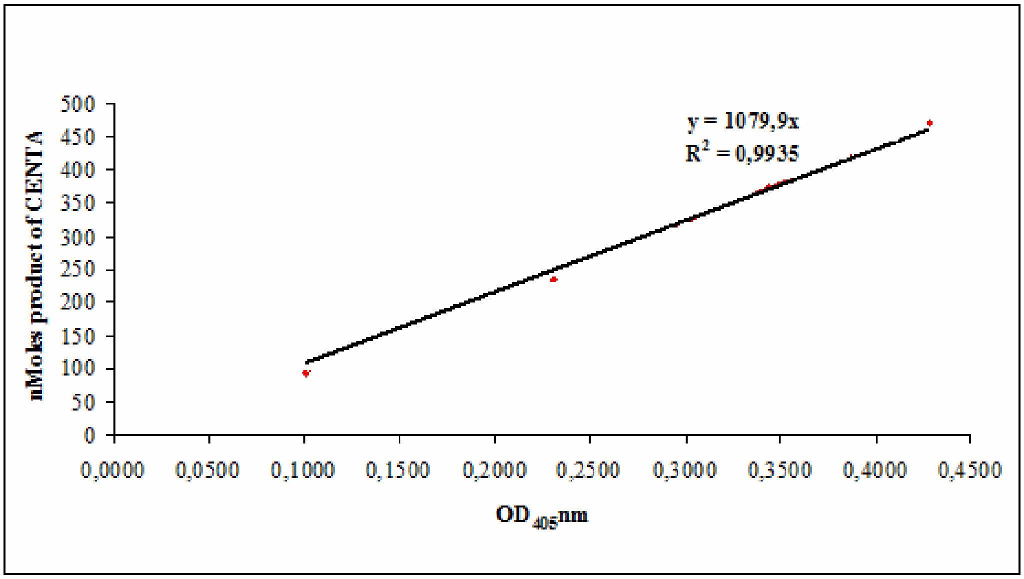

Figure D.1. CENTA Calibration Curve

APPENDIX E

d_A/d_T VALUES FOR CALCULATION ENZYME ACTIVITIES IN UNITS

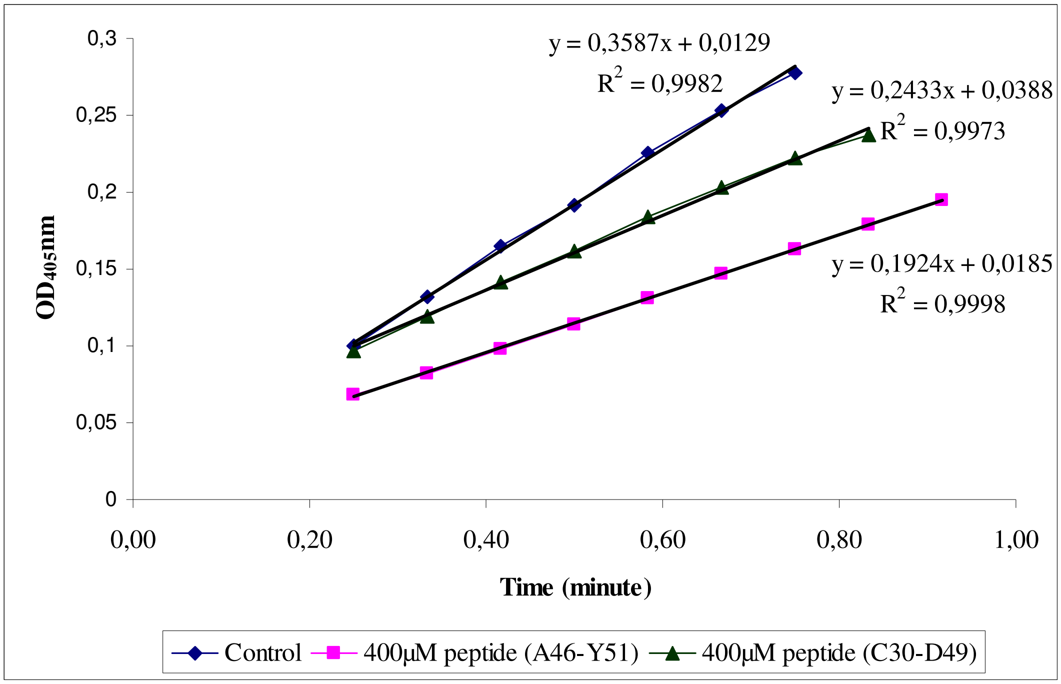

Figure E.1. d_A/d_T values for calculation enzyme activities in Units.

AUTOBIOGRAPHY

I graduated from the Biology Department with a second rank and Molecular Biology and Genetics Department from Istanbul University. I enrolled in the Bioengineering MSc Program at Marmara University in 2007.

Projects

- Glucose Effect of Oxidative Stress Response In The Yeast, *Schizosaccharomyces pombe* (2007). Istanbul Univ., Molecular Biology & Genetics Dep.Term Project
- Collagen I gene polymorphism in Scleroderma. (09.2006-01.2007). Istanbul Univ., Molecular Biology & Genetics Dep., Participant as an asistant student.

Publication

- **Büdeyri N,** Sarıyar Akbulut B, Yavuztürk B, Kazan D. β-GALACTOSIDASE BY MODERATELY HALOPHILIC *Halomonas sp.* MU10: Production and Optimization. Submitted.

Selected Posters

- **Büdeyri N,** Özkırımlı Ölmez E, Sarıyar Akbulut B. (2009) Investigation of *in-vivo* Beta-Lactamase Inhibition by Beta-Lactamase-Inhibitor-Protein Based Peptides. 34th FEBS Congress, Prague-Czech Republic, July 4-9.
- Kanlıkılıçer P, **Büdeyri N,** Sarıyar Akbulut B, Hortaçsu A, Özkırımlı Ölmez E. (2009). Dynamic Analysis of β-Lactamase Ligand Recognition. Biophysical Society 53rd Annual Meeting, Boston-USA, February 28- March 4
- **Büdeyri N**, Kanlıkılıçer P, Sarıyar Akbulut B, Hortaçsu A, Özkırımlı Ölmez E. (2008). Dynamic Analysis of Beta-Lactamase Ligand Recognition. ECCB'08 European Conference on Computational Biology, Cagliari, Sardinia-Italy September 22-26.
- **Büdeyri N**, Sarıyar B, Kazan D. (2008). The optimization of beta-galactosidase production by *Halomonas sp.* using response surface methodology. UKMK-8, 8th National Chemical Engineering Congress, Malatya-TURKEY, August 26-29.